Nuclear Safety
NEA/CSNI/R(2020)11
October 2022
www.oecd-nea.org

OECD/NEA X-FEM Benchmark Final Report

OECD BETTER POLICIES FOR BETTER LIVES
NEA NUCLEAR ENERGY AGENCY

Nuclear Energy Agency

NEA/CSNI/R(2020)11

Unclassified **English text only**

4 October 2022

NUCLEAR ENERGY AGENCY
COMMITTEE ON THE SAFETY OF NUCLEAR INSTALLATIONS

OECD/NEA X-FEM Benchmark Final Report

This document is available in PDF format only.

JT03504034

ORGANISATION FOR ECONOMIC CO-OPERATION AND DEVELOPMENT

The OECD is a unique forum where the governments of 38 democracies work together to address the economic, social and environmental challenges of globalisation. The OECD is also at the forefront of efforts to understand and to help governments respond to new developments and concerns, such as corporate governance, the information economy and the challenges of an ageing population. The Organisation provides a setting where governments can compare policy experiences, seek answers to common problems, identify good practice and work to co-ordinate domestic and international policies.

The OECD member countries are: Australia, Austria, Belgium, Canada, Chile, Colombia, Costa Rica, the Czech Republic, Denmark, Estonia, Finland, France, Germany, Greece, Hungary, Iceland, Ireland, Israel, Italy, Japan, Korea, Latvia, Lithuania, Luxembourg, Mexico, the Netherlands, New Zealand, Norway, Poland, Portugal, the Slovak Republic, Slovenia, Spain, Sweden, Switzerland, Türkiye, the United Kingdom and the United States. The European Commission takes part in the work of the OECD.

OECD Publishing disseminates widely the results of the Organisation’s statistics gathering and research on economic, social and environmental issues, as well as the conventions, guidelines and standards agreed by its members.

NUCLEAR ENERGY AGENCY

The OECD Nuclear Energy Agency (NEA) was established on 1 February 1958. Current NEA membership consists of 34 countries: Argentina, Australia, Austria, Belgium, Bulgaria, Canada, the Czech Republic, Denmark, Finland, France, Germany, Greece, Hungary, Iceland, Ireland, Italy, Japan, Korea, Luxembourg, Mexico, the Netherlands, Norway, Poland, Portugal, Romania, Russia (suspended), the Slovak Republic, Slovenia, Spain, Sweden, Switzerland, Türkiye, the United Kingdom and the United States. The European Commission and the International Atomic Energy Agency also take part in the work of the Agency.

The mission of the NEA is:

- to assist its member countries in maintaining and further developing, through international co-operation, the scientific, technological and legal bases required for a safe, environmentally sound and economical use of nuclear energy for peaceful purposes;
- to provide authoritative assessments and to forge common understandings on key issues as input to government decisions on nuclear energy policy and to broader OECD analyses in areas such as energy and the sustainable development of low-carbon economies.

Specific areas of competence of the NEA include the safety and regulation of nuclear activities, radioactive waste management and decommissioning, radiological protection, nuclear science, economic and technical analyses of the nuclear fuel cycle, nuclear law and liability, and public information. The NEA Data Bank provides nuclear data and computer program services for participating countries.

COMMITTEE ON THE SAFETY OF NUCLEAR INSTALLATIONS

The Committee on the Safety of Nuclear Installations (CSNI) addresses Nuclear Energy Agency (NEA) programmes and activities that support maintaining and advancing the scientific and technical knowledge base of the safety of nuclear installations.

The Committee constitutes a forum for the exchange of technical information and for collaboration between organisations, which can contribute, from their respective backgrounds in research, development and engineering, to its activities. It has regard to the exchange of information between member countries and safety R&D programmes of various sizes in order to keep all member countries involved in and abreast of developments in technical safety matters.

The Committee reviews the state of knowledge on important topics of nuclear safety science and techniques and of safety assessments, and ensures that operating experience is appropriately accounted for in its activities. It initiates and conducts programmes identified by these reviews and assessments in order to confirm safety, overcome discrepancies, develop improvements and reach consensus on technical issues of common interest. It promotes the co-ordination of work in different member countries that serve to maintain and enhance competence in nuclear safety matters, including the establishment of joint undertakings (e.g. joint research and data projects), and assists in the feedback of the results to participating organisations. The Committee ensures that valuable end-products of the technical reviews and analyses are provided to members in a timely manner, and made publicly available when appropriate, to support broader nuclear safety.

The Committee focuses primarily on the safety aspects of existing power reactors, other nuclear installations and new power reactors; it also considers the safety implications of scientific and technical developments of future reactor technologies and designs. Further, the scope for the Committee includes human and organisational research activities and technical developments that affect nuclear safety.

Acknowledgements

This report would not have been possible without the contributions of the benchmark participants. They helped develop the benchmark problems, conducted the requested analyses, performed additional sensitivity analyses on their own, documented their results, and helped author and review this manuscript.

The benchmark participants thankfully acknowledge the co-ordination by Isabelle Delvallée Nunio from the IRSN (France).

Finally, Dr Diego Escrig Forano is recognised for his contribution as NEA scientific secretary for the CSNI Working Group for Integrity and Ageing of Components and Structures (WGIAGE). Dr Escrig Forano helped ensure that projects were running smoothly and deliverables were completed on time.

Table of contents

Tables

Figures

List of abbreviations and acronyms

CAPS	CSNI Activity Proposal Sheet
CSNI	Committee on the Safety of Nuclear Installations (NEA)
FEM	Finite Element Method
IRSN	Institut de Radioprotection et de Sûreté Nucléaire (Institute of Radiological Protection and Nuclear Safety, France)
LOCA	Loss-of-coolant accident
NEA	Nuclear Energy Agency
OECD	Organisation for Economic Co-operation and Development
SIF	Stress Intensity Factor
WGIAGE	Working Group for Integrity and Ageing of Components and Structures (NEA)
X-FEM	eXtended Finite Element Method

Executive summary

This report summarises the work done for the activity: "Benchmark analysis on the eXtended Finite Element Method (X-FEM) calculation technology in its use to evaluate the fracture mechanics stress intensity parameters K_I, K_{II} and K_{III} for different types of loadings (mechanical, thermal) in metal components and structures".

The benchmark study was initiated due to the growing need for an efficient and effective tool that can be used in the evaluation of the harmfulness of a nuclear component or structure. This growing need is inherent to the fact that many nuclear power plants in many countries are reaching the end of their design lifetimes, and these lifetimes have already been or will be extended in the near future. With these extensions, the probability of detecting a flaw or planar crack in components and structures increases. As most of the components of the primary circuit or secondary circuit are not easily replaceable, tools that can estimate the harmfulness of flaws must be available and easy to use for any component and crack(s) geometry. In this context, the eXtended Finite Element Method (X-FEM) may be a useful tool.

Until recently, the use of X-FEM has been limited in fracture mechanics analysis in the nuclear industry. X-FEM has only been implemented in a few commercial and research codes. A general technical introduction to the X-FEM technology implemented in these codes is provided in Section 1. The benchmark objective is to compare X-FEM results (the stress intensity factors K_I, K_{II} and K_{III}) obtained by these different codes and by different participants on a few predefined and mostly straightforward exercises under tension, bending or thermal transient loadings. Furthermore, and even more importantly, the purpose is to identify good practices and limits in the use of X-FEM.

Annex G lists the participants and includes information on their organisations. In total, 18 organisations from 9 countries in Asia, Europe and North America participated in this benchmark. Participants included technical support organisations (TSOs), research centres as well as licensee (support) organisations and nuclear industry organisations.

The X-FEM results on the benchmark are divided into three main cases: cases A (A1, A2 and A3), B and C (C1). These results are summarised in Section 2 of this report. Another benchmark case (C2) was defined; however, the results are not summarised in this report as only a small number of participants reported results and these results varied greatly from one participant to the next. The case C2, which is the most complex, could possibly be kept for a future second stage of the project, if there is still sufficient interest.

In Section 2, the participant results are also compared to the corresponding reference solutions. The tables and graphs provided show that the X-FEM results are on average compatible with the reference solutions. The excessively large deviations that may have been observed were not directly related to X-FEM but rather to modelling issues. For example, incorrect boundary conditions and/or incorrect loading applications, in some cases, led to inadequate shear stresses and thermo-mechanical stress distributions acting on the crack.

Section 3 summarises the good practices and the limits of the X-FEM technology as experienced by the participants. Much attention has been paid to mesh effect on X-FEM results. The effect of element size, element order, mesh homogeneity and meshing methodology on the accuracy of the X-FEM results has been described. Also, the effect of the stress intensity factor calculation method on the convergence of the X-FEM calculations has been investigated.

The following good practices on X-FEM use in fracture mechanics were identified from these benchmark analyses:

- First, the general good practices of FEM still need to be applied in modelling geometry and loading specificities.
- A mesh size of $1/10^{th}$ or $1/20^{th}$ of the smallest crack dimension is recommended around the crack tip.
- A homogeneous mesh size on the crack front is recommended.
- The results along the whole crack front are overall more accurate with a quadratic mesh than with a linear mesh; the linear mesh can cause oscillations of the calculated solution around the reference solution. The oscillation may nevertheless be alleviated by using a mesh size smaller than $1/10^{th}$ of crack depth.
- Refining the mesh solely around the crack tip is recommended to avoid large models that are computationally too demanding. To that purpose, the availability of automatic local meshing tools should be systematised in codes to avoid modelling manually, which is too time-consuming. This enhances the application of the benefits of X-FEM.
- When using the integration method to determine stress intensity factors, it is recommended that care be taken – as for conventional FEM – to obtain the solution convergence, which depends on the defined contours. To reach convergence, a more refined mesh at the crack area may be required than with conventional FEM.
- When the convergence of stress intensity factors obtained by the integration method is not obtained on a given model, the displacement method can be a successful alternative to provide good accuracy with the same model.

Similarly, some limits of X-FEM, such as currently implemented in research and industrial codes for fracture analysis, were identified during this benchmark. These are listed below:

- There is a restricted number of element types for X-FEM in several codes.
- The modelling of cracks on symmetric planes is not possible.
- The application of X-FEM on a crack between two different materials is not possible.
- Extensive computer resources are required when no care is taken for limiting model size. Indeed, the degree of freedom greatly increases for enriched nodes.
- A displacement method to estimate stress intensity factors from X-FEM calculation is not available in all codes.

In conclusion, the results of the academic benchmark cases confirm that X-FEM is an efficient alternative tool for fracture analyses compared to conventional methods for simple fracture analysis cases. In an industrial context, and for complex structural applications that are almost impossible to study with conventional FEM, X-FEM may also be a good alternative. However, in some codes, developments appear necessary to improve the modelling efficiency in order to take full advantage of the use of X-FEM compared to the conventional FEM (e.g. computation time-saving, crack meshing possibilities).

1. Project identification

1.1. Framework

The CSNI has initiated several working groups that periodically meet in order to discuss common issues, operating experience, research programmes, regulations and joint undertakings[1].

The idea for the joint project under consideration here on the topic of "Benchmark analysis on the eXtended Finite Element Method (X-FEM) calculation technology in its use to evaluate the fracture mechanics stress intensity parameters K_I, K_{II} and K_{III} for different types of loadings (mechanical, thermal) in metal components and structures", was launched during the annual meeting of the Working Group for Integrity and Ageing of Components and Structures (WGIAGE) (metals subgroup). It can be considered as a follow-up activity of the finalised WGIAGE activity that provided the published CSNI report "Benchmark Results on the Analytical Evaluation of the Fracture Mechanic Parameters K and J" (NEA, 2017).

1.2. Context

With the lifetime extension of nuclear power plants, the probability of detecting a flaw or planar crack in components and structures increases. As most of the components of the primary circuit or secondary circuit are not easily replaceable, tools that can estimate the harmfulness of flaws must be available and easy to use, whatever the geometry of the component and whatever the geometry of the crack. Existing analytical formulas are mostly only developed for structures and cracks with simple geometry, and are not always easy to apply. In that frame, the eXtended Finite Element Method may be a useful tool.

X-FEM is a method that enriches the standard finite element method to take into account the presence of a discontinuity or a singularity, such as a crack in a structure, without requiring a special mesh that is often very time-consuming to develop. The simplicity of meshing also makes it possible to model a crack in complex structures (nozzle welding) and to model the propagation of a crack without re-meshing. Hence, X-FEM represents a good alternative when no analytical solutions are available or when more realistic models are needed to obtain results which fulfil the regulatory requirements.

X-FEM was developed in the 1990s and makes use of the assumption that the displacement field of a crack can be divided into three main parts (Belytschko and Black, 1999):

1. The part from the standard Finite Element.
2. The part from the enrichment to describe the discontinuity, i.e. the crack tips (enrichment with Heaviside function).
3. The part from the enrichment to describe the singularity to approximate the behaviour at the crack tip (an asymptotic displacement).

1. Joint undertakings that need follow-up are usually treated in so-called CSNI Activity Proposal Sheets (CAPS) or joint projects.

Figure 1.1. Circled nodes are enriched with the Heaviside function while squared nodes are enriched by tip functions

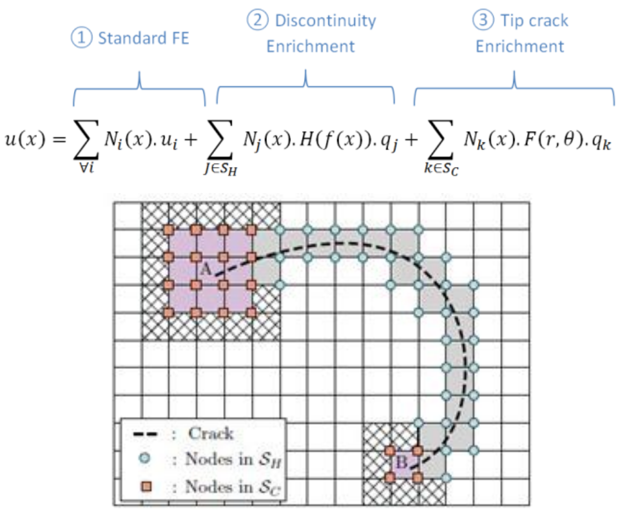

Until recently, the use of X-FEM has been limited in fracture mechanics analysis in the nuclear industry. The wider use of X-FEM enables quicker results for decision making on issues of safety significance. Nevertheless, due to its quite recent implementation in calculation codes, one needs to gain experience in its use and confidence in its capability to assess the structural integrity of primary or secondary components.

X-FEM has been implemented in different commercial codes (ABAQUS, ANSYS, SYSTUS, LMS SAMCEF, VIRFAC Crack, etc.) and in research codes (CODE_ASTER, CAST3M, etc.). It would be interesting to compare the X-FEM results and capabilities of these different codes. It is in that framework that the current X-FEM benchmark was launched in the WGIAGE metal workgroup.

The expected users of the results of this benchmark are the utilities and TSOs. The results may be used in their evaluations of the harmfulness of cracks detected on components that cannot be removed.

This project will provide an opportunity for staff members in the participating organisations to learn how to apply X-FEM in fracture mechanics analyses to predict margins against crack failure.

1.3. Project description

To enable a comparison of the X-FEM capabilities of the codes used in the nuclear industry, the current benchmark proposes that each participating member perform a few predefined benchmark analyses with the X-FEM code which is normally used in the organisation of the participating member. Three rather basic benchmark exercises are proposed in the project with a straightforward analytical solution. These exercises can be found in Section 2 of this report. Currently, the scope is limited to the evaluation of the KI parameter. In a later stage of the project, more complex benchmark analyses and other fracture mechanics parameters can be considered, in order to challenge the capabilities of the FEM/X-FEM codes.

The first stage of the project consisted of refining the proposed benchmark exercises according to the wishes of all participating members, or defining additional basic exercises.

In the second stage of the project, each member performed the necessary calculations in order to obtain the results demanded in each defined benchmark problem.

The final expected output of each participating member of this second stage of the project was a Summary Report which included at least the following elements:

- A short description of the code used.
- The methodology used to obtain the requested results. It should contain the following information:
  - meshing methodology (in particular mesh refinement criteria around the crack);
  - number of elements;
  - type of elements;
  - refined mesh around the crack: type, size, etc.;
  - K_I calculation method;
  - problems encountered during modelling or calculation (e.g. modifications required to obtain a converged solution towards analytical results).
- Overview of the results obtained. It was asked that at least the following results be included in the report:
  - the numerical integration scheme of X-FEM;
  - an overview of the mesh;
  - a view of the crack mesh;
  - an Excel file given the displacements, normal stress, normal strain and K_I at the crack front as a function of the position along the crack front;
  - a graph illustrating the evolution of K_I along the crack front using conventional FEM techniques, if available;
  - a graph illustrating the evolution of K_I along the crack front using X-FEM;
  - the comparison of the X-FEM results to the analytical solutions.

1.4. Project objectives

The principal objectives of the project are the following:

- To compare K_I obtained by the classical FEM, i.e. with a fine mesh of crack tip, or obtained with analytical formulas (like those in RSE-M code) to K_I obtained by X-FEM.
- To identify and summarise the limitations of X-FEM: mechanical behaviour (elastic, plastic...), loadings (mechanical, thermal...).
- To identify and summarise good practices in the use of X-FEM: size of meshing, type of mesh….

2. Benchmark exercises: definition and results intercomparison

2.1. Benchmark A: Semi-elliptical surface flaw in a plate

2.1.1. Definition

Geometry

Figure 2.1. Semi-elliptical surface crack in a plane

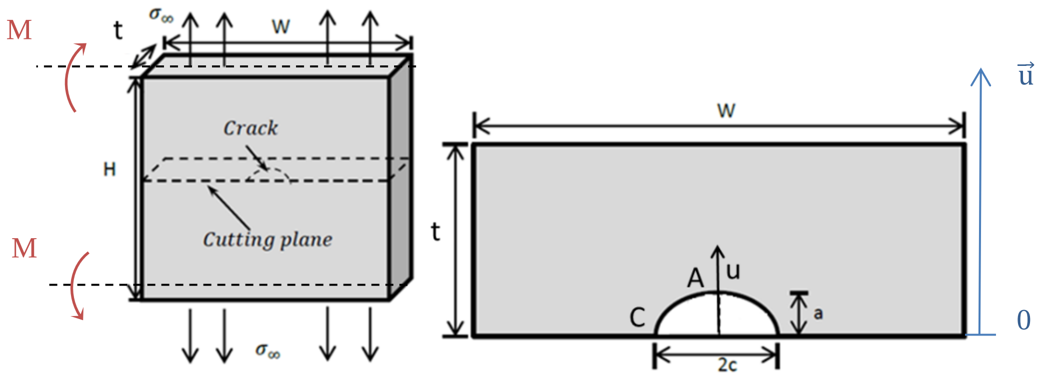

Note: H = 2 m ; W = 2 m ; t = 0.1 m ; a = 0.01 m ; 2c = 0.04 m. The cutting plane is at half height of the structure (H/2).

Modelling type

A 3D model is requested. The choice of the type of element used, linear or quadratic, is left to the discretion of the participant. This choice depends mainly on the available X-FEM elements in the software used.

Material properties

The material behaviour is postulated linear elastic. The mechanical properties are those given in Annex A for ferritic steel at 20°C except for the thermal loading case, where they are considered as temperature dependent.

Boundary conditions

Despite the symmetry of the problem (Figure 2.1), a complete model of the structure is suggested in a first use of the X-FEM crack modelling. Quarter or half models might be also considered in a second approach.

Figure 2.2. Definition of plane A, points P and R

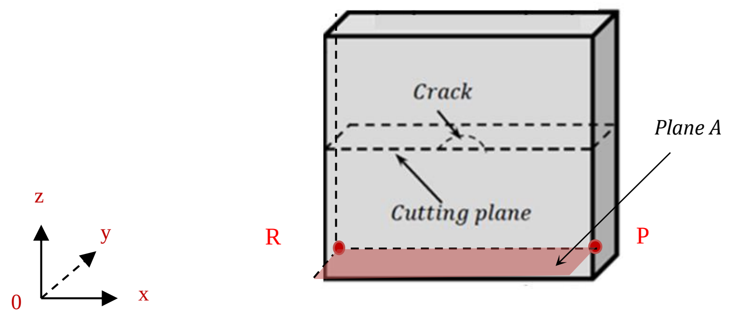

Note: Plane A: Uz = 0; Point P: Ux, Uy= 0; Point R: Uy = 0; where Ux, Uy, Uz are the displacements respectively according to x, y and z.

Reference solution

The reference solution of the stress intensity factor KI given by influence coefficients method (RSE-M code) is:

$$K_I = \sqrt{\pi a} \sum_{j=0}^{3} \sigma_j \, i_j \left(\frac{a}{L}\right)^j$$

where σ_i are the polynomial coefficients of the approximated normal stress (σ_n) to the crack plane:

$$\sigma_n(u) = \sum_{j=0}^{3} \sigma_j \left(\frac{u}{L}\right)^j$$

and L = t and u as defined on Figure 2.1.

The influence coefficients extracted from RSE-M Appendix 5.4 are given in the Table 2.1.

Table 2.1. Influence coefficients for case A at the surface and deepest points

a/c='0.5' and a/t=0.1	i_0	i_1	i_2	i_3
Point A	0.884	0.567	0.449	0.383
Point C	0.712	0.113	4.05E-2	2.05E-2

For a membrane load or a bending load, the solution can be determined by directly using the previous equations if the load is well known. The solution is unique. For the loading cases A1 and A2 defined in Loading cases, the solutions are the following:

Table 2.2. Intensity parameter K_I for cases A1 and A2 at deepest and surface points.

K_I	Case A1	Case A2
	Membrane stresses	Bending stresses
Point A (deepest point)	31.34	27.32
Point C (surface point)	25.24	24.44

In the case of thermal transients, which are usually encountered on the components of nuclear reactors, a bending moment-type loading is generated. To calculate the reference solution, it is first necessary to define the normal stress profile in the crack section of the sound structure. This should be evaluated by each participant to avoid introducing deviation at this step (see details in Case A 3: thermal transient 1).

Loading cases

Case A1: Membrane load

$\sigma_\infty = 200$ MPa

Case A2: Bending load

$\sigma_\infty = 200\ [1 - (2u)/t]$ MPa with u and t as defined on Figure 3.1.

Case A3: Thermal transient 1

- The material properties are temperature dependent.
- Strain free condition assumed to be at 150°C.
- Initial state: homogeneous temperature at 150°C.
- Thermal transient applied as shown on Figure 2.3. The temperature varies linearly from 150°C to 20°C in 60 s and remains constant (at 20°C) from 60 s to 600 s.

Figure 2.3. Zone of application of the thermal transient

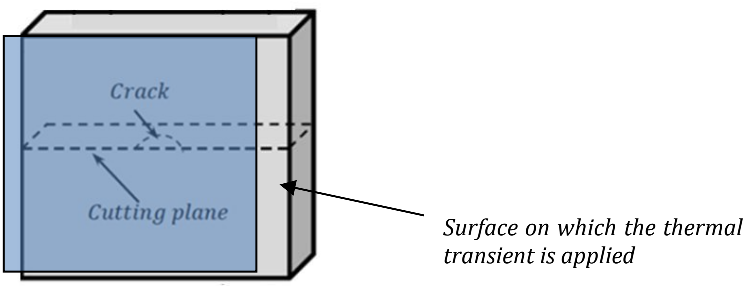

- Thermal exchange coefficient: 20 000 W/m²/°C.
- No heat exchange at the other surfaces (adiabatic conditions).

2.1.2. Results

The difference between the X-FEM solution ($\mathrm{Sol}_{\mathrm{X-FEM}}$) and the reference solution $\mathrm{Sol}_{\mathrm{REF}}$) is evaluated according to the following equation:

$$\mathrm{Diff} = \frac{\mathrm{Sol}_{\mathrm{X-FEM}} - \mathrm{Sol}_{\mathrm{REF}}}{\mathrm{Sol}_{\mathrm{REF}}}$$

Case A1: Uniaxial tension

For a mesh size in the vicinity of the crack between a/33 and 2a/3, the X-FEM solution is quite close to the reference solution (Table 2.3). As seen in Table , the difference between the X-FEM solution and the reference solution is 2% ± 4% at the deepest point, and 3% ± 7% at the surface points. The difference with the reference solution is slightly higher at the surface points as can also be observed with standard finite element calculation.

Furthermore, Figure 2.4, which represents differences as a function of mesh size, seems to suggest that the magnitude of the deviation is not correlated to mesh size. Nevertheless, a comparison of the three data sets of roughly the same mesh size, encircled on Figure 2.4, shows that the scatter in deviations is lesser for a mesh size surrounding the crack of a/20 than for higher mesh size of a/10 and a/5.

Annex B includes graphs of KI along the crack front of all the calculations performed by the participants for the benchmark case A1.

Figure 2.4. Case A1 – Difference according mesh size in the vicinity of crack

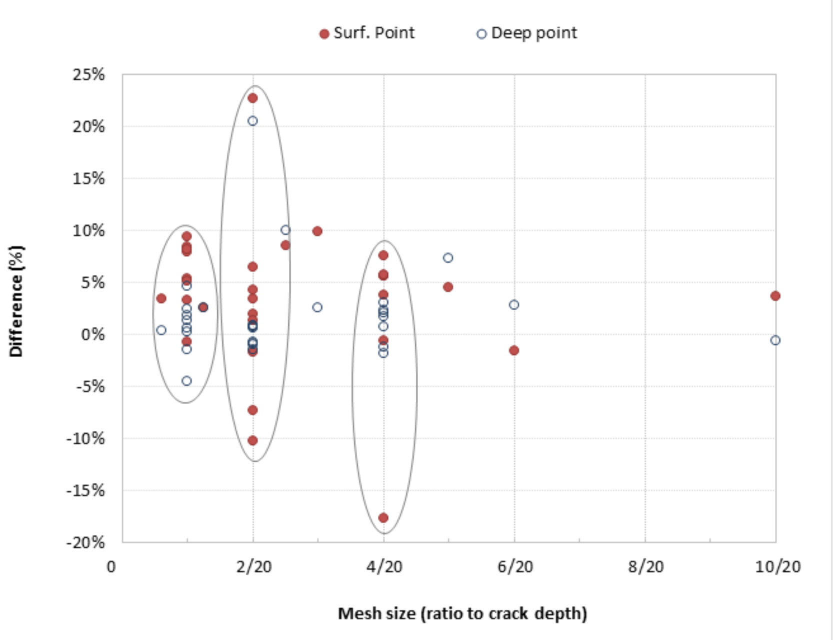

Table 2.3. Case A1 - Deviation with the reference solution for each participant

Participant	Code	Mesh element			SIF calculation method	Difference	
		Order	type	Mesh size (*)		Deep point	Surf. Point
1	Abaqus	Linear	Hexahedral	1/20	Integral	1.4%	5.2%
2	Morfeo crack	Linear	Tetrahedral	1/10	Integral	-0.9%	-2.0%
3	Abaqus	Linear	Hexahedral	1/10	Integral	0.6%	22.7%
	Ansys	Linear	Hexahedral	1/10	Integral	0.7%	-1.7%
4	Code-Aster	Quadratic	Tetrahedral	1/10	Integral	-0.8%	1.3%
				1/20	Integral	0.6%	8.5%
5	Systus	Quadratic	Hexahedral	1/10	integral	0.9%	4.3%
6	Code-Aster	Linear	Tetrahedral	1/20	Integral	-4.5%	-0.7%
		Quadratic	Tetrahedral	1/5	Integral	1.7%	3.8%
				1/10	Integral	-0.9%	3.4%
				1/20	Integral	0.3%	3.3%
				1/20	Integral	1.8%	5.4%
7	Abaqus	Linear	Hexahedral	1/5	Integral	-1.8%	-0.6%
				1/20	Integral	2.4%	9.4%
8	Abaqus	Linear	Hexahedral	1/2	Integral	-0.6%	3.7%
				1/10	Integral	20.5%	6.5%
9	Abaqus	Linear	Hexahedral	1/10	Integral	-1.4%	-10.3%
10	NLXFEM3Dstruct	Linear	Hexahedral	1/10	Integral	-0.7%	-7.3%
11	Abaqus	Linear	Hexahedral	1/5	Integral	3.1%	5.8%
12	Abaqus	Linear	Hexahedral	1/20	Displacement	4.7%	8.0%
13	Abaqus	Linear	hexahedral	1/5	Integral	-1.1%	-17.7%
14	Abaqus	Linear	Hexahedral	1/20	Integral	-1.4%	8.2%
15	Abaqus	Linear	Hexahedral	1/5	Integral	2.2%	5.6%
16	Abaqus	Linear	Hexahedral	1/4	Integral	7.3%	4.6%
				1/8	Integral	10.0%	8.6%
				1/16	Integral	2.6%	2.6%
17	Abaqus	Linear	Hexahedral	1/33	Integral	0.4%	3.5%
18	Abaqus	Linear	Hexahedral	1/5	Integral	0.8%	5.6%
				3/10	Integral	2.8%	-1.6%
				3/20	Integral	2.6%	9.9%
				1/5	Integral	2.3%	7.5%

Note: (*) Mesh size in the crack area (ratio to crack depth).

Table 2.4. Case A1 – Mean and standard deviation of the differences between X-FEM and reference solutions

Difference	Deep point	Surface point
Min	-5%	-18%
Max	20%	23%
Mean	2%	3%
Standard deviation	4%	7%

Case A2: Bending load

Overall, for a mesh size in the vicinity of the crack between a/33 and 2a/3, the X-FEM solution is quite close to the reference solution (Table 2.6). As seen in Table 2.6, the difference between the X-FEM solution and the reference solution is 1% ± 6% at the deepest point, and 1% ± 7% at the surface points. The difference with reference solution is similar at the surface points and at the deepest point.

In Figure 2.5, it can be observed that the deviation between the X-FEM solution and the reference solution does not increase significantly if the mesh size surrounding the crack is increased from a/20 to a/5.

As for case A1 (see Figure 2.4), it can be observed for the data sets of same size circled on Figure 2.5 that the deviation scattering is smaller for mesh sizes surrounding the crack of a/20 than for higher mesh sizes of a/10 and a/5.

Annex C includes graphs of KI along the crack front of all the calculations performed by the participants for the benchmark case A2.

Figure 2.5. Case A2 – Difference according mesh size in the vicinity of crack

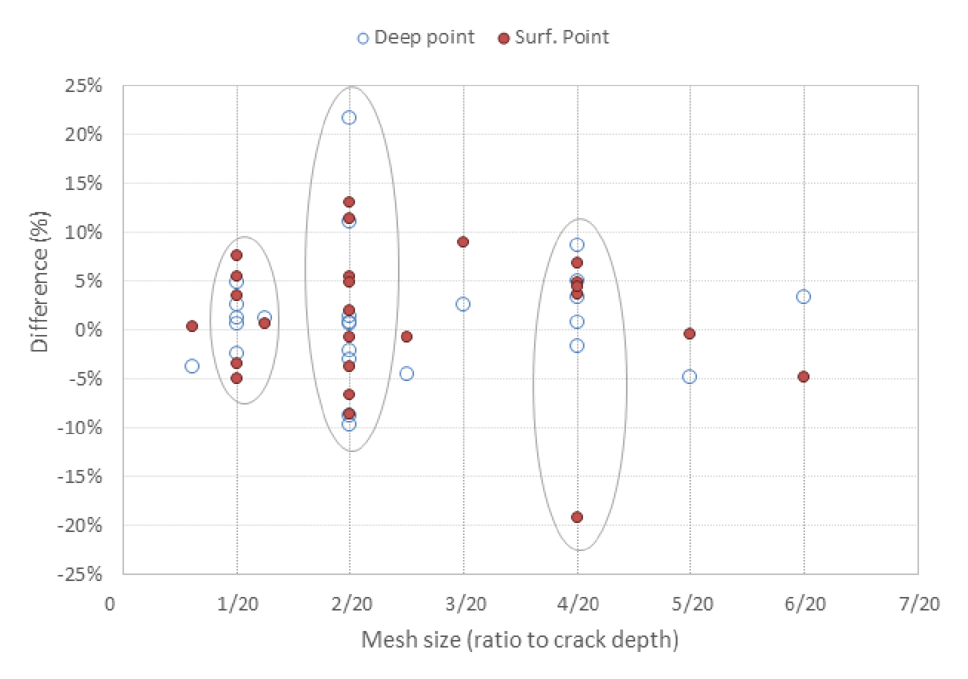

Table 2.5. Case A2 - Deviation with the reference solution for each participant

Participant	Code	Mesh element			SIF calculation method	Difference	
		Order	type	Mesh size (*)		Deep point	Surf. Point
1	Abaqus	Linear	Hexahedral	1/20	Integral	1.3%	5.5%
2	Morfeo crack	Quadratic	Tetrahedral	1/10	Integral	-0.7%	-2.0%
3	Abaqus	Linear	Hexahedral	1/10	Integral	-9.7%	13.1%
	Ansys	Linear	Hexahedral	1/10	Integral	-8.7%	-3.8%
4	Code_Aster	Quadratic	Tetrahedral	1/10	Integral	-2.1%	-0.7%
				1/20	Integral	0.7%	-3.4%
5	Systus	Quadratic	Hexahedral	1/10	Integral	0.8%	5.5%
6	Code_Aster	quadratic	Hexahedral	1/20	Integral	2.7%	3.6%
7	Abaqus	Linear	Hexahedral	1/5	Integral	3.4%	6.9%
				1/10	Integral	11.1%	11.4%
8	Abaqus	Linear	Hexahedral	1/2	Integral	0.1%	2.1%
				1/10	Integral	21.8%	4.9%
9	Abaqus	Linear	Hexahedral	1/10	Integral	1.4%	-6.6%
10	NLXFEM3Dstruct	Linear	Hexahedral	1/10	Integral	-2.9%	-8.6%
11	Abaqus	Linear	Hexahedral	1/5	Integral	5.0%	4.5%
12	Abaqus	Linear	Hexahedral	1/20	Displacement	4.9%	-4.9%
13	Abaqus	Linear	Hexahedral	1/5	Integral	8.7%	-19.2%
14	Abaqus	Linear	Hexahedral	1/20	Integral	-2.4%	7.6%
15	Abaqus	Linear	Hexahedral	1/5	Integral	-1.6%	3.7%
16	Abaqus	Linear	Hexahedral	1/4	Integral	-4.8%	-0.4%
				1/8	Integral	-4.5%	-0.7%
				1/16	Integral	1.2%	0.7%
17	Abaqus	Linear	Hexahedral	1/33	Integral	-3.7%	0.4%
18	Abaqus	Linear	Hexahedral	1/5	Integral	0.7%	5.0%
				3/10		3.3%	-4.8%
				3/20		2.7%	9.0%

Note: (*) Mesh size in the crack area (ratio to crack depth).

Table 2.6. Case A2 – Mean and standard deviation of the difference between X-FEM and reference solutions

Difference	Deep point	Surface point
Min	-10%	-19%
Max	22%	13%
Mean	1%	1%
Standard deviation	6%	7%

Case A3: Thermal transient

Participants were asked to provide:

- the K_I evolution at crack tip as a function of time;
- the K_I evolution on the crack front at t=120 s.

In order to determine the reference solution as described in Reference solution" at the beginning of Section 2, and finally the deviation induced solely by the X-FEM calculation method, participants were also asked to provide the normal stress distribution they obtained in the sound structure under the thermal transient, in the section where the defect would be located. Following the approach defined in "Reference solution", the stress distribution was then expressed as a polynomial of third order.

Hence, the difference between the X-FEM solution and the reference solution was calculated by considering the most relevant stress profile. The objective was to rule out differences induced by thermo-mechanical calculation itself. This calculation is more complex and requires two steps. First, a thermal calculation must be performed to determine the temperature field in the structure and then the temperature field must be projected onto the mesh on which the mechanical calculation is performed. Different projection algorithms can be used. Second, the mechanical stresses generated by the temperature field are determined.

In addition, differences may arise from one code to another depending on whether or not an initial thermal deformation of the structure has been implemented in the codes.

Thermal deformation is proportional to the difference between the temperature T and the reference temperature T_{ref}, defined as the temperature at which the structure is assumed to be free of deformation of thermal origin or by misuse of language free of stress of thermal origin. This is expressed as follows:

$$\varepsilon^{th} =\cdot \overline{\alpha}(\mathrm{T}) \cdot (\mathrm{T} - \mathrm{T_{ref}})$$

with $\overline{\alpha}(T)$ the thermal expansion coefficient between the temperatures T and T_{ref} $\overline{\alpha}(T)$ is deduced from the thermal expansion coefficient α defined experimentally between the temperature T and the definition temperature, T_{def} (20°C in the present benchmark). In general, $\overline{\alpha}(T)$ is calculated automatically in codes after entering α(T), T_{def} and T_{ref}, from the expression given below.

$$\overline{\alpha}(\mathrm{T}) = \frac{\alpha(\mathrm{T}) \cdot (\mathrm{T} - \mathrm{T_{def}}) - \alpha(\mathrm{T_{ref}}) \cdot (\mathrm{T_{ref}} - \mathrm{T_{def}})}{(\mathrm{T} - \mathrm{T_{ref}})}$$

Case A3 appeared more difficult to perform by participants due to the complexity of the loading.

Table 2.7 presents the deviation of the X-FEM solution with the reference solution for each participant. Among results from 13 participants for which it was possible to calculate the deviation from the reference solution, the X-FEM solution is quite close to the reference solution on average but with a slightly increased standard deviation. As seen in Table 2.8, the difference between the X-FEM solution and the reference solution is -1 % ± 8 % at the deepest point, and -3% ± 8 % at the surface points.

Refining the mesh does not seem to improve the accuracy of the X-FEM solution as observed on Figure 2.6.

Annex D includes graphs of KI along the crack front of all the calculations performed by the participants for the benchmark case A3.

Figure 2.6. Case A3 – Differences according mesh size in the vicinity of crack

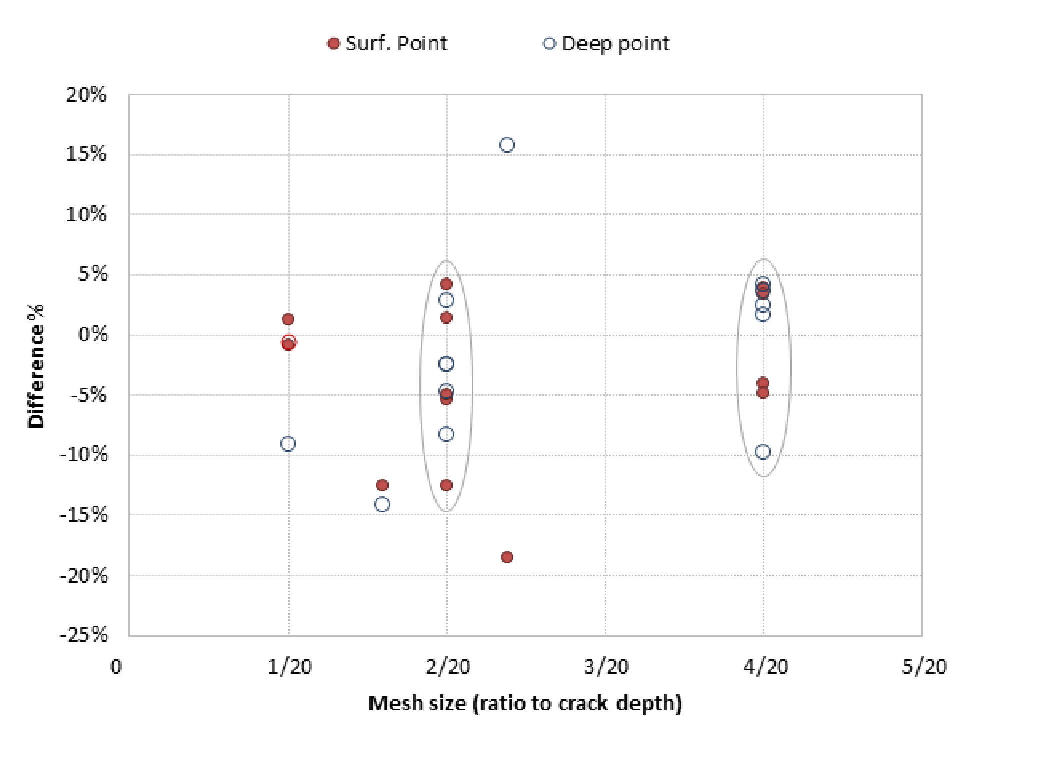

Table 2.7. Case A3 - Deviation with the reference solution for each participant

Particip.	Code	Mesh element			SIF calculation method	Difference		Remarks
		Order	type	Mesh size (*)		Deep point	Surf. Point	
1	Abaqus	No X-FEM result for benchmark A3						
2	Morfeo/Crack	Quadratic	Tetrahedral	1/10	Integral	-4.7%	-5.4%	
3	Ansys	Linear	Hexahedral	1/10	Integral	4.1%	7.8%	Results strongly dependent on integration contour
4	Code_Aster	Quadratic	Tetrahedral	1/5	Displacement	3.6%	3.9%	Gtheta method did not provide accurate SIF according to Code_Aster criteria
				1/10	Displacement	-2.5%	4.2%	
5	Systus	Quadratic	Hexahedral	1/10	Integral	-2.5%	1.4%	
6	Code_Aster	Quadratic	Hexahedral	1/20	Integral	-0.6%	-0.8%	Differences were estimated with the conventionnal FEM solution calculated by participant 6
7	Abaqus	Linear	Hexahedral	1/10	Integral	-	-	Reference solution not estimated as normal stress evolution not transmitted
8	Abaqus	Linear	Hexahedral	1/2	Integral	-9.8%	-4.0%	Results strongly dependent on integration contour. Differences given for contour 4
				1/6 to 1/14	Integral	15.8%	-18.6%	
9	Abaqus	Linear	Hexahedral	1/10	Integral	2.9%	-12.5%	
10	NLXFEM3Dheat NLXFEM3Dstruct	Linear	Hexahedral	1/10	Integral	-8.3%	-5.0%	
11	Abaqus	Linear	Hexahedral	1/5	integral	4.2%	-4.8%	Results at 60s
12	Abaqus	Linear	Hexahedral	1/20	Displacement	-9.0%	1.3%	
13	Abaqus	Linear	Hexahedral	1/5	Integral	High	High	Results far from the expected results
14	Abaqus	Linear	Hexahedral	2/25	Integral	-14.2%	-12.5%	KI strongly dependent of the integration field
15	Abaqus	Linear	Hexahedral	1/5	Integral	1.6%	-	
16	Abaqus	Linear	Hexahedral	1/4 to 1/8	Integral	-	-	Reference solution not estimated as normal stress evolution not transmitted
17	Abaqus	Linear	Hexahedral	-	Integral	High	High	Results have been discarded by the participant as too far from the reference solution
18	Abaqus	Linear	Hexahedral	1/5	Integral	2.4% (**)	3.4% (**)	KI strongly dependent of the integration contour. The convergence of solution is not obtained. Difference evaluated with an average value of the solutions on selected integration contours as proposed by participant 18.

Note: (*) Mesh size in the crack area (ratio to crack depth).
(**) Differences obtained for KI on contour 3 are 28.8% and 16.1% for the deep and surface points respectively.

Table 2.8. Case A3 – Mean and standard deviation of the differences between X-FEM and reference solutions on available results

Difference	Deep point	Surface point
Min	-14%	-19%
Max	16%	8%
Mean	-1%	-3%
Standard deviation	8%	8%

2.2. Benchmark B: Embedded elliptical crack in a plate submitted to shear load

2.2.1. Definition

Geometry

Figure 2.7. Crack in a plate submitted to shear load

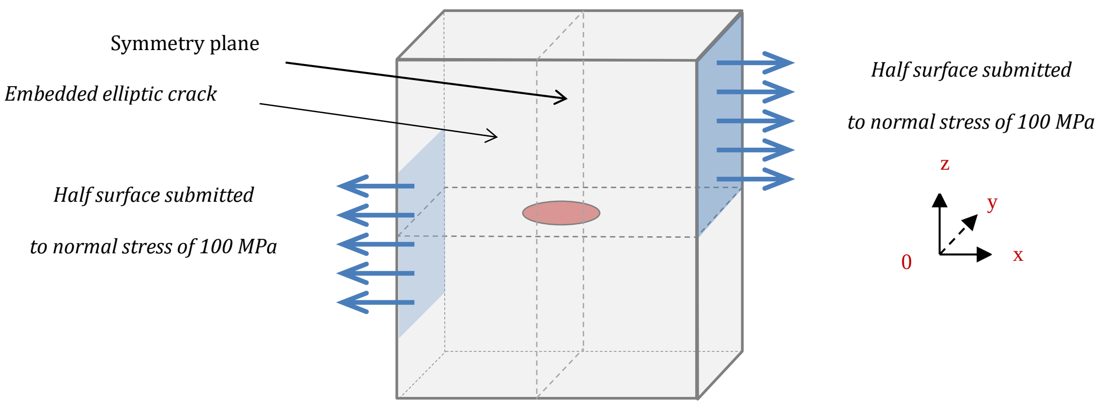

Note: The plate is the same size as the one shown on Figure 2.1 (identical to those of the case A): Thickness (t) = 0.1 m, Height (H) = 2 m, Width (W) = 2 m. The crack dimensions are the following: 2a = 0.01 m, 2c = 0.04m. The cutting plane is at half height of the structure (H/2).

Model

The model is tridimensional.

Material properties

The material behaviour is considered linear elastic. The mechanical properties are those of the ferritic steel at 20°C given in Annex A.

Boundary conditions

Figure 2.8. Definition of plane A, points P and R

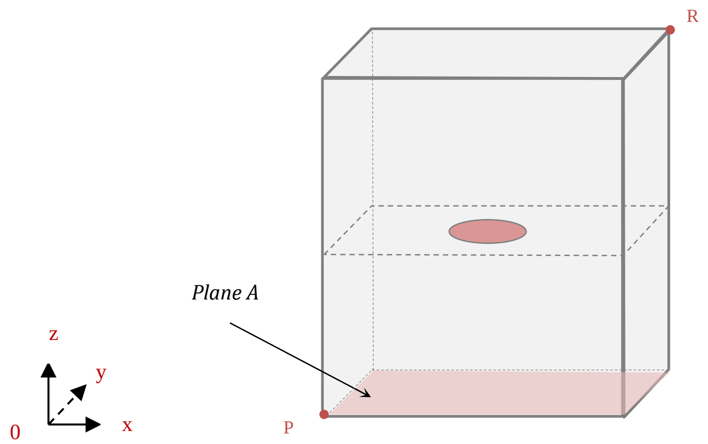

Note: Plane A: Uz = 0. Point P: Ux, Uy= 0. Point R: Uy = 0. Where Ux, Uy, Uz are the displacements respectively according to x, y and z.

Loading

A shear stress τ is induced in the crack plane by a normal stress of 100 MPa applied to the plate as shown in Figure 2.7 τ must be determined beforehand by the finite element method in the loaded structure without cracks. Its value in the area where the crack would be is 57.5 MPa.

Reference solution

Figure 2.9. Point A on the crack front

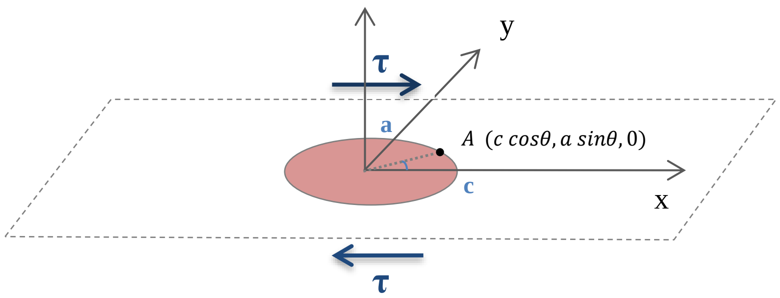

The stress intensity factors at a point A of the crack front, defined on Figure 2.9, is given by the Handbook Tada-Paris-Irwin Third Edition and recalled below (Tada et al., 2000).

$$K_{IIA} = \frac{\tau \cdot \sqrt{\pi a} \cdot k^2}{\left[sin^2\theta + \left(\frac{a}{c}\right)^2 cos^2\theta\right]^{1/4}} \left(\frac{k'}{B} \; cos\theta\right)$$

$$K_{IIIA} = -\frac{\tau \cdot \sqrt{\pi a} \cdot (1-\mathcal{V}) \cdot k^2}{\left[sin^2\theta + \left(\frac{a}{c}\right)^2 cos^2\theta\right]^{1/4}} \left(\frac{1}{B} \; sin\theta\right)$$

Where:

$$B = (k^2 - \mathcal{V})\, E(k) + \; \mathcal{V} \quad \frac{a^2}{c^2}\, K(k)$$

$$C = \left(k^2 + \mathcal{V}\, \frac{a^2}{c^2}\right) \cdot \; E(k) - \; \mathcal{V} \quad \frac{a^2}{c^2}\, K(k)$$

With:

$$k^2 = 1 - \left(\frac{a}{c}\right)^2, \quad k' = \frac{a}{c}$$

$$K(k) = \int_0^{\pi/2} \frac{d\varphi}{\sqrt{1 - k^2 sin^2\varphi}}$$

$$E(k) = \int_0^{\pi/2} \sqrt{1 - k^2 sin^2\varphi} \quad d\varphi$$

From Figure 2.10, it can be observed that the obtained K_{II} and K_{III} solutions are very close to the ones obtained by conventional FEM solutions by participants 3 and 6.

Figure 2.10. Comparison of the finite element solution with the theoretical solution

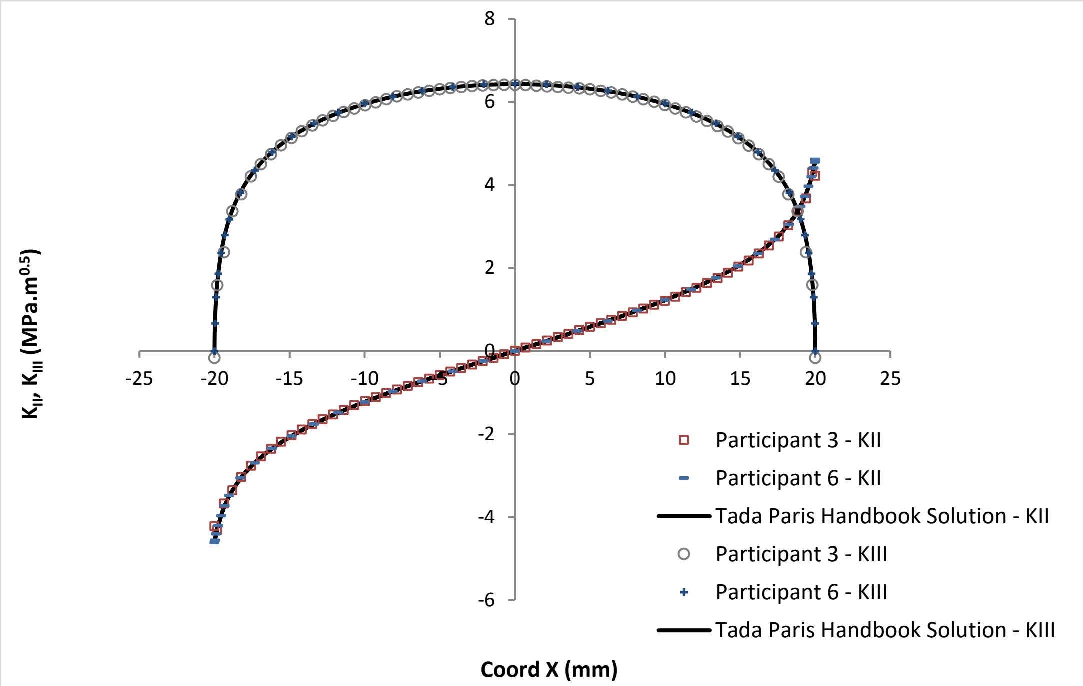

2.2.2. Results

Table 2.9 shows the relative deviations of the participant X-FEM results with respect to the reference solution determined according to the equations in Figure 2.9.

The values for the stress intensity factor of the 1st mode K_I have not been tabulated, as they can be neglected with respect to the K_{II} and K_{III} values.

For the stress intensity factor of the 2nd mode K_{II}, the relative difference of the participant X-FEM results with respect to the reference solution is only reported at the surface points at x = -20 mm and x = +20 mm, because the relative deviation at the deep point of the crack is theoretically infinite using the equation given in 2.1.2 (K_{II} at the deep point is 0 MPa $m^{1/2}$). For the sake of simplicity, the average of the differences at the surface points (positions x = -20 mm and x = +20 mm) is reported in Table 2.9.

For the stress intensity factor for the 3 rd mode K_{III}, the relative difference of the participant result with respect to the reference solution is only reported at the deep point of the crack, because the relative deviation at the surface points of the crack are theoretically infinite using the equation in 2.1.2 (K_{III} at the surface points is 0 MPa $m^{1/2}$).

It can be observed that, in general, the deviations with respect to the reference solution are higher for benchmark B than for benchmarks A1, A2 and A3. The more complex loading may explain this observation.

From Table 2.10, it can be seen that the mean difference between the X-FEM results and the reference solution is 3% ± 26% at the surface points for K_{II}, and 5% ± 17% at the deep point for K_{III}.

It was observed that excessively large deviations were obtained by participant 3 with ANSYS and by participant 10 with NLXFEM3DStruct. These had a significant impact on the mean and standard deviation given in Table 2.10 but they may not be attributed to X-FEM. Indeed, no excessive deviation was observed on the X-FEM calculations performed with ANSYS or NLXFEM3DStruct for cases A1 and A2 also concerning mechanical loading. For these cases, the accuracy of the X-FEM results is overall lower or equal than 10% in absolute value (see Table 2.3 and Table 2.5). For these reasons, the mean and standard deviation of the differences – without taking into account theses highest values – are also represented in Table 2.11. They are -2%±14% at the surface point for K_{II} and 2%±8% at the deep point for K_{III}.

For the K_{II} values at the surface points, the relative significant deviations with respect to the reference solution can in some cases also be explained by the fact that the gradient of the evolution of K_{II} with respect to the position x is large at these locations. A small increase in the position x near to the surface points leads to a significantly different K_{II} value. This may have an effect on the evaluation of the relative deviation with respect to the reference solution as tabulated in Table 2.9. After all, it can be observed from the graphs in Annex E that the shapes of the K_{II} graphs as function of x are in many cases compatible with the reference solution, but that the relative significant deviations are just due to the gradient of the K_{II} solution at the extremities. This explanation is not applicable for the relative significant deviations for K_{III} at the deep point, as the gradient of the evolution of K_{III} with respect to the position x is small at that location.

As seen on Figure 2.11, the relation between the deviation of X-FEM results and the mesh size is rather weak. No pronounced relationship between the scatter in X-FEM deviations and the mesh size can be identified as was the case for load cases A1, A2, A3 (smaller scatter in deviations for smallest mesh size).

Table 2.9. Case B – Deviation with the reference solution for each participant

Participant	Code	Mesh element			SIF calculation method	Difference	
						K_{II}	K_{III}
		Order	type	Mesh size (*)		Surf. Point	Deep point
1	Abaqus	No X-FEM result for K_{II} and K_{III} for benchmark B					
2	Morfeo crack	Quadratic	Tetrahedral	1/10	Integral	-32.6%	-16.9%
3	Ansys	Linear	Hexahedral	1/10	Integral	92.9%	64.5%
	Abaqus	Linear	Hexahedral	1/10	Integral	-8.1%	11.7%
4	Code-Aster	Quadratic	Tetrahedral	1/10	Displacement	6.1%	1.6%
5 (**)	Systus	Quadratic	Hexahedral	1/5	Integral	19.2%	-0.2%
6 (***)	Code-Aster	No X-FEM result for KII and KIII for benchmark B					
7	Abaqus	Linear	Hexahedral	1/5	Integral	20.7%	9.6%
		Linear	Hexahedral	2/5	Integral	4.4%	14.3%
8	Abaqus	Linear	Hexahedral	2/5	Integral	-1.9%	20.0%
9	Abaqus	Linear	Hexahedral	1/5	Integral	-12.1%	-1.4%
				1/10	Integral	-1.1%	-2.1%
10 (****)	NLXFEM3Dstruct	Linear	Hexahedral	1/10	Integral	66.5%	14.7%
11	Abaqus	Linear	Hexahedral	1/5	Integral	-8.4%	-1.0%
12	Abaqus	Linear	Hexahedral	1/10	Displacement	-1.2%	-5.2%
13	Abaqus	Linear	Hexahedral	3/50	Integral	2.8%	3.8%
14	Abaqus	Linear	Hexahedral	13/100	Integral	-14.1%	0.5%
15	Abaqus	Linear	Hexahedral	1/10	Integral	-4.2%	-2.6%
16	Abaqus	Linear	Hexahedral	1/50 (non-uniform)	Integral	11.7%	-4.0%
				1/50 (uniform)	Integral	-6.9%	-4.3%
17	Abaqus	Linear	Hexahedral	3/50	Integral	14.5%	-0.4%
18	Abaqus	Linear	Hexahedral	2/5	Integral	-25.2%	6.9%

Notes: (*) Mesh size in the crack area (ratio to crack depth)

(**) A conventional FEM analysis was executed with the following relative differences with respect to the reference solution as described in Figure 2.9: K_{II}, surf. point = 0.5%; K_{III}, deep point = 0.2%

(***) A conventional FEM analysis was executed with the following relative differences with respect to the reference solution: δKII, surf. point = 4% K_{III}, deep point = -1.2%

(****) According participant 10, his X-FEM results is close to his FEM results

Table 2.10. Case B – Mean and standard deviation of the differences between X-FEM and reference solutions

Difference	K_{II}	K_{III}
	Surface point	Deep point
Min	-33%	-17%
Max	93%	65%
Mean	3%	5%
Standard deviation	26%	17%

Table 2.11. Case B – Mean and standard deviation of the differences between X-FEM and reference solutions except the excessively large differences from ANSYS and NLXFEM3DStruct calculations

Difference	K_{II}	K_{III}
	Surface point	Deep point
Min	-33%	-17%
Max	21%	20%
Mean	-2%	2%
Standard deviation	14%	8%

Figure 2.11. Case B – Differences according to mesh size in the vicinity of crack - Except unexplained highest values from ANSYS calculation obtained by participant 3

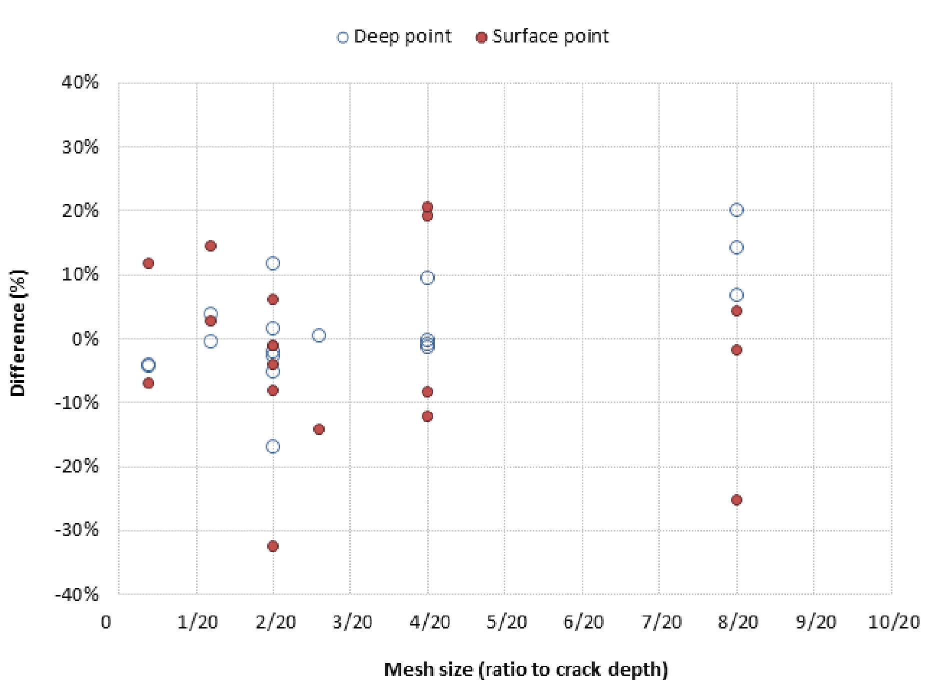

2.3. Benchmark C: semi-elliptical underclad crack in the core shell of a reactor pressure vessel

2.3.1. Definition

Geometry

The structure considered in the current exercise is a cylindrical vessel shell with dimensions as defined in Figure 2.12.

Figure 2.12. Cylindrical vessel shell with an axial underclad crack

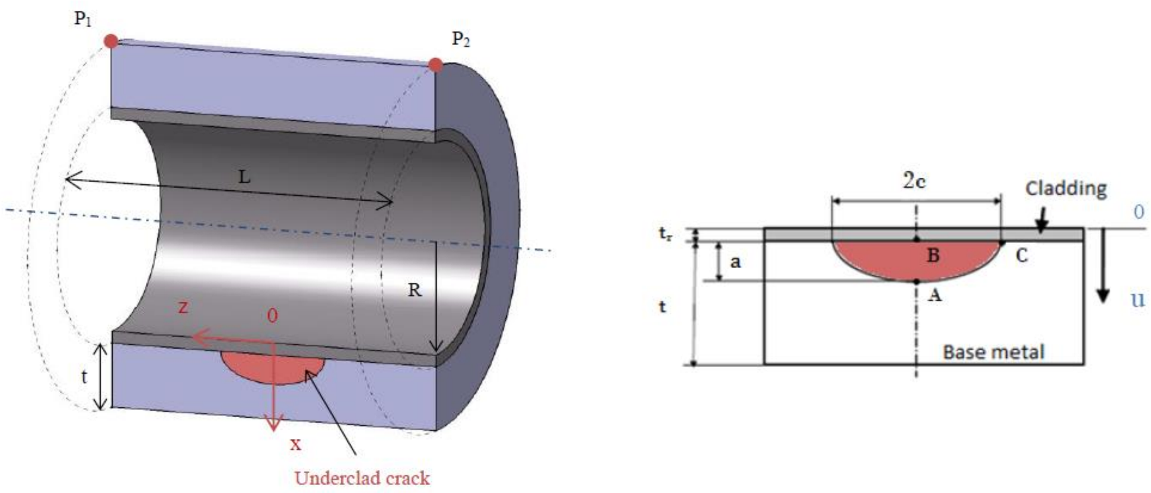

Note: Internal radius R = 2 m ; t = 0.2 m ; a = 0.01 m ; a/c = 1/3; tr = 0.0075 m; L = 2 m. Where t, tr are respectively the base metal and cladding thicknesses.

Model

The model is tridimensional.

Material properties

Two sub-cases will be considered with one optional

C-1) Linear elastic

C-2) Optional - Elasto-plastic (Von Mises with linear kinematic work hardening)

The materials properties retained are given in Table A.1. in Annex A for the stainless steel cladding and in Table A.2. in Annex A for the ferritic steel base metal.

Boundary conditions

For the sake of simplification, the structure is assumed to be strain-free at the initial temperature of the thermal transient. The structure can freely expand.

A half model of the structure is suggested. Other models or boundary conditions are allowed, if these are equivalent to those proposed here.

- Oxz symmetry plane: Uy = 0 (except on the crack surface)
- Ux (P1) = Ux (P2) = 0
- Uz (P1) = 0

Referential stress intensity factor (SIF) solution

An accurate solution can be determined by FEM calculation.

Furthermore, given that the ratio t/R is small, the solution can be approximated by that obtained for an underclad crack in a plate given in RSE-M code:

$$K_I = \left(\sum_{0}^{3} \sigma_j . i_j \cdot \left(\frac{a + t_r}{t + t_r} \right)^j \right) \cdot \sqrt{\pi \cdot a}$$

Where σ_j are the coefficients of the approximated normal stress in the base metal in the form of a polynomial trend curve:

$$\sigma_n(u) = \sum_{j=0}^{3} \sigma_j \left(\frac{u}{t + t_r} \right)^j$$

u: local co-ordinate as defined in Figure 2.12.

And ij are given in Table 2.12.

Table 2.12. Influence coefficients at different points on the crack front

Point	i0	i1	i2	i3
A	0.688	0.587	0.516	0.463
B	0.690	0.397	0.243	0.157
C	0.230	0.109	0.053	0.027

Loading

Two types of loadings were considered for this exercise, so-called C-1 and C-2 detailed below.

C-1) First study

The materials properties are postulated constant, corresponding to the temperature of 289°C (case C-1 in *Material properties*). The loading is a thermal transient equivalent to that induced by a loss-of-coolant accident (LOCA) and applied on the inner surface (see Table 2.13). The outside surface is perfectly insulated (Q=0).

C-2) Second study (optional)

The material properties depend on temperature (case C-2 in *Material properties*). The loading applied in the inner surface is a thermal transient equivalent to that induced by a LOCA (see Figure 2.13 and Table 2.13). The outside surface is perfectly insulated (Q=0). At the initial state, the temperature is homogeneous in the vessel shell. For the sake of simplification, the structure is assumed to be strain-free at 289 °C.

Figure 2.13. LOCA thermal transient

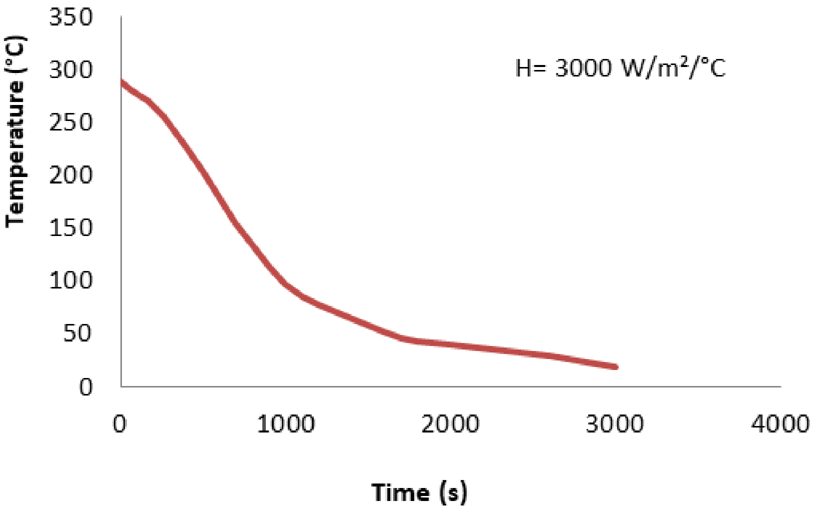

Table 2.13. Thermal transient definition

Time (s)	Fluid temperature (°C)
0	289
60	282
120	275
160	271
200	265
260	255
400	227
500	203
600	179
700	156

Table 2.13. Thermal transient definition (Continued)

Time (s)	Fluid temperature (°C)
800	133
900	114
1 000	98
1 100	85
1 200	78
1 600	52
1 700	47
1 800	43
2 000	40
2 600	30
3 000	20

2.3.2. Results

Case C1

Table 2.14 summarises the difference between the reference solution and the X-FEM solution by each participant for case C1 and comments on difficulties encountered to achieve case C1. As for case A3: thermal transient 1, participants were asked to provide the normal stress in the crack section in order to determine the reference solution for the reasons detailed in Case A3: Thermal transient 1 and then, to determine the difference between this solution and the X-FEM solution.

Of the 18 participants, 12 achieved the X-FEM calculation for case C1.

Two participants (participants 1 and 4) gave up performing case C1 because modelling complex geometry requires special care to partition the geometry to account for loading and geometry specificities. Indeed, the use of X-FEM does not alleviate this constraint. A fine mesh is necessary in the crack area to reach a solution at an acceptable level of accuracy. Without an ad hoc automatic meshing tool, the modelling is too time-consuming when meshing optimisation is sought in view of limiting the model size. In addition, when no precaution is taken for refining mesh solely around the crack zone – as for conventional FEM – the half model becomes very voluminous (in terms of number of nodes or elements), increasing greatly the computing resources needed for the calculation.

The other participants failed to achieve a result consistent with the thermal load applied for reasons unrelated to X-FEM and they discarded their results.

Among the 12 participants who completed case C1, the X-FEM solution is in quite good agreement with the reference solution. The difference between the X-FEM and reference solutions is 6% on average at the deepest point in the base metal, with a standard deviation of 10%; these mean and standard deviations were established excluding the difference determined with non-convergent solutions.

Annex F includes graphs of K_I along the crack front of all the calculations performed by the participants for the benchmark case C1.

Table 2.14. Case C1 – Deviation with the reference solution at the deep point for each participant

Particip.	Code	Mesh element			SIF calculation method	Difference at Deep point	Comments
1	ABAQUS	No X-FEM result for benchmark C1					
2	MORFEO CRACK	Linear (pt C) + Quadra. (pt A - B)	Tetra.	1/10 (Pt A) 1/50 (Pt C)	Integral	5.5%	In order to obtain reasonable calculation times, only a section of 10° (instead of 180°) of the vessel is modelled, with the crack positioned in the centre. Model of 746 000 elements
3	ANSYS	Linear	Hexa.	1/10	Integral	14.1%	Quarter model. K_I strongly dependant on the integration contours (no convergence). Difference estimated by participant 3 from an average value of K_I.
4	CODE_ASTER	No X-FEM result for benchmark C1					Same difficulties for meshing as for conventional crack FEM analysis. In Code_Aster, the methods of calculation of Gtheta and SIF do not correctly estimate the values of G and K at the points at the interface of the base metal and the cladding. The same applies to the X-FEM implemented in Code_Aster => K_I erroneous at points B and C located at the interface of the two materials.
5	SYSTUS	Quadra.	Hexa.	1/10	Integral	2.0%	Half model of 43 400 elements and 134 484 nodes.
6	CODE_ASTER	Quadra.	Hexa.	1/25	Integral	-3.8%	Half model of 140 000 nodes.
7	ABAQUS	No X-FEM result for benchmark C1					For benchmark C, several problems occurred during modelling with ABAQUS 6.14 • It appears, that the X-FEM implementation in ABAQUS won't allow putting the crack plane into a symmetry plane of a model • Also, ABAQUS has problems when two adjacent materials are close to the X-FEM-crack.

Table 2.14. Case C1 – Deviation with the reference solution at the deep point for each participant (Continued)

Particip.	Code	Mesh element			SIF calculation method	Difference at Deep point	Comments
8	ABAQUS	Linear	Hexa.	1/8 to 1/10	Integral	0.2%	Full model. In the X-FEM enrichment zone, only one material can be considered.
				1/10 to 1/20	Integral	0.2%	
9	ABAQUS	Linear	Hexa.	1/10	Integral	-2.6%	
10	NLXTFEM3D heat & struct	Linear	Hexa.	1/20	Integral	-1.1%	Half model of ~403 000 nodes and ~387 000 elements.
11	ABAQUS	Linear	Hexa.	1/5	Integral	20.6%	The analysis was carried out assuming 10% of the original cladding thickness as the base metal, the crack tip is assumed to pass through the base metal.
12	ABAQUS	Linear	Hexa.	1/10	Displac.	15.9%	X-FEM implemented invalid at the interface between the cladding and the base metal. To bypass this problem, 10% of cladding thickness in contact with base metal was changed to base metal. According participant 12, there is little difference in stress gradient including the crack front against the original conditions.
13	ABAQUS	Linear	Hexa.	1/33	Integral	-	Half model of ~174 000 nodes. The reference solution has not been evaluated since the stress distribution was not transmitted.
14	ABAQUS	Linear	Hexa.	1/10	Integral	27.3%	Full model - 10% of cladding thickness in contact with base metal was changed to base metal.
15	ABAQUS	Linear	Hexa.	1/10	Integral	2.8%	
16	ABAQUS	Linear	Hexa.	1/28	Integral	6.5%	Deviation established from the reference solution determined by the participant.
17	ABAQUS	No X-FEM result for benchmark C1					
18	ABAQUS	No X-FEM result for benchmark C1					

(*) Mesh size in the crack area (ratio to crack depth)

Case C2

For the case C2, less than half of the participants reported results, and the problem was experienced as too complex by various participants. Moreover, the results of several participants were varied significantly.

For this reason, the benchmark organisers (IRSN and Bel V) decided to temporarily withdraw the benchmark case C2 from the X-FEM benchmark problem and to base the conclusions on the more straightforward benchmark cases. In a second phase of the project, case C2 and eventually other more complex cases can be considered.

3. Feedback on the participant results and experiences

3.1. General feedback

In total, 18 organisations from 9 countries participated in the benchmark and sent their results to the X-FEM project leaders. These results were produced by 6 X-FEM codes:

- ABAQUS (9 participants);
- CODE_ASTER (2 participants);
- ANSYS (1 participant);
- MORFEO CRACK (1 participant);
- SYSTUS (1 participant);
- NLX-FEM3D (1 participant).

The stress intensity factors calculated with X-FEM can be distinguished into two main groups, those evaluated from the displacement based method and those from the energy based method (G_θ, J-integral).

In order to evaluate the accuracy of the obtained X-FEM solutions, a mix of the following reference solutions was used:

- Formulas from the RSE-M code (AFCEN, 2020);
  - (for case A and C1 - see tables of deviations above) (AFCEN, 2020);
- Formulas from the Handbook Tada-Paris-Irwin (Tada et al., 2000);
  - (for case B – see Table 3.9 above);
- Formulas from the Handbook Raju-Newman (Newman et al., 1984);
  - (for figures B.17 et C.17 related to case A1 and A2 in the annexes from participant 17);
- Conventional FEM evaluation, using refined and focused meshing around the crack tip (for case B).

For a few participants, the contribution was restricted to a limited number of benchmark exercises due to a lack of resources or capability. All the contributions that were effectively provided were generally of good quality as the deviations with respect to the reference solutions were mostly at an acceptable level.

3.2. Good practices to be implemented during X-FEM modelling

The benchmark exercises provided a good opportunity to compare the X-FEM modelling methods and techniques among the participants, and to search for good practices which can be implemented to efficiently make use of the X-FEM technology. The following good practices were identified during the intercomparison of the participant results:

1. 1/10th or 1/20th of smallest crack dimension is a good mesh size around crack tip

The most common mesh size around the crack tip used by participants was 1/10th to 1/20th of the smallest crack size. This mesh size proved to provide accurate results with a fairly good coherence with the reference solution. Nevertheless, some participants were able to get good, or at least acceptable, accuracy with a mesh size up to 5 times more coarse than this.

As an example, Figure 3.1 provides the K_I results along the crack front for the benchmark case A1, calculated by participant 6. The chosen elements at the crack tip are quadratic and have a size of 1/10th of the smallest crack dimension (a). A very good coherence with theory and with conventional FEM results can be observed.

Figure 3.1. K_I along crack tip calculated by participant 6 for the benchmark case A1

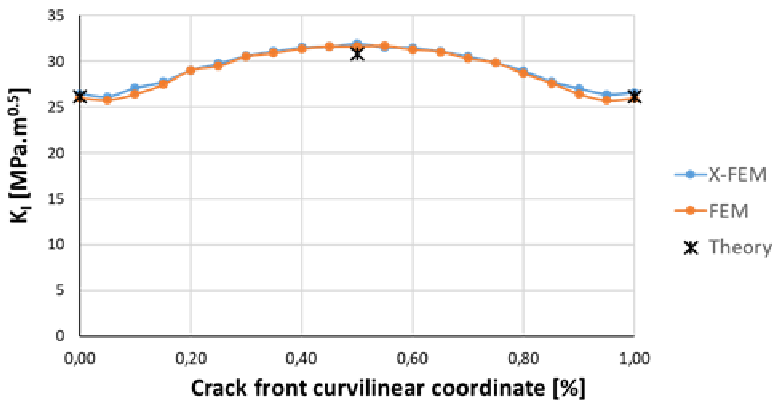

Note: Mesh size = a/10 at crack tip – quadratic elements.

Some participants used a coarser mesh (up to 1/3rd of the smallest crack dimension) in order to decrease the computation time. For the results of these participants, the correlation with the theoretic values is smaller, and the results are less accurate as the curve representing the evolution of K_I along the crack front is not as smooth as in Figure 3.1. This can for example be observed from Figure , which shows the calculated K_I values along the crack front for benchmark case A1, done by participant 18 for a mesh size of 1/3rd of the smallest crack dimension around the crack tip using linear elements.

Figure 3.2. K_I along crack tip calculated by participant 18 for the benchmark case A1

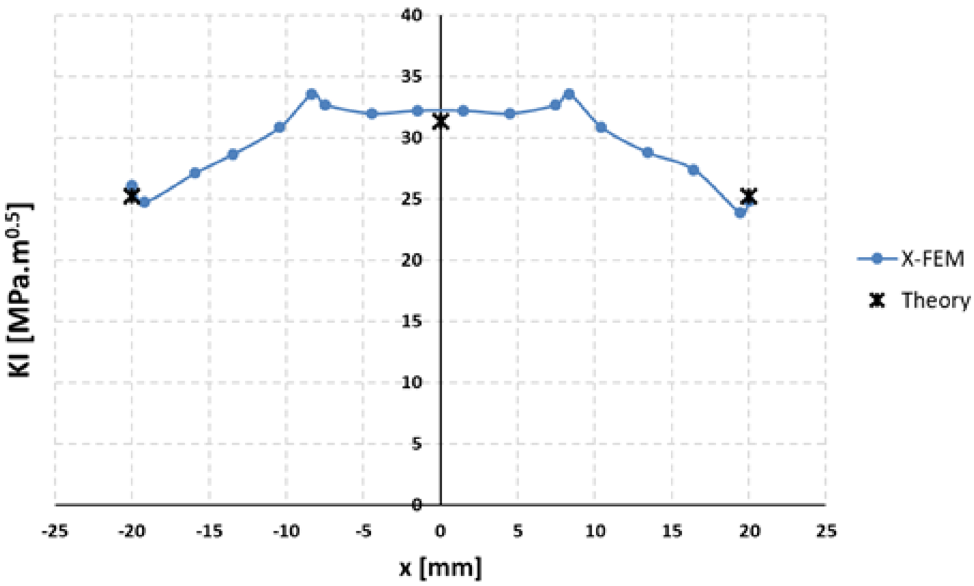

Note: Mesh size = a/3 – linear elements.

Other participants calculated the stress intensity factors using a finer mesh (up to 1/50 of the smallest crack size). This only slightly improves the calculation results but, generally speaking, it can be concluded that a mesh size at the crack tip of 1/10th or 1/20th of the smallest crack size provides satisfying results with respect to the reference solution.

Furthermore, it was observed by the participants that the crack curvature has an important effect on the element size around the crack which should be applied in order to obtain reasonable results: the sharper the crack, the finer the required mesh should be.

Some participants also made use of a tool for automatic refinement of the mesh size at the crack tip (e.g. Tool Homard in code_Aster). Such a tool is useful when using X-FEM as it enables a large reduction of the numbers of elements and consequently the computing time, especially for large and complex models. In Figure 3.3, the mesh resulting from such a tool is illustrated. When compared to a model with a propagated mesh through the whole model, as illustrated in Figure 3.4, there is a large gain in computing efficiency.

Figure 3.3. Mesh obtained for case A1 by participant 4 with a local mesh refinement tool resulting in 30 000 elements for accurate results

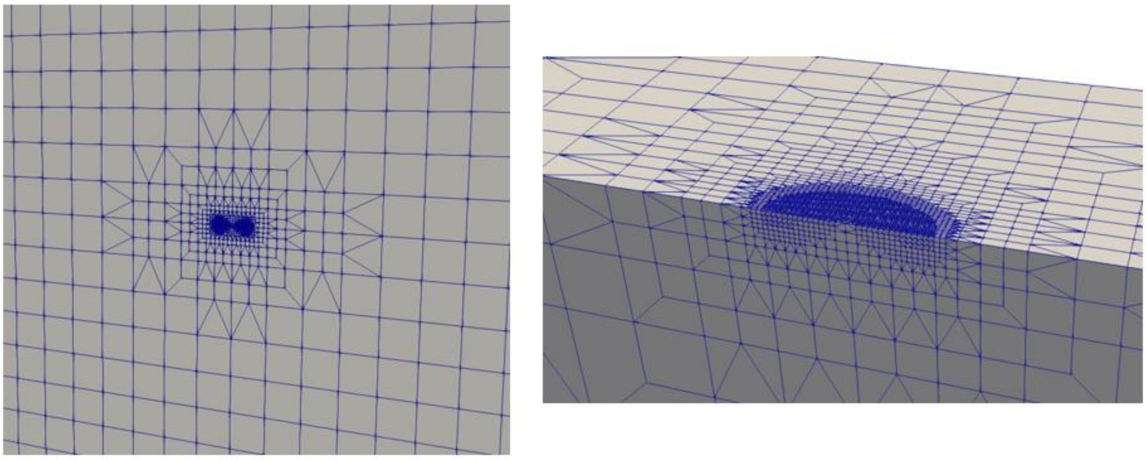

Figure 3.4. Mesh obtained for case A1 by participant 8 by propagation resulting in 556 800 elements for accurate results

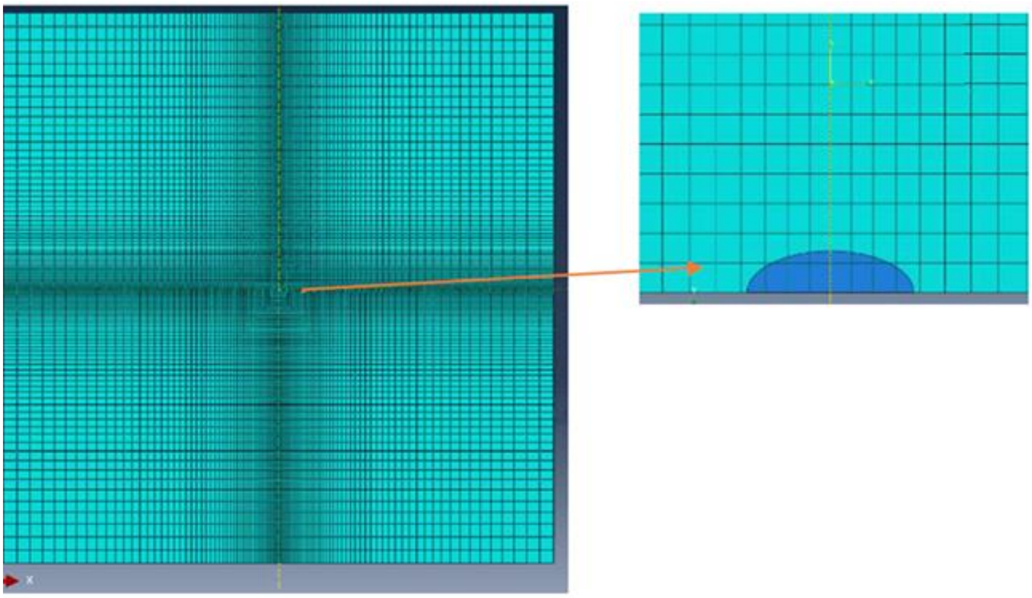

As a conclusion on the crack tip mesh size to be used in X-FEM calculations, it must be mentioned that, whatever the mesh size, the convergence of the solution must be verified when integration methods are used to determine the stress intensity factors. More details are given on the convergence aspect in 3.3. If the convergence of the solution is not obtained, a more refined mesh shall be used to improve the convergence and therefore the accuracy of the solution. Another option is to determine the stress intensity factor by the displacement method.

2. Quadratic elements give better results than linear elements

It can generally be observed from the participant results that quadratic elements provide results that are closer to the theoretic values. Especially for linear elements, the stress intensity factor along the crack tip shows some high scatter in the oscillations (see also limitation 4 of 3.2). A drawback of the use of quadratic elements is the computation time, which is several orders higher.

Figure 3.5 shows a comparison of the K_I result along the crack front as calculated by participant 12 using a linear mesh and by participant 54 using a quadratic mesh for benchmark A2. It can be clearly seen that the quadratic mesh provides much better results.

Figure 3.5. K_I along crack tip calculated by participant 12 (mesh size = a/10 - linear elements) and participant 5 (mesh size = a/10 - quadratic elements) for the benchmark case A2

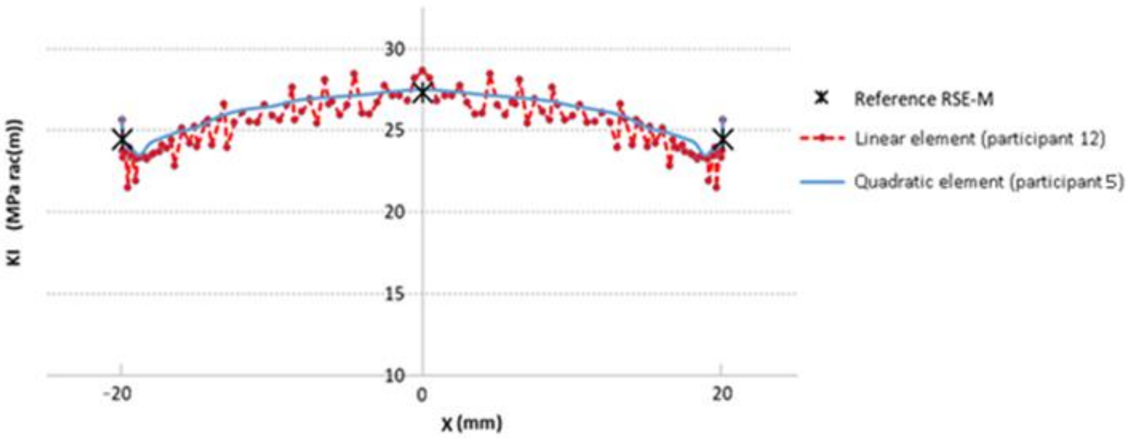

When using linear elements, a good practice may be to perform a polynomial fitting of the obtained stress intensity factor solution along the crack front, as has been done by participant seven for benchmark A1, A2 and A3 (see Figure 3.6). As it has been observed, this approximation correlates better with the solution obtained by a calculation with a quadratic mesh and also with the reference solution.

Figure 3.6. K_I along crack tip calculated by participant 7 (mesh size = a/10 - linear elements) for benchmark case A2, compared to a polynomial fit of the 6th order

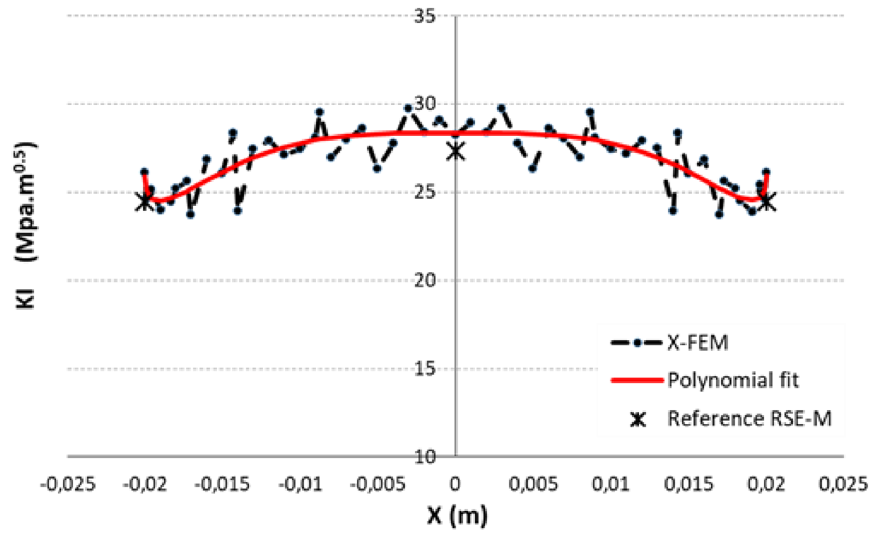

Another method to improve the accuracy of the results when using linear elements is to make the mesh size at the crack tip as homogeneous as possible. This can be observed from the graph in Figure 3.7, which compares the K_I results along the crack front for case A2 as calculated by participant 9 for 2 linear meshes, with the results from a quadratic mesh obtained by participant 4 and with the theoretic values at the deep point and the surface points. It can be observed that the results for the second linear mesh are more accurate and closer to the reference solution. This is apparently related to the fact that this mesh is more homogeneous at the crack tip (element size varies between 0.9 mm and 1.3 mm) than the first mesh (element size varies between 1 mm and 2 mm).

Figure 3.7. K_I along crack tip calculated by participant 9 (mesh size = a/10 - linear elements) for benchmark case A2, compared to the results from participant 4 (mesh size = a/10 – quadratic elements) and theory

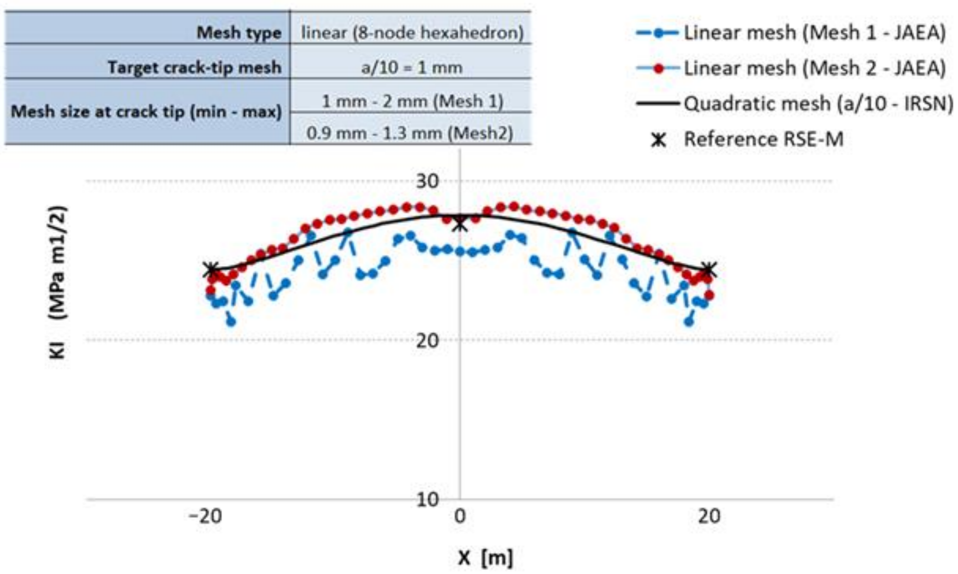

Mesh type	linear (8-node hexahedron)
Target crack-tip mesh	a/10 = 1 mm
Mesh size at crack tip (min - max)	1 mm - 2 mm (Mesh 1)
	0.9 mm - 1.3 mm (Mesh2)

3. Use a sufficiently large area of refined and regular mesh around the crack tip

Some participants could significantly improve their calculated results by enlarging the region with refined and regular mesh around the crack tip. This can be explained by the fact that the path dependence in the energy based method G_θ for large theta fields will improve. In order to obtain accurate results with X-FEM, the theta field should have an inner radius which is on the one hand small enough and at least equal to the smallest element size at the crack tip, but on the other hand also large enough (but not too large).

4. Modelling of a small fillet at sharp edges

Several participants reported problems in obtaining accurate X-FEM results at the sharp edge of the flaw (point C) for benchmark C. As a solution, some participants modelled this edge by a fillet with a small radius and refining the mesh at this location. This technique provided much better results.

3.3. Limits of X-FEM modelling encountered by the participants

The main benefit of X-FEM is commonly known to be the ability to model cracks in a component without the need to manually create a special, time-consuming mesh around the crack tip, as required for a conventional FEM. This simplicity of meshing is supposed to offer the possibility to model a crack or even multiple cracks in complex structures such as nozzle welds, and to model the propagation of cracks without the need for continuously re-meshing the zone around the crack tip.

Nevertheless, the X-FEM application may also be subjected to certain limitations and drawbacks. It is specifically the purpose of this benchmark to identify these limitations and drawbacks. The following limitations and drawbacks were identified by certain participants:

1. Difference between X-FEM results and analytical solutions (and conventional FEM)

For the participants who also calculated conventional FEM results, it was observed that the divergence of the X-FEM results was typically larger than the divergence of the FEM results.

A certain divergence between the X-FEM and FEM solutions is not abnormal as the meshes of the FEM and X-FEM models are not the same. Even for two FEM models with a different mesh, some divergence can be observed. In this framework, it should be mentioned that a good meshing strategy also for X-FEM is extremely important, as it is the key to finding a good balance between accuracy and computing time.

A certain divergence between the X-FEM and reference solutions can be related to a combination of causes, e.g. not an optimal mesh, bad choice of elements, wrong boundary conditions, etc. A careful setting of the X-FEM parameters is therefore crucial in this aspect.

2. Inability to model a crack on a symmetry plan

Some participants reported that for some codes (e.g. ABAQUS and Code Aster), it is not possible (yet) to model a crack on a symmetry plane using X-FEM, while this is effectively possible using the conventional FEM.

However, as X-FEM is a method specifically developed for complex structures with a complex loading (without symmetry), this limitation does not really affect the performance of the method for the problems for which it is designed.

3. Restricted number of usable element types for X-FEM

For some codes, the participants reported the issue that only a limited number of element types (mainly linear elements) is available when using X-FEM, which is not the case when using conventional FEM.

Although the list of available element types includes elements that can generally be used in most applications, this issue might cause problems in specific applications, e.g. for combined thermal and fracture mechanics problems, as the accuracy of the thermo-mechanical stresses calculated may depend on the type (linear or quadratic) of element used.

4. Oscillation of K_I results when using a linear mesh

Some participants using a linear mesh with X-FEM observed an oscillation of the K_I results on the crack front, while for conventional FEM a linear mesh provides a smoother evolution of K_I along the crack front. This is observed for mesh sizes at the crack tip in the order of a/10, but not for smaller mesh sizes in the order of a/30, as can be observed in Figure 3.1. This figure shows the K_I results for the benchmark case A1 calculated by participant 16 (3 larger meshes) and participant 17 (1 small mesh) as a function of position x by using linear hexahedral elements.

Furthermore, this observation cannot be made at all for quadratic meshes.

Figure 3.8. Figure illustrating oscillations in the SIF calculation results when using a coarse mesh (> a/30) using linear elements

K_I as function of x for benchmark A1, obtained with linear hexahedral elements

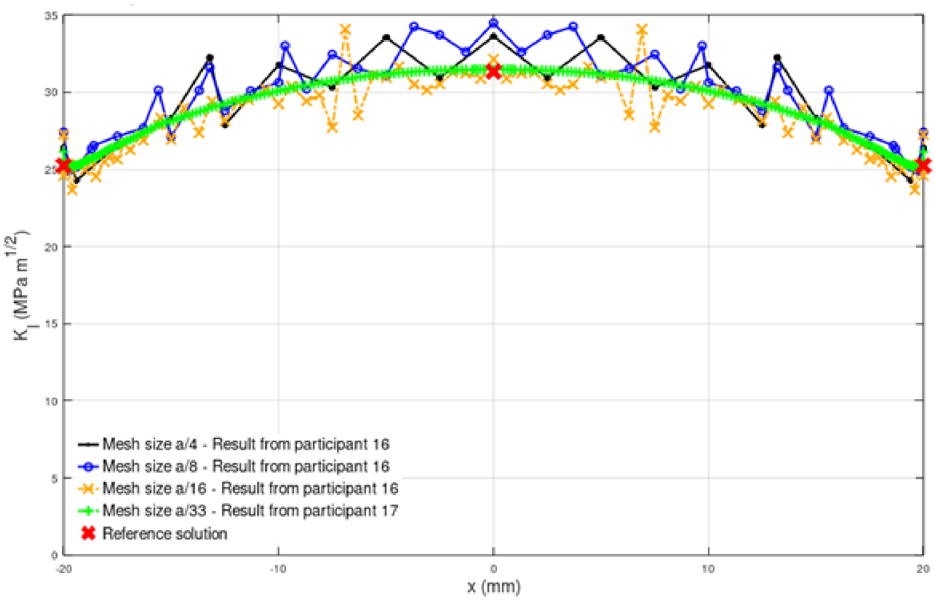

In order to solve this problem, some participants tried out an X-FEM linear mesh that follows the crack geometry (see Figure as an example). Such a mesh gave a much better result but is necessarily more time-consuming. However, the beneficial effect of X-FEM can then put into question in this case as being a mesh independent tool for fracture mechanics analyses, in comparison to classical FEM which is less demanding in terms of calculation time. Guiding the mesh along the crack front might not be the philosophy of X-FEM as it makes the mesh dependent on the crack shape, and may introduce the same difficulties as for the conventional FEM, making the technique less efficient and more time-consuming.

Figure 3.9. Figure illustrating an X-FEM mesh following the crack geometry

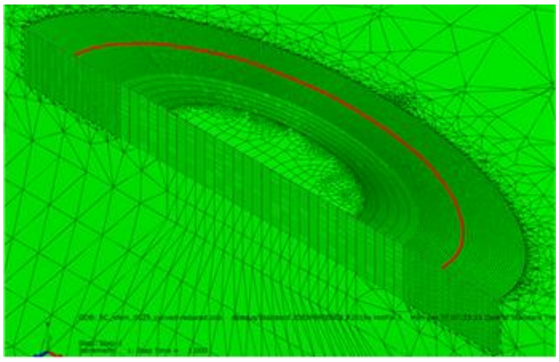

5. Inability to apply X-FEM on a crack between two different materials

For benchmark case C1, a crack was assumed with a crack front partly lying on the interface of a base metal and its cladding, made of two different materials with different properties. For some codes (e.g. ABAQUS, CODE_ASTER), participants reported that it was not possible to apply X-FEM on a crack which concerns two different materials (at the interface of the two materials). Three methods to bypass this limitation - schematically illustrated in Figure 3.10 - can be considered to rule out this problem:

- For the mechanical calculation only, the same Young modulus was assigned to the cladding (e.g. participant 8). The error introduced on K_I at the deepest point is negligible as the Young modules of the stainless steel cladding and the ferritic steel base metal are close to each other.
- For the mechanical calculation only, the thickness of the cladding was reduced by 10% and replaced by base metal such that the crack is contained completely in the base metal (e.g. participants 11, 12, 13, 14). The normal stress distribution in the base metal is not significantly affected by the change.
- The surface points to be considered on the interface of the base metal and the cladding are not those at the interface of the base metal and the cladding but those just behind the cladding (thus in the base metal) and closest to the cladding.

This issue might cause problems in dissimilar welds between materials for which the mechanical properties are significantly different. However, in practice, the design codes state that dissimilar welds should not be made of materials that differ significantly in yield strength and thus in Young modulus.

Only methods 1 and 2 were considered by the participants who went through to the end of benchmark C1.

Figure 3.10. Figure illustrating an X-FEM mesh following the crack geometry

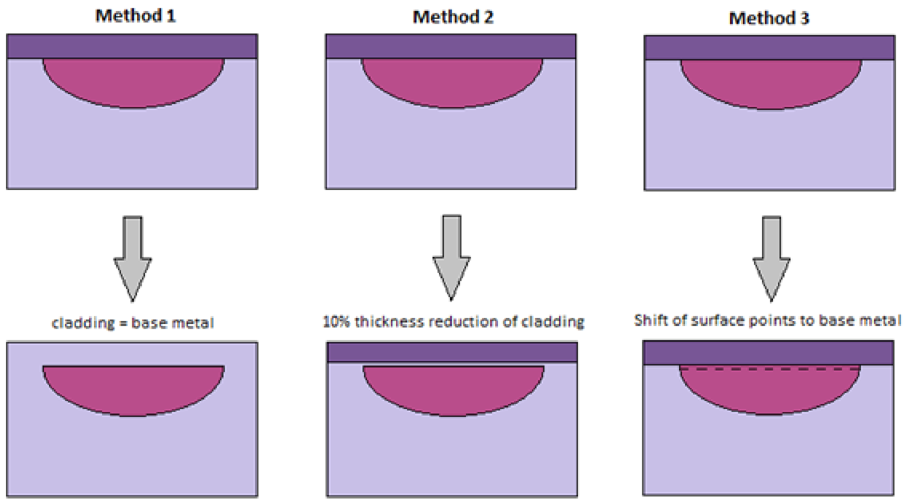

6. Computational effort too large

Some participants reported that the requested model for case C, in combination with the desired mesh (fine enough to get accurate results) required too great a computational effort. Therefore, additional symmetry was added to the model, decreasing the number of elements and the computational effort to an acceptable level.

Compared with conventional FEM, X-FEM is expected to demand a greater computation effort as the elements are enriched and therefore present significantly more degrees of freedom than in the case of classical 3D modelling. For this reason, an effective mesh strategy resulting in an optimal mesh is even more important for X-FEM than for conventional finite element modelling.

For models with a complex geometry and/or complex loadings, the followed strategy of introducing symmetry would not be an option. That is effectively the reason why the models requested in the benchmark exercises are large in size, as it obliges the user to search for an X-FEM mesh strategy that is efficient in terms of time spent but also computationally efficient.

7. No convergence on the X-FEM contour integral

Some participants that used the X-FEM SIF integral calculation method reported that convergence of the X-FEM solution with the integration contours is not systematic, even when the refinement of the mesh appears adequate (a/10 for instance). This is observed whatever code is used.

Participant 17 considers that it is inherent to X-FEM that the contour integrals are not fully path independent, although the path dependence can be minimised through mesh refinement and contouring. Because of these effects, Participant 17 has reported SIF values that are the average of the SIF values calculated from 5 contours.

It was further observed by participant 17 that the path dependency and the corresponding convergence of the SIF results may be improved by using a larger zone of homogeneous and high density mesh (Figure 3.11).

According to participant 4, using the displacement method makes it possible to eliminate the problem of convergence of the X-FEM solution from the integral method. The displacement method for determining K_I, K_{II}, K_{III} gives more accurate X-FEM solutions than the integral methods, without convergence problems (see Figure 3.12).

Limitations two, three and five demonstrate that for the most finite element codes, not all functionalities are available yet for X-FEM that are already implemented for conventional FEM modelling. This makes complex studies (with contact friction, dynamics, large strains, etc.) hardly feasible with X-FEM. Therefore, it is important that the necessary efforts are made to continuously improve and develop the X-FEM technology.

Figure 3.11. Figure illustrating the difficulty of finding converging SIF results using the SIF integral calculation method. A large density homogeneous mesh (2) improves the path independency of the SIF results compared to a coarser density homogeneous mesh (1)

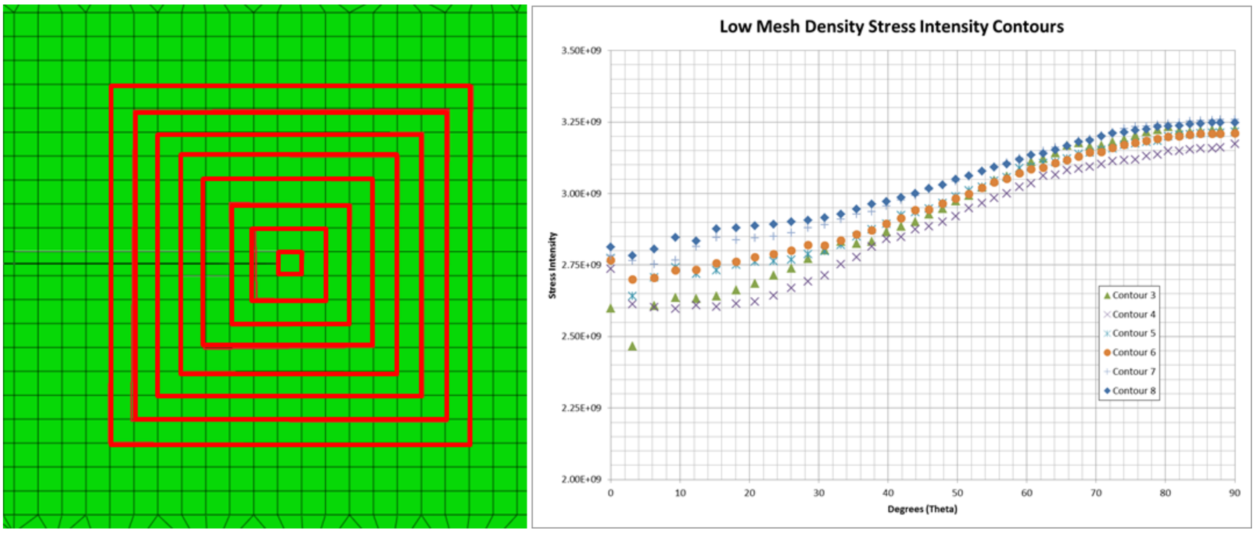

1) Low density mesh (a/10) with contours highlighted and stress intensity factor results

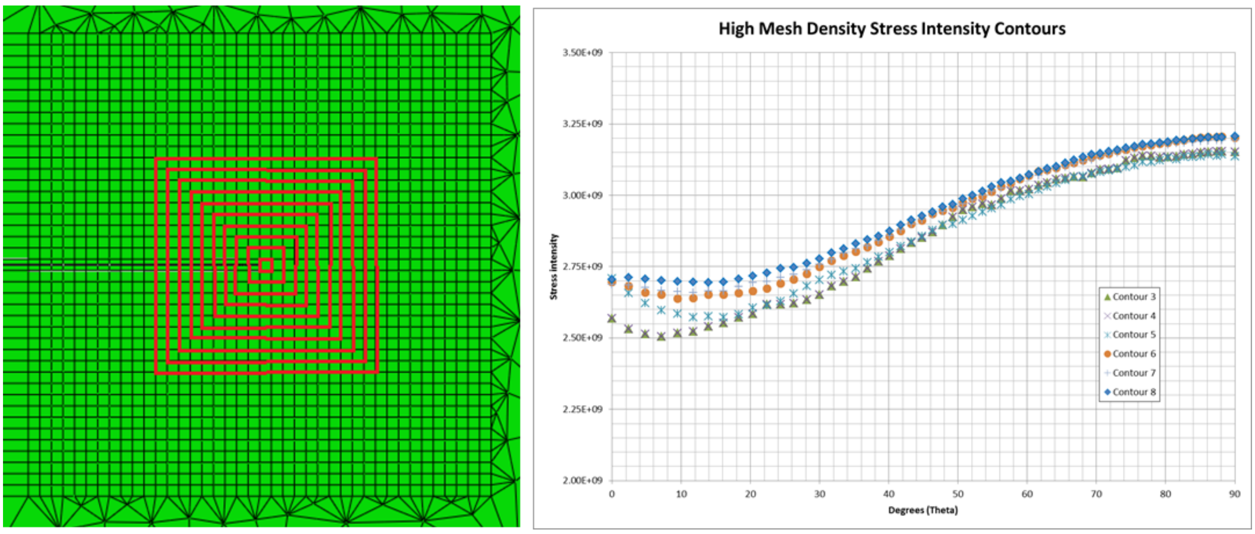

2) High density mesh (~a/30) with contours highlighted and stress intensity factor results

Figure 3.12. Figure comparing case B results obtained with the displacement method and the integration (participant 4). The solution accuracy is better for the displacement method as observed on K_{II} evolution (1) and K_{III} evolution (2).

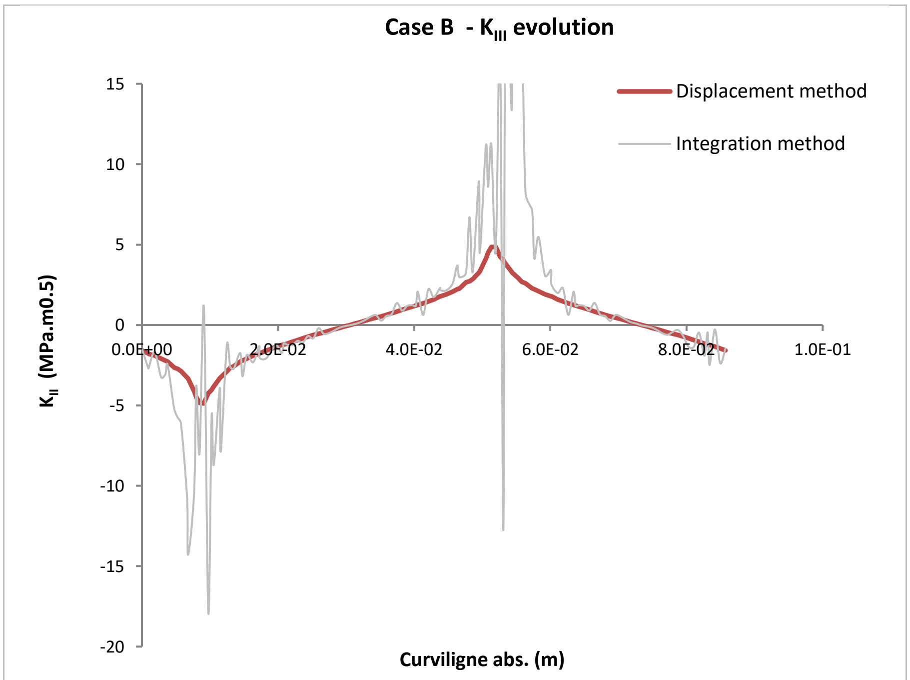

(1)

Figure 3.12. Figure comparing case B results obtained with the displacement method and the integration (participant 4). The solution accuracy is better for the displacement method as observed on K_{II} evolution (1) and K_{III} evolution (2). (Continued)

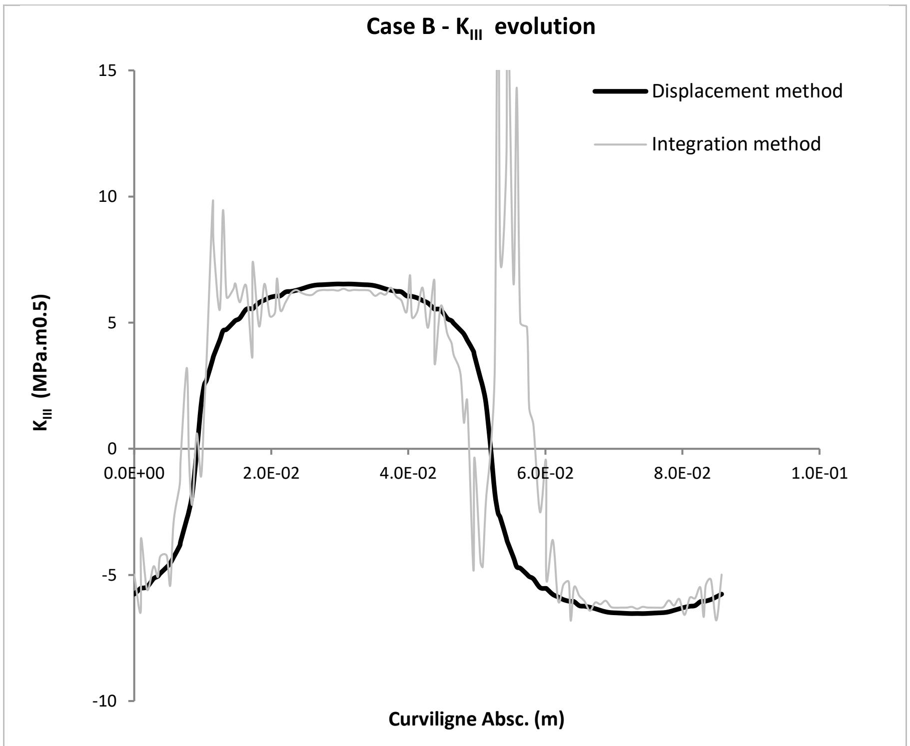

(2)

4. Conclusion

The aim of the eXtended Finite Element Method (X-FEM) benchmark was twofold. The first objective was to verify the accuracy of the Fracture Mechanics Parameters K_I, K_{II}, K_{III} determined by X-FEM for metal components and structures under various loadings, namely tension, bending and thermal transient. The second objective, considered to be at least as important as the first one, was to gather the good practices and limits of X-FEM, which is just beginning to be used in industry.

Eighteen organisations from nine countries in Asia, Europe and North America were keen to participate in this X-FEM benchmark, which consisted of three rather academic cases and one more complex practical case related to the justification of reactor pressure vessel fitness for service.

The comparison of the deviations of the X-FEM solution from the reference solution obtained by the participants shows that X-FEM results are on average compatible with the reference solutions. The excessively large deviations that may have been observed were not directly related to X-FEM but rather to modelling issues. For example, incorrect boundary conditions and/or loading applications have led, in some cases, to inadequate t shear stresses and thermal stresses acting on the crack. The results of all the calculations performed by each participant are detailed in five annexes.

Some good practices were drawn from this benchmark. These are summarised below:

- First, the general good practices of FEM still need to be applied in modelling geometry and loading specificities.
- A mesh size of 1/10th or 1/20th of the smallest crack dimension is recommended around the crack tip.
- A homogeneous mesh size on the crack front is recommended.
- The results along the whole crack front are overall more accurate with a quadratic mesh than a linear mesh, for which oscillations of the calculated solution on the crack front around the reference solution can be observed. The oscillation may nevertheless be alleviated when a mesh size smaller than 1/10th of crack depth is used.
- Refining the mesh solely around the crack tip is preferable to avoid large models that are too demanding in terms of computing resources. To that purpose, the availability of automatic local meshing tools should be systematised in codes to avoid modelling that is manually too time-consuming. This enhances the application of the benefits of X-FEM.
- When using the integration method to determine stress intensity factors, care must be taken – as for conventional FEM – to obtain the solution convergence that depends on the defined contours. To reach convergence, a more refined mesh at the crack area may be required than with conventional FEM.
- When the convergence of stress intensity factors obtained by the integration method is not reached on a given model, the displacement method can be a successful alternative to provide good accuracy with the same model.

Similarly, some limits of X-FEM, as it is presently implemented in research and industrial codes for facture analysis, were identified during the benchmark. These are listed below:

- There is a restricted number of element types for X-FEM in several codes.
- The modelling of cracks on symmetric planes is not possible.
- The application of X-FEM on a crack between two different materials is not possible.
- Extensive computer resources are required when no care is taken to limiting model size. Indeed, the degree of freedom greatly increases for enriched nodes.
- The displacement method to estimate stress intensity factors from X-FEM calculation is not available in all codes.

In conclusion, the results of the academic benchmark cases confirm that X-FEM is an efficient alternative tool for fracture analyses compared to conventional methods for simple fracture analyses. In an industrial context and for complex structural applications that are almost impossible to study with the conventional FEM, X-FEM may also be a good alternative. However, in some codes, developments appear necessary to improve the modelling efficiency in order to take full advantage of the use of X-FEM compared to the conventional FEM (e.g. computation time-saving, crack meshing possibilities).

5. References

AFCEN (2020), “Règles de Surveillance en Exploitation des Matériels Mécaniques des Ilots Nucléaires REP”, RSE-M, AFC196, AFCEN.

Belytschko, T., R. Gracie and G. Ventura (2009), “A review of Extended/Generalized Finite Element Methods for Material Modelling”, *Modelling Simul. Mater. Sci. Eng.*, Volume 17, DOI: 10.1088/0965-0393/17/4/043001.

Belytschko, T. and T. Black (1999), “Elastic crack growth in finite elements with minimal remeshing”, *Internat. J. Numer. Methods Engrg*, Volume 45, pp. 601-620.

Duflot, M. (2008), “The extended finite element method in thermoelastic fracture mechanics”, *Internat. J. Numer. Methods Engrg*, Volume 74, 827-847, DOI: 10.1002/nme.2197.

Moës, N. (2015), “The eXtended Finite Element Method (X-FEM)” in *Encyclopedia of Applied and Computational Mathematics*, pp.472-477.

NEA (2017), “Benchmark Results on the Analytical Evaluation of the Fracture Mechanic Parameters K and J”, OECD Publishing, Paris, www.oecd-nea.org/jcms/pl_19798.

Newman, J.C. and I.S. Raju (1984), “Stress-Intensity Factor Equations for Cracks in Three-Dimensional Finite Bodies Subjected to Tension and Bending Loads”, *NASA Technical Memorandum*.

Tada, H., P.C. Paris and G.R. Irwin (2000), *The Stress Analysis of Cracks Handbook*, Third Edition, ASME Press, DOI: 10.1115/1.801535.

Annex A. Materials properties

Table A.1. Forged ferritic steel (~SA 508 Cl3) material properties from the RCC-M code

Temperature (°C)	Young Modulus (MPa)	Yield Strength (MPa)	Expansion a (*) (/°C)	Conductivity λ (W/m/°C)	Density ρ (kg/m³)	Specific heat Cp J/kg/°C	Diffusivity λ/ρ.Cp m/s
0	205000	420	11.22E-6	37.7	7800	447.12	10.8E-06
20	204000	420	11.22E-6	37.7	7800	447.12	10.8E-06
50	203000	414	11.45E-6	38.6	7800	460.35	10.7E-06
100	200000	393	11.79E-6	39.9	7800	483.95	10.6E-06
150	197000	380	12.14E-6	40.5	7800	503.62	10.3E-06
200	193000	374	12.47E-6	40.5	7800	523.95	9.91E-06
*250	189000	365	12.78E-6	40.2	7800	547.12	9.42E-06
300	185000	355	13.08E-6	39.5	7800	567.09	8.93E-06

Table A.2. Stainless steel material properties from the RCC-M code

Temperature (°C)	Young Modulus (MPa)	Yield Strength (MPa)	Expansion a (*) (/°C)	Conductivity λ (W/m/°C)	Density ρ (kg/m³)	Specific heat Cp J/kg/°C	Diffusivity λ/ρ.Cp m/s
0	198500	376	16.40E-6	14.7	7800	461.92	4.08E-06
20	197000	370	16.40E-6	14.7	7800	461.62	4.08E-06
50	195000	360	16.54E-6	15.2	7800	479.98	4.06E-06
100	191500	344	16.80E-6	15.8	7800	500.16	4.05E-06
150	187500	328	17.04E-6	16.7	7800	526.05	4.07E-06
200	184000	312	17.20E-6	17.2	7800	533.93	4.13E-06
250	180000	296	17.50E-6	18.0	7800	546.85	4.22E-06
300	176500	280	17.70E-6	18.6	7800	550.72	4.33E-06

(*) The linear expansion coefficients indicated in the tables are the mean values between 20°C and the considered temperature.

A.1. Strain-stress curve

The stress-strain curve is modelled as mentioned on Figure A.1. with:

- Base material (ferritic steel): ET/Sy = 1/56 T + 36/7, where T is the temperature and Sy is the yield strength given in Table A.1.;
- Cladding (stainless steel): ET/Sy = 5.1, where Sy is the yield strength given in Table A.2.

Figure A.1. Stress-strain curve

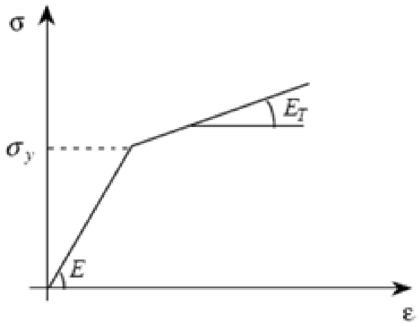

Annex B. Resulting graphs for benchmark A1

Figure B.1. Summary data for all participants on benchmark A1

Figure	Participant	Code	Curve	Mesh element: Order	Mesh element: type	Mesh element: target size (ratio to crack depth a)	SIF calculation method	More information
B.1	1	Abaqus	Curve 1	Linear	Hexahedral	1/20	Integral	
B.2	2	Morfeo crack	Curve 1	Linear	Tetrahedral	1/10	Integral	
B.3	3	Abaqus	Curve 1	Linear	Hexahedral	1/10	Integral	
		Ansys	Curve 2	Linear	Hexahedral	1/10		Regular mesh / elements of size 0,9 mm
			Curve 3			1/10		Regular mesh / elements of size 1,1 mm
			Curve 4			1/10		Conformed mesh / elements of size 1,1 mm
B.4	4	Code-Aster	Curve 1	Quadratic	Tetrahedral	1/10	Integral	Integration domain: R_{min} = 4 mm; R_{max} = 8 mm
			Curve 2					Integration domain: R_{min} = 0,8 mm; R_{max} = 2 mm
			Curve 3					Integration domain: R_{min} = 0,4 mm; R_{max} = 2 mm
			Curve 4			1/20	Integral	Integration domain: R_{min} = 2,8 mm; R_{max} = 5,7 mm
			Curve 5					Integration domain: R_{min} = 0,4 mm; R_{max} = 2,5 mm
			Curve 6					Integration domain: R_{min} = 0,4 mm; R_{max} = 5 mm
			Curve 7					Integration domain: R_{min} = 0,4 mm; R_{max} = 1,5 mm
B.5	5	Systus	Curve 1	Quadratic	Hexahedral	1/10	Integral	Integration domain: R_{min} = 0,5 mm; R_{max} = 2 mm / XY and YZ symmetry used
			Curve 2					Integration domain: R_{min} = 0,5 mm; R_{max} = 3 mm / XY and YZ symmetry used
			Curve 3					Integration domain: R_{min} = 0,5 mm; R_{max} = 4 mm / XY and YZ symmetry used
			Curve 4					Integration domain: R_{min} = 0,5 mm; R_{max} = 2 mm / no symmetry used
			Curve 5					Integration domain: R_{min} = 0,5 mm; R_{max} = 3 mm / no symmetry used
			Curve 6					Integration domain: R_{min} = 0,5 mm; R_{max} = 4 mm / no symmetry used
B.6	6	Code-Aster	Curve 1	Linear	Tetrahedral	1/20	Integral	Integration domain: R_{min} = 1 mm; R_{max} = 2 mm / topological crack-tip enrichment / 6 refinement steps (XL6TT mesh)
			Curve 2					Integration domain: R_{min} = 1 mm; R_{max} = 3 mm / topological crack-tip enrichment / 6 refinement steps (XL6TT mesh)
			Curve 3					Integration domain: R_{min} = 1 mm; R_{max} = 2 mm / geometrical crack-tip enrichment / 6 refinement steps (XL6TG mesh)
			Curve 4					Integration domain: R_{min} = 1 mm; R_{max} = 3 mm / geometrical crack-tip enrichment / 6 refinement steps (XL6TG mesh)
			Curve 5	Quadratic		1/5		Integration domain: R_{min} = 4 mm; R_{max} = 8 mm / geometrical crack-tip enrichment / 4 refinement steps (XQ4TG mesh)
			Curve 6					Integration domain: R_{min} = 4 mm; R_{max} = 12 mm / geometrical crack-tip enrichment / 4 refinement steps (XQ4TG mesh)
			Curve 7					Integration domain: R_{min} = 4 mm; R_{max} = 8 mm / geometrical crack-tip enrichment / 4 refinement steps (XQ4TG mesh) / integral method with Legendre polynomials

Figure	Participant	Code	Curve	Mesh element			SIF calculation method	More information
				Order	type	target size (ratio to crack depth a)		
B.6	6	Code-Aster	Curve 8	Quadratic	Tetrahedral	1/10	Integral	Integration domain: R_{min} = 2 mm; R_{max} = 4 mm / geometrical crack-tip enrichment / 5 refinement steps (XQ5TG mesh)
			Curve 9					Integration domain: R_{min} = 2 mm; R_{max} = 6 mm / geometrical crack-tip enrichment / 5 refinement steps (XQ5TG mesh)
			Curve 10					Integration domain: R_{min} = 2 mm; R_{max} = 4 mm / geometrical crack-tip enrichment / 5 refinement steps (XQ5TG mesh) / integral method with Legendre polynomials
			Curve 11			1/20		Integration domain: R_{min} = 1 mm; R_{max} = 2 mm / geometrical crack-tip enrichment / 6 refinement steps (XQ6TG mesh)
			Curve 12					Integration domain: R_{min} = 1 mm; R_{max} = 3 mm / geometrical crack-tip enrichment / 6 refinement steps (XQ6TG mesh)
			Curve 13					Integration domain: R_{min} = 1 mm; R_{max} = 2 mm / geometrical crack-tip enrichment / 6 refinement steps (XQ6TG mesh) / integral method with Legendre polynomials
			Curve 14		Hexahedral	1/20		Integration domain: R_{min} = 1 mm; R_{max} = 2 mm / geometrical crack-tip enrichment / 5 refinement steps (XQ5HG mesh)
			Curve 15					Integration domain: R_{min} = 1 mm; R_{max} = 3 mm / geometrical crack-tip enrichment / 5 refinement steps (XQ5HG mesh)
			Curve 16					Integration domain: R_{min} = 1 mm; R_{max} = 2 mm / geometrical crack-tip enrichment / 5 refinement steps (XQ5HG mesh) / integral method with Legendre polynomials
		Code-Aster (FEM)	Curve 17	Quadratic	Tetrahedral	1/25		Integration domain: R_{min} = 0,8 mm; R_{max} = 1,6 mm / Zcrack integral method
			Curve 18					Integration domain: R_{min} = 0,8 mm; R_{max} = 2,4 mm / Zcrack integral method
			Curve 19					Integration domain: R_{min} = 0,8 mm; R_{max} = 1,6 mm / BlocFissure integral method
			Curve 20					Integration domain: R_{min} = 0,8 mm; R_{max} = 2,4 mm / BlocFissure integral method
			Curve 21					Integration domain: R_{min} = 0,8 mm; R_{max} = 1,6 mm / BlocFissure integral method with Legendre polynomials
B.7	7	Abaqus	Curve 1	Linear	Hexahedral	1/20	Integral	
			Curve 2					Curve 2 is a polynomial fit (degree 6) of the data points from Curve 1
			Curve 3			1/5		
			Curve 4					Curve 4 is a polynomial fit (degree 6) of the data points from Curve 3
B.8	8	Abaqus	Curve 1	Linear	Hexahedral	1/2	Integral	
			Curve 2			1/10		
B.9	9	Abaqus	Curve 1	Linear	Hexahedral	1/10	Integral	Element size at crack tip varying from 1 mm to 2 mm
			Curve 2	Linear	Hexahedral	1/10		Element size at crack tip varying from 0,9 mm to 1,3 mm

Figure	Participant	Code	Curve	Mesh element			SIF calculation method	More information
				Order	type	target size (ratio to crack depth a)		
B.10	10	NLXFEM3Dstruct	Curve 1	Linear	Hexahedral	1/10	Integral	
B.11	11	Abaqus	Curve 1	Linear	Hexahedral	1/5	Integral	
B.12	12	Abaqus	Curve 1	Linear	Hexahedral	1/20	Displacement	
B.13	13	Abaqus	Curve 1	Linear	Hexahedral	1/5	Integral	
B.14	14	Abaqus	Curve 1	Linear	Hexahedral	1/20	Integral	
B.15	15	Abaqus	Curve 1	Linear	Hexahedral	1/5	Integral	
B.16	16	Abaqus	Curve 1	Linear	Hexahedral	1/4	Integral	
			Curve 2			1/8		
			Curve 3			1/16		
		Abaqus (FEM)	Curve 4			1/25		
B.17	17	Abaqus	Curve 1	Linear	Hexahedral	1/33	Integral	
		Abaqus (FEM)	Curve 2					
		Theory of Raju-Newman	Curve 3					
B.18	18	Abaqus	Curve 1	Linear	Hexahedral	1/5	Integral	Results present average of 5 integration domains / Crack plane on element face
			Curve 2			1/3		Results present average of 5 integration domains / Crack plane in middle of element
			Curve 3			3/20		Results present average of 5 integration domains / Crack plane in middle of element
			Curve 4			1/5		Results present average of 5 integration domains / Crack plane in middle of element
B.19	18	Abaqus	Curve 1	Linear	Hexahedral	1/5	Integral	Integration domain 1 (domain not specified, but increasing from 1 to 5) / Crack plane on element face
			Curve 2					Integration domain 2 (domain not specified, but increasing from 1 to 5) / Crack plane on element face
			Curve 3					Integration domain 3 (domain not specified, but increasing from 1 to 5) / Crack plane on element face
			Curve 4					Integration domain 4 (domain not specified, but increasing from 1 to 5) / Crack plane on element face
			Curve 5					Integration domain 5 (domain not specified, but increasing from 1 to 5) / Crack plane on element face
			Curve 6					Resuls present average of the 5 integration domains / Crack plane on element face

Figure	Participant	Code	Curve	Mesh element			SIF calculation method	More information
				Order	type	target size (ratio to crack depth a)		
B.20	18	Abaqus	Curve 1	Linear	Hexahedral	1/3	Integral	Integration domain 1 (domain not specified, but increasing from 1 to 5) / Crack plane in middle of element
			Curve 2					Integration domain 2 (domain not specified, but increasing from 1 to 5) / Crack plane in middle of element
			Curve 3					Integration domain 3 (domain not specified, but increasing from 1 to 5) / Crack plane in middle of element
			Curve 4					Integration domain 4 (domain not specified, but increasing from 1 to 5) / Crack plane in middle of element
			Curve 5					Integration domain 5 (domain not specified, but increasing from 1 to 5) / Crack plane in middle of element
			Curve 6					Results present average of the 5 integration domains / Crack plane in middle of element
B.21	18	Abaqus	Curve 1	Linear	Hexahedral	3/20	Integral	Integration domain 1 (domain not specified, but increasing from 1 to 5) / Crack plane in middle of element
			Curve 2					Integration domain 2 (domain not specified, but increasing from 1 to 5) / Crack plane in middle of element
			Curve 3					Integration domain 3 (domain not specified, but increasing from 1 to 5) / Crack plane in middle of element
			Curve 4					Integration domain 4 (domain not specified, but increasing from 1 to 5) / Crack plane in middle of element
			Curve 5					Integration domain 5 (domain not specified, but increasing from 1 to 5) / Crack plane in middle of element
			Curve 6					Results present average of the 5 integration domains / Crack plane in middle of element

Figure	Participant	Code	Curve	Mesh element			SIF calculation method	More information
				Order	type	target size (ratio to crack depth a)		
B.22	18	Abaqus	Curve 1	Linear	Hexahedral	1/5	Integral	Integration domain 1 (domain not specified, but increasing from 1 to 5) / Crack plane in middle of element
			Curve 2					Integration domain 2 (domain not specified, but increasing from 1 to 5) / Crack plane in middle of element
			Curve 3					Integration domain 3 (domain not specified, but increasing from 1 to 5) / Crack plane in middle of element
			Curve 4					Integration domain 4 (domain not specified, but increasing from 1 to 5) / Crack plane in middle of element
			Curve 5					Integration domain 5 (domain not specified, but increasing from 1 to 5) / Crack plane in middle of element
			Curve 6					Results present average of the 5 integration domains / Crack plane in middle of element

Figure B.2. Participant 1 – Benchmark A1

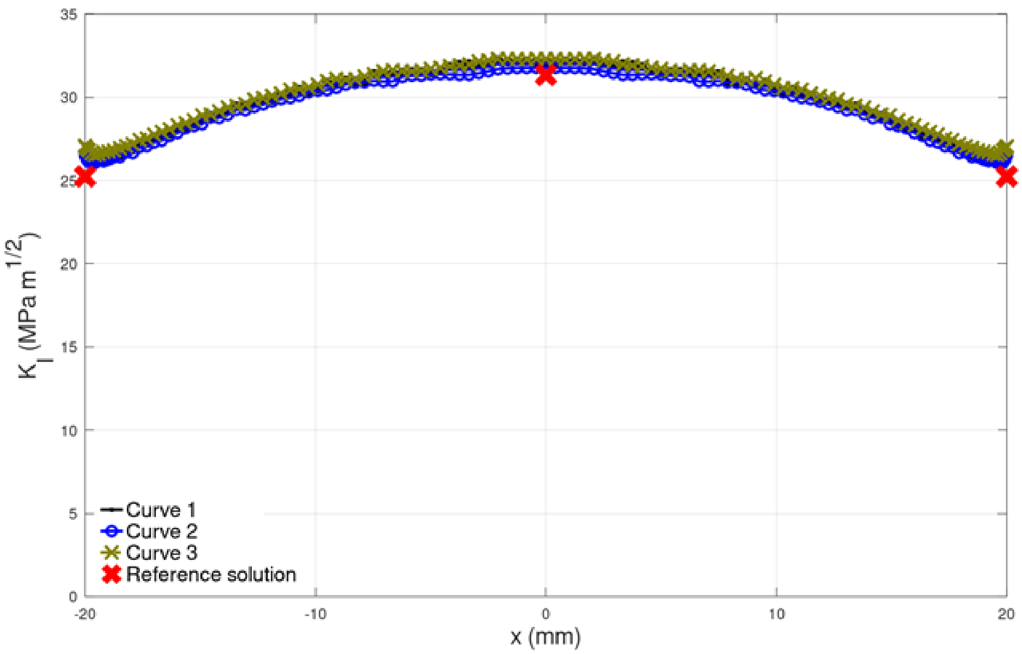

Figure B.3. Participant 2 – Benchmark A1

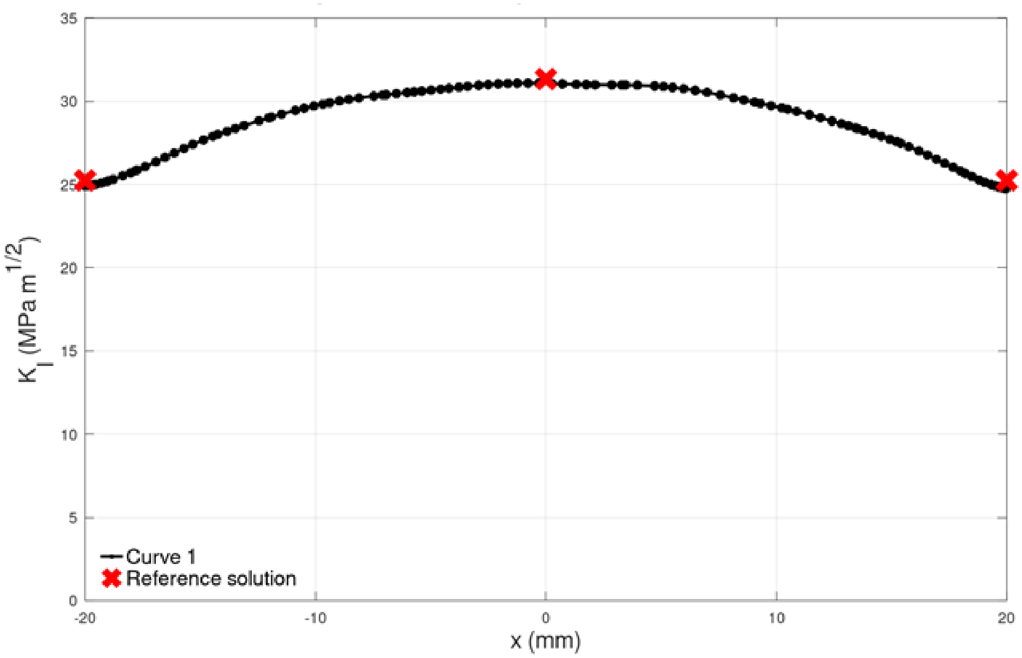

Figure B.4. Participant 3 – Benchmark A1

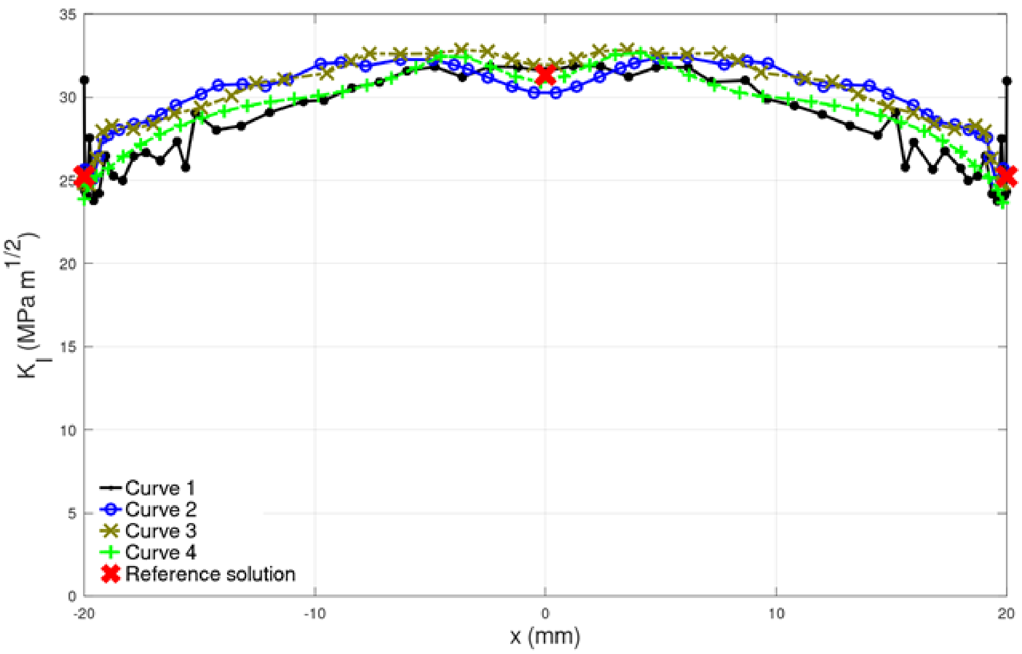

Figure B.5. Participant 4 – Benchmark A1

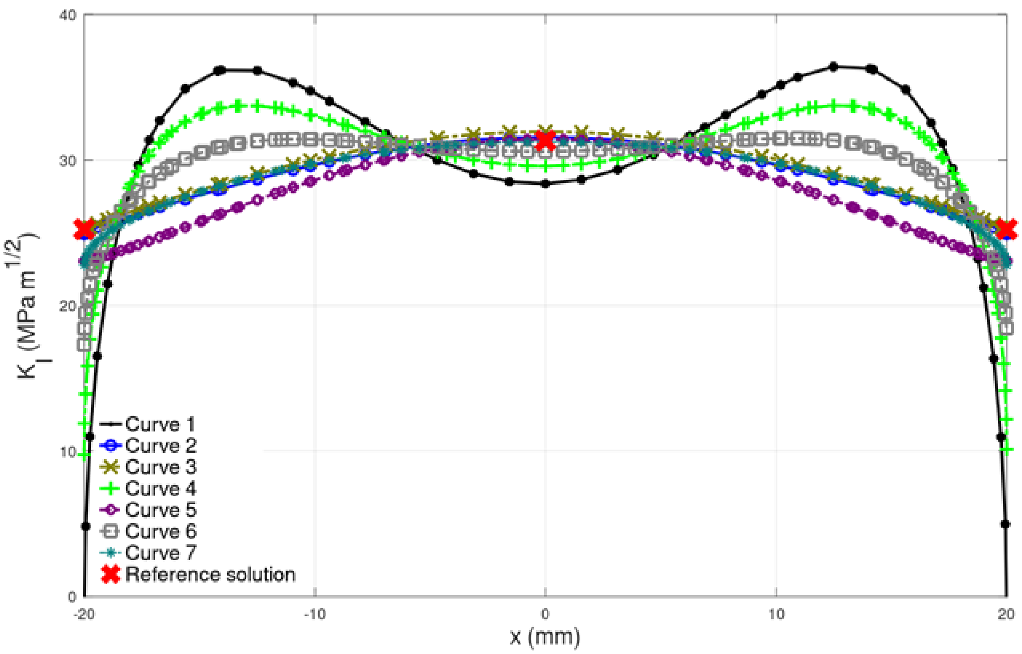

Figure B.6. Participant 5 – Benchmark A1

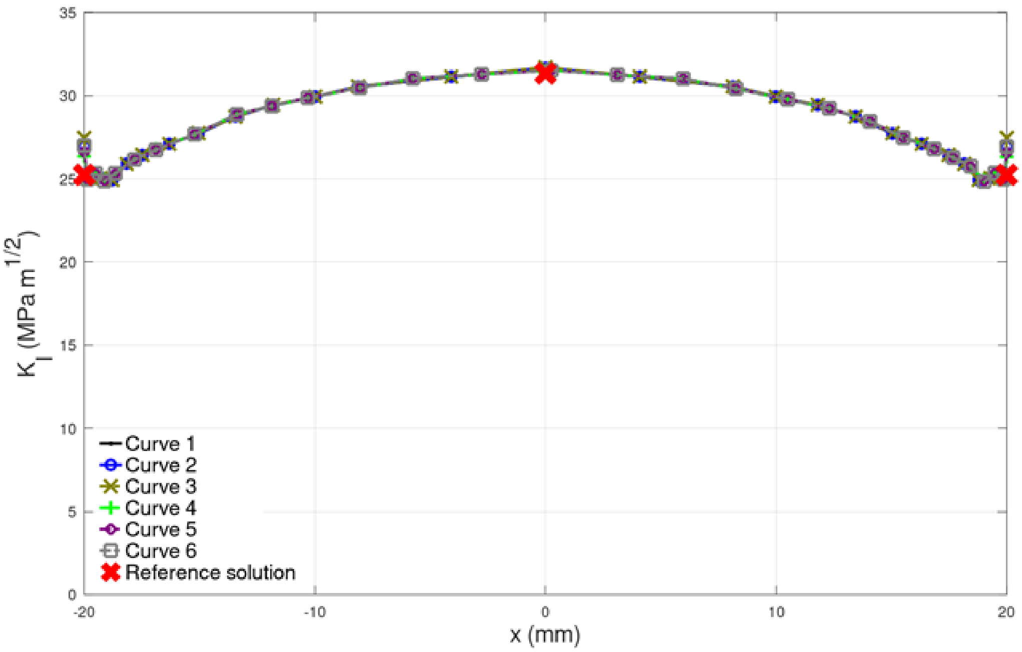

Figure B.7. Participant 6 – Benchmark A1

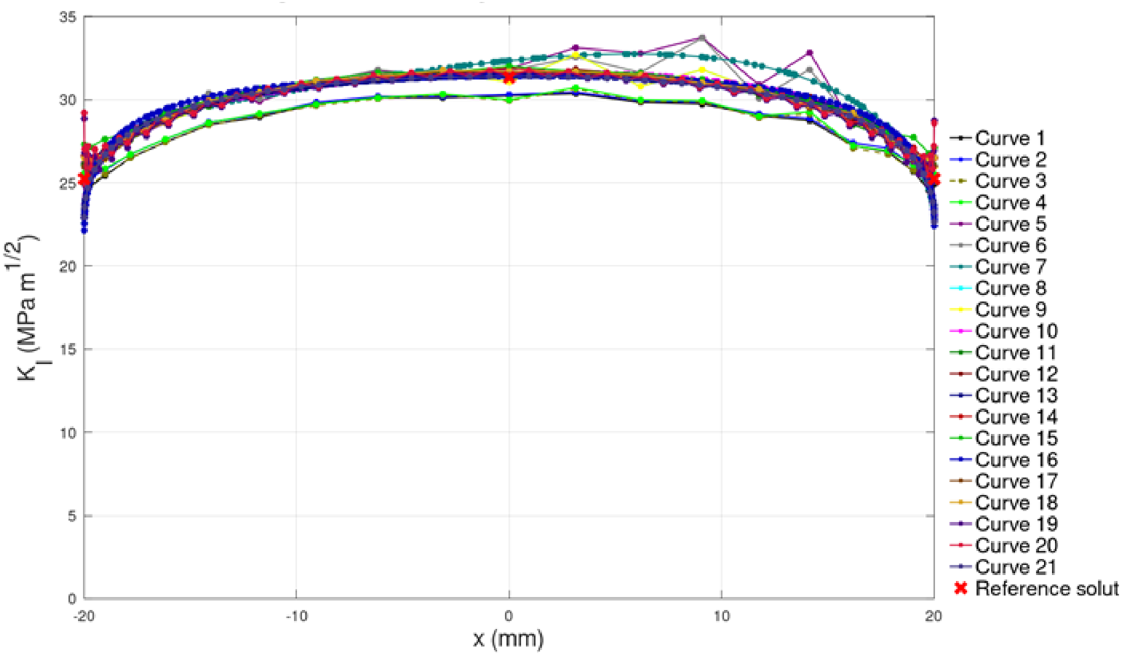

Figure B.8. Participant 7 – Benchmark A1

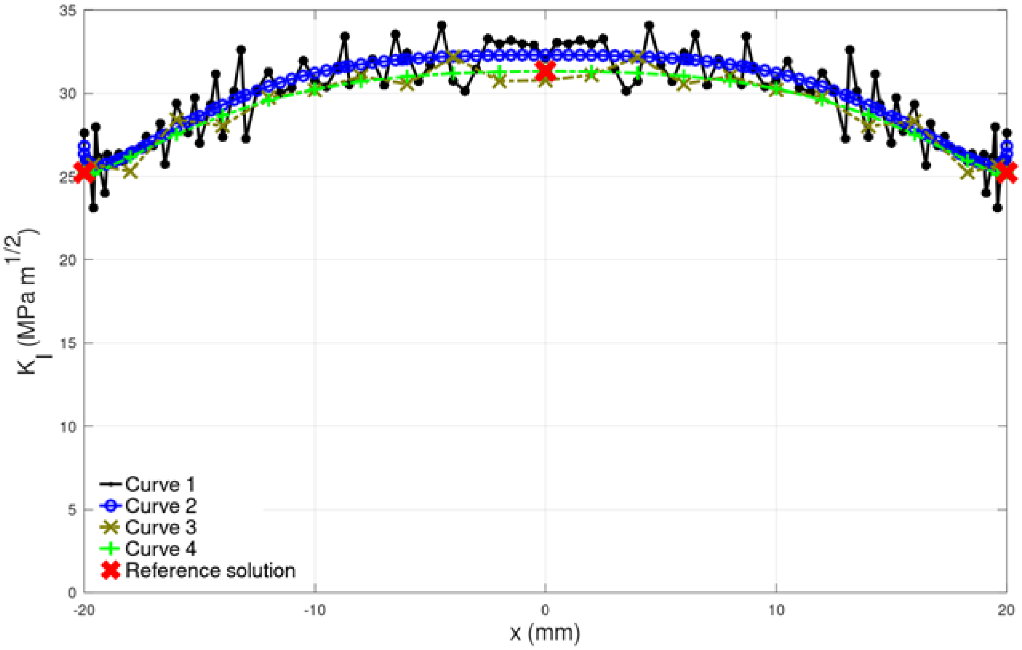

Figure B.9. Participant 8 – Benchmark A1

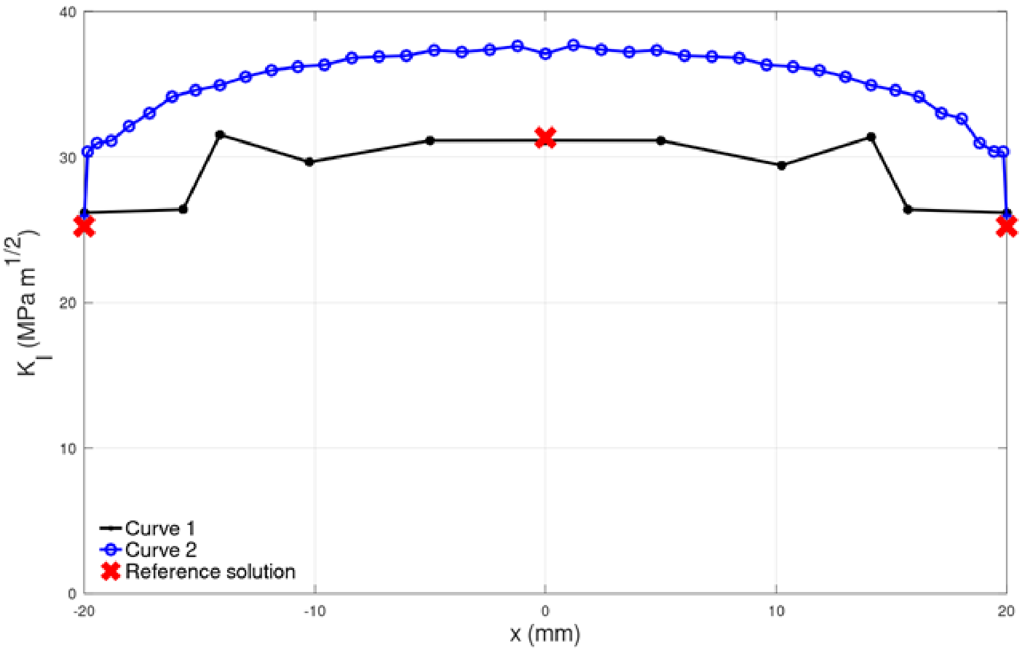

Figure B.10. Participant 9 – Benchmark A1

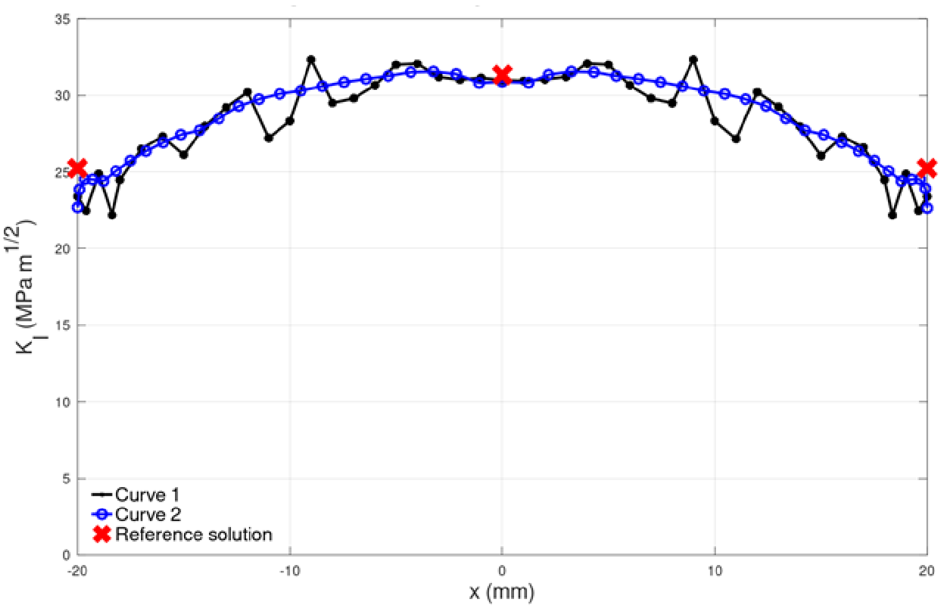

Figure B.11. Participant 10 – Benchmark A1

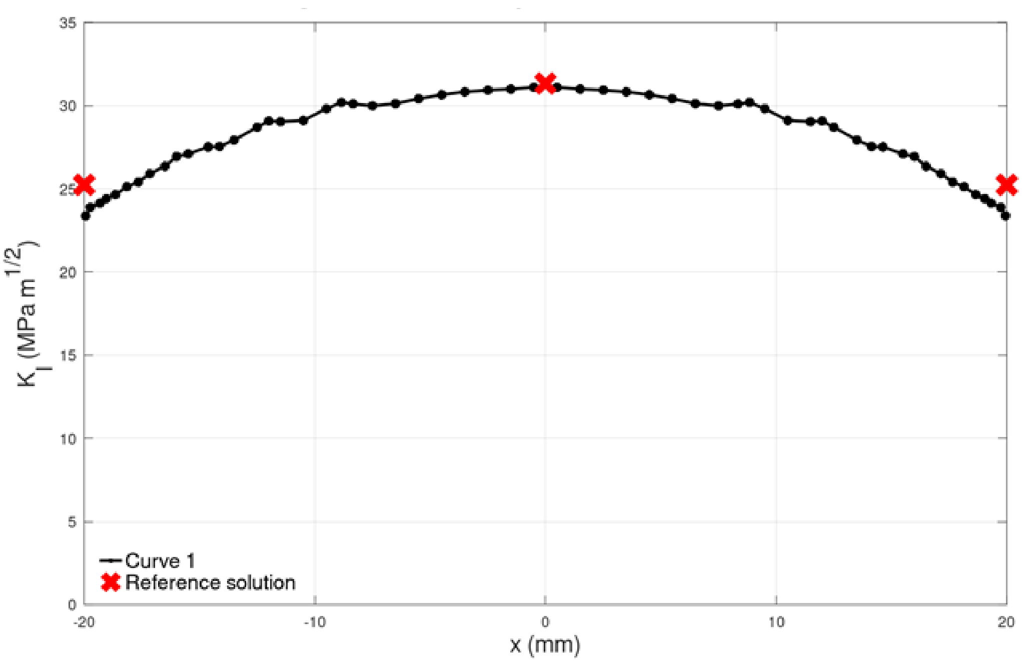

Figure B.12. Participant 11 – Benchmark A1

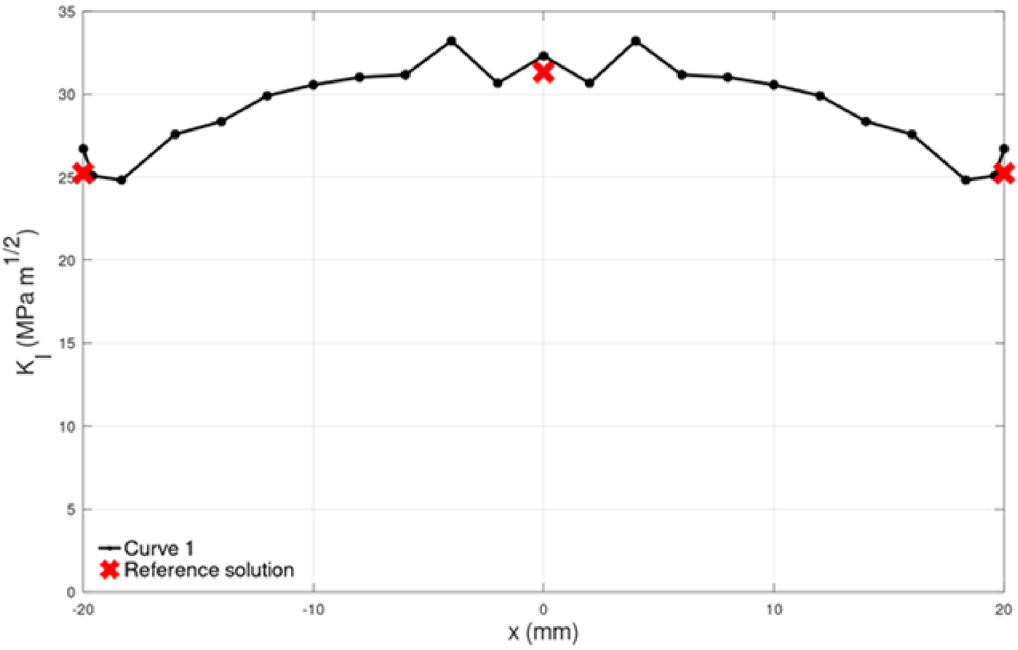

Figure B.13. Participant 12 – Benchmark A1

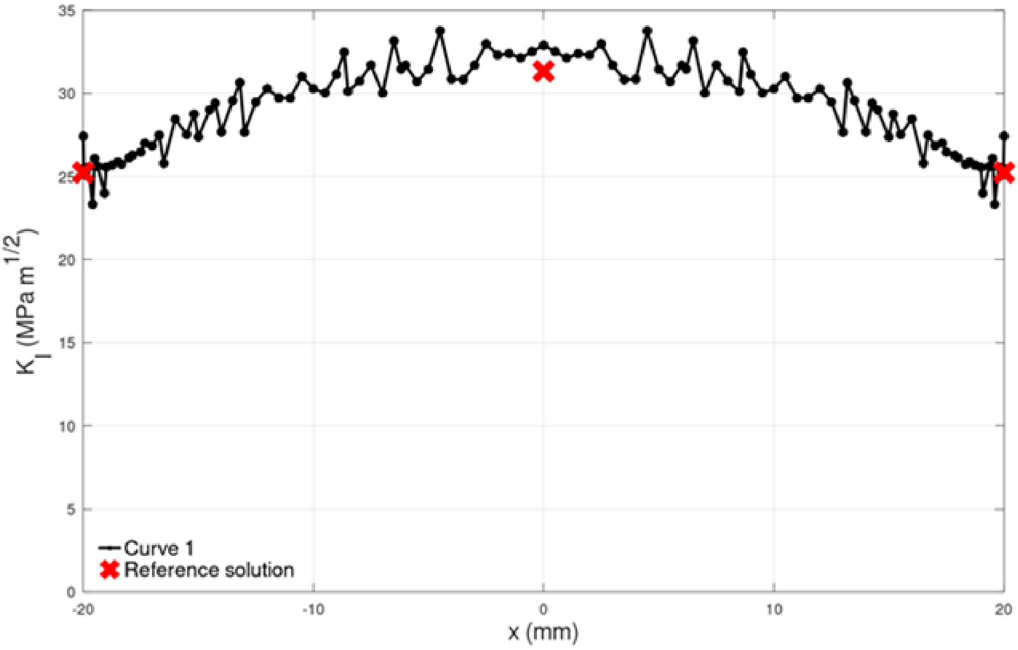

Figure B.14. Participant 13 – Benchmark A1

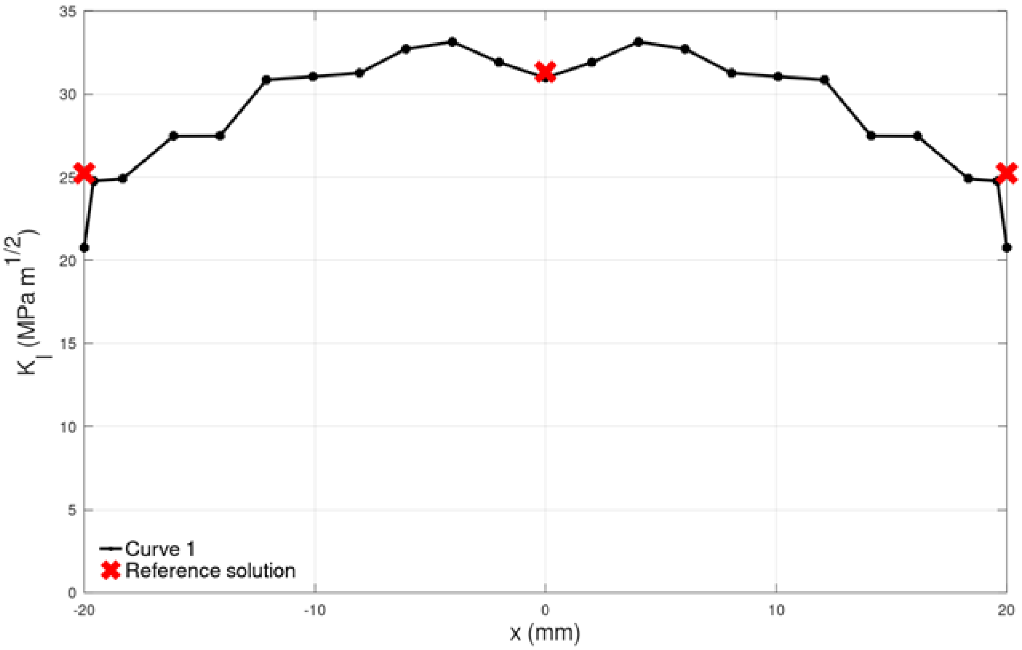

Figure B.15. Participant 14 – Benchmark A1

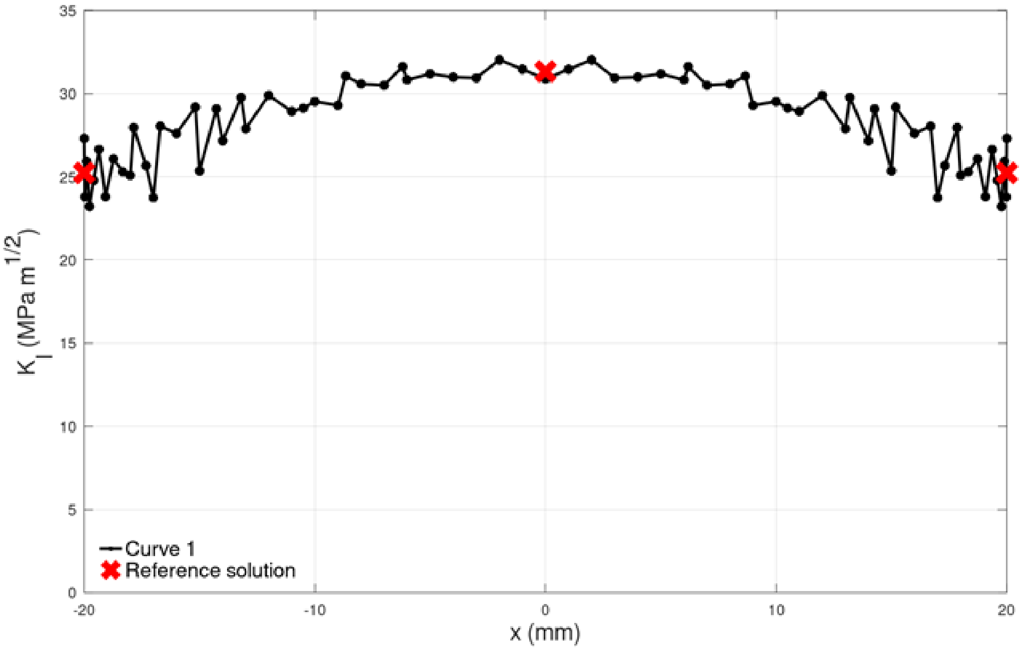

Figure B.16. Participant 15 – Benchmark A1

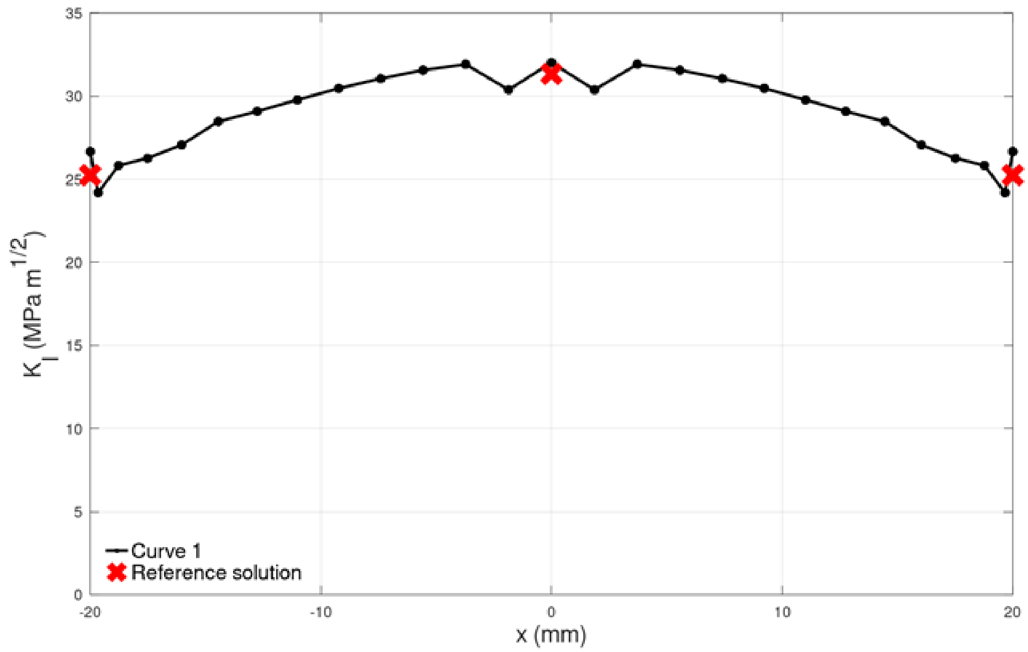

Figure B.17. Participant 16 – Benchmark A1

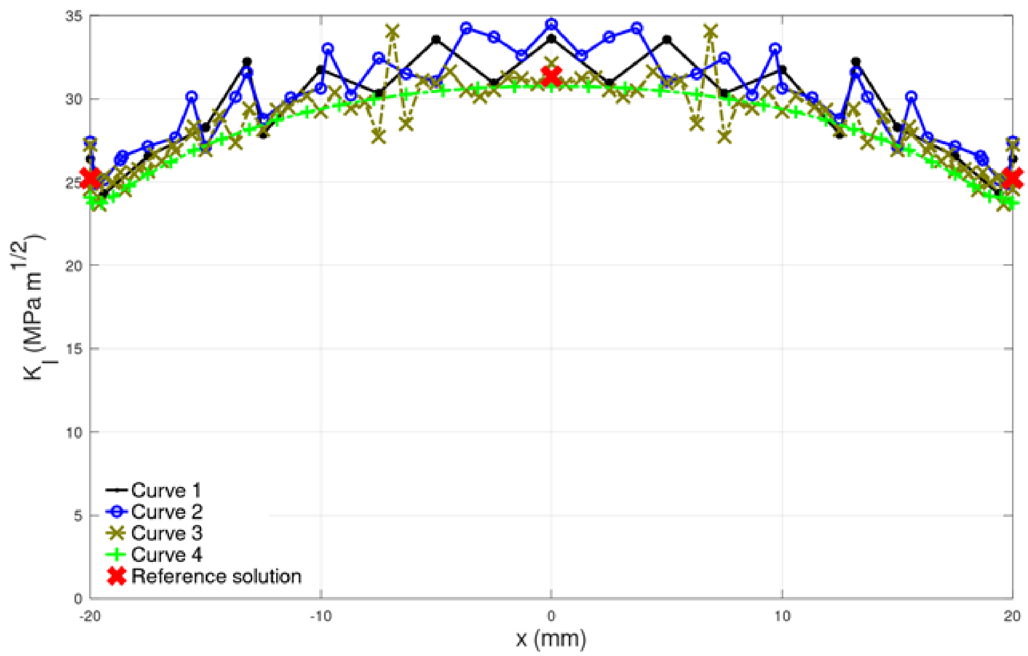

Figure B.18. Participant 17 – Benchmark A1

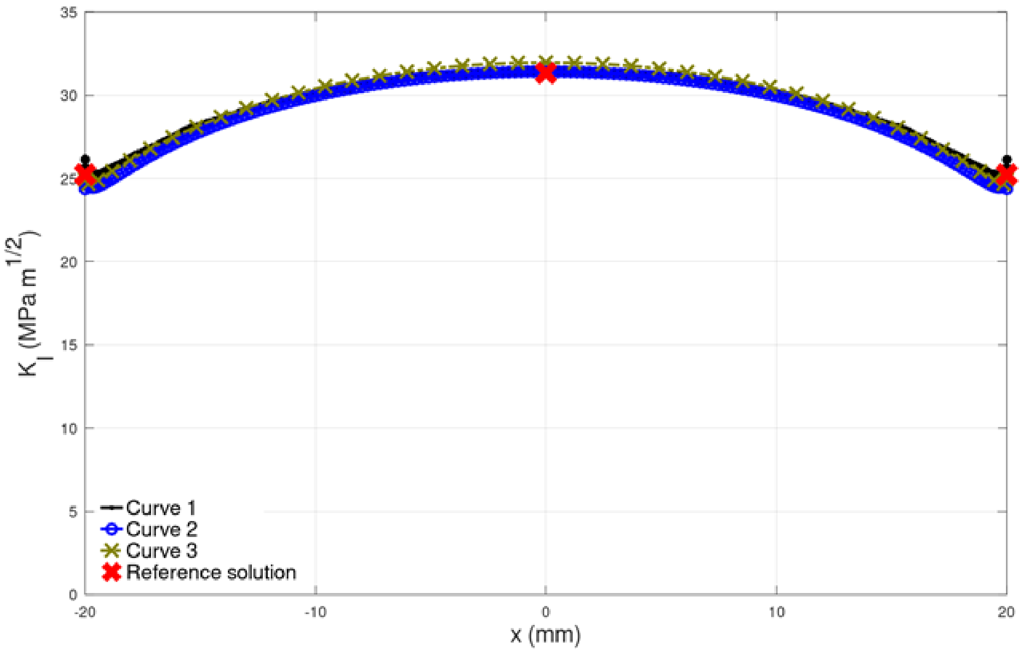

Figure B.19. Participant 18 – Benchmark A1

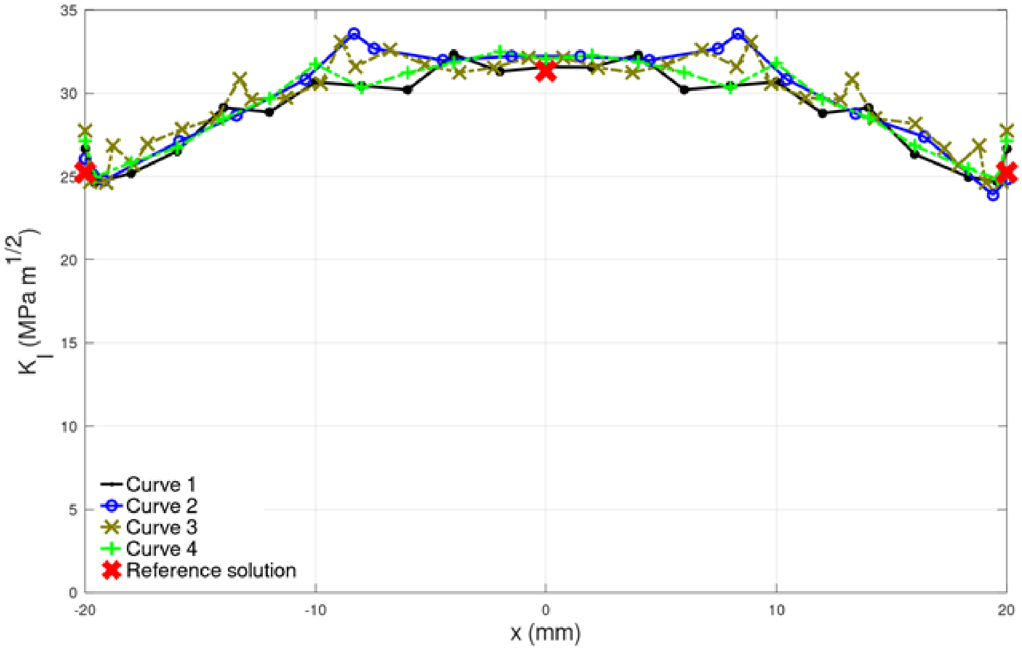

Figure B.20. Participant 18 – Benchmark A1 - Mesh 1

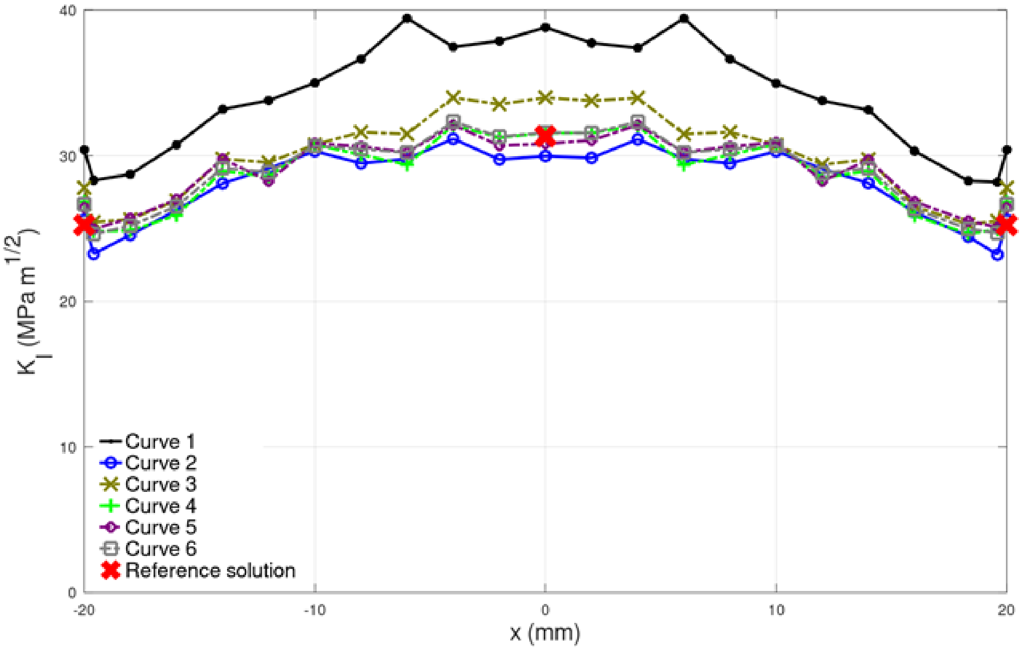

Figure B.21. Participant 18 – Benchmark A1 - Mesh 2

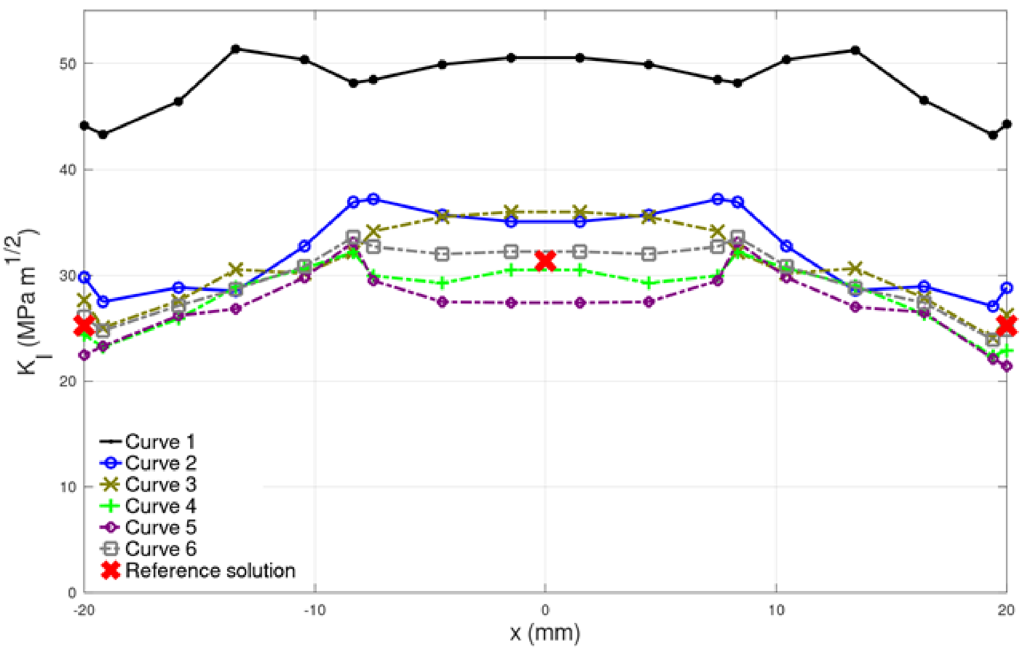

Figure B.22. Participant 18 – Benchmark A1 - Mesh 3

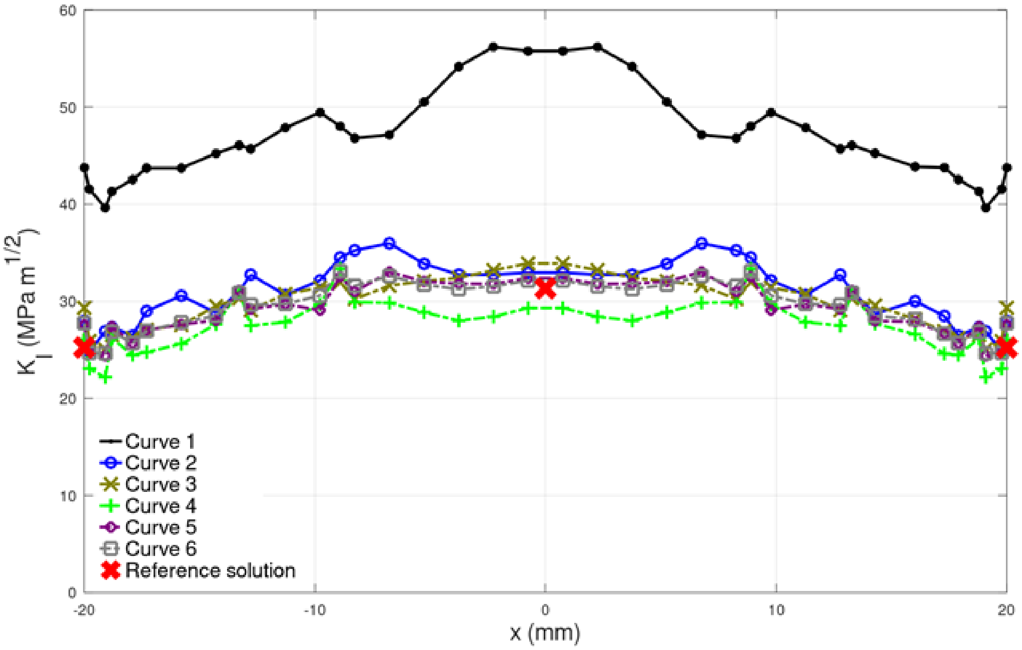

Figure B.23. Participant 18 – Benchmark A1 - Mesh 4

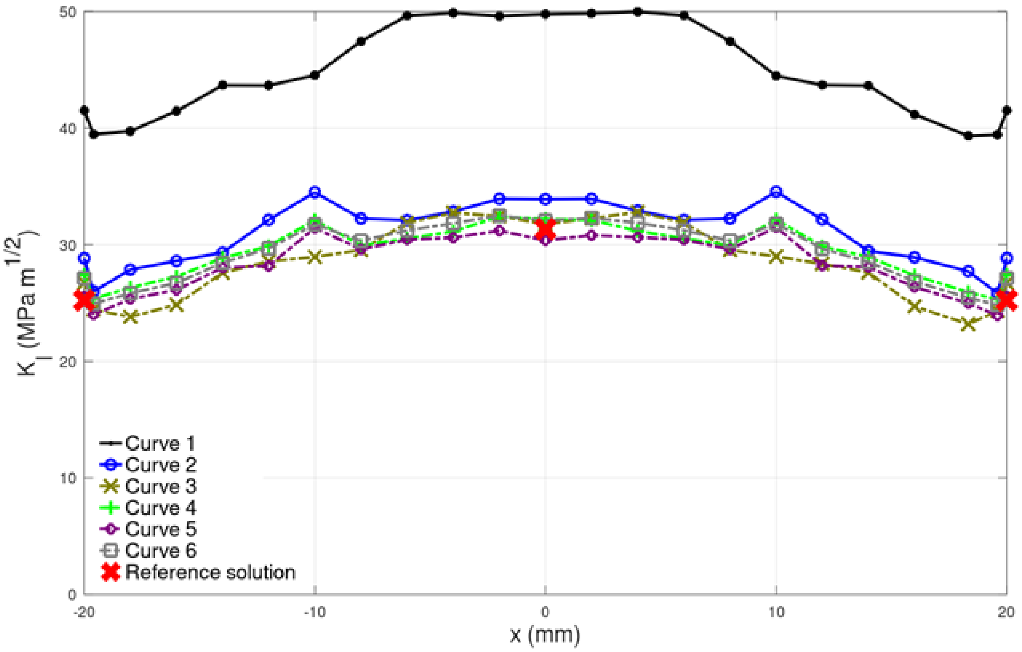

Annex C. Resulting graphs for benchmark A2

Figure C.1. Summary data for all participants on benchmark A2

Figure	Participant	Code	Curve	Mesh element: Order	Mesh element: type	Mesh element: target size (ratio to crack depth a)	SIF calculation method	More information
C.1	1	Abaqus	Curve 1	Linear	Hexahedral	1/20	Integral	
C.2	2	Morfeo crack	Curve 1	Quadratic	Tetrahedral	1/10	Integral	
C.3	3	Abaqus	Curve 1	Linear	Hexahedral	1/10	Integral	
		Ansys	Curve 2	Linear	Hexahedral	1/10		Regular mesh
C.4	4	Code-Aster	Curve 1	Quadratic	Tetrahedral	1/10	Integral	Integration domain: R_{min} = 4 mm; R_{max} = 8 mm
			Curve 2					Integration domain: R_{min} = 0,4 mm; R_{max} = 2 mm
			Curve 3					Integration domain: R_{min} = 0,4 mm; R_{max} = 5 mm
			Curve 4			1/20	Integral	Integration domain: R_{min} = 2,8 mm; R_{max} = 5,7 mm
			Curve 5					Integration domain: R_{min} = 0,4 mm; R_{max} = 1,5 mm
			Curve 6					Integration domain: R_{min} = 0,4 mm; R_{max} = 2,5 mm
			Curve 7					Integration domain: R_{min} = 0,4 mm; R_{max} = 5 mm
C.5	5	Systus	Curve 1	Quadratic	Hexahedral	1/10	Integral	Integration domain: R_{min} = 0,5 mm; R_{max} = 2 mm / XY and YZ symmetry used
			Curve 2					Integration domain: R_{min} = 0,5 mm; R_{max} = 3 mm / XY and YZ symmetry used
			Curve 3					Integration domain: R_{min} = 0,5 mm; R_{max} = 4 mm / XY and YZ symmetry used
C.6	6	Code-Aster	Curve 1	Quadratic	Hexahedral	1/20	Integral	Integration domain: R_{min} = 1 mm; R_{max} = 2 mm / geometrical crack-tip enrichment / 5 refinement steps (XQ5HG mesh)
			Curve 2					Integration domain: R_{min} = 1 mm; R_{max} = 3 mm / geometrical crack-tip enrichment / 5 refinement steps (XQ5HG mesh)
			Curve 3					Integration domain: R_{min} = 1 mm; R_{max} = 2 mm / geometrical crack-tip enrichment / 5 refinement steps (XQ5HG mesh) / integral method with Legendre polynomials
		Code-Aster (FEM)	Curve 4		Tetrahedral	1/25		Integration domain: R_{min} = 0,8 mm; R_{max} = 1,6 mm / Zcrack integral method
			Curve 5					Integration domain: R_{min} = 0,8 mm; R_{max} = 2,4 mm / Zcrack integral method
C.7	7	Abaqus	Curve 1	Linear	Hexahedral	1/10	Integral	
			Curve 2					Curve 2 is a polynomial fit (degree 6) of the data points from Curve 1
			Curve 3			1/5		
			Curve 4					Curve 4 is a polynomial fit (degree 6) of the data points from Curve 3
C.8	8	Abaqus	Curve 1	Linear	Hexahedral	1/2	Integral	
			Curve 2			1/10		
C.9	9	Abaqus	Curve 1	Linear	Hexahedral	1/10	Integral	Element size at crack tip varying from 1 mm to 2 mm
			Curve 2	Linear	Hexahedral	1/10		Element size at crack tip varying from 0,9 mm to 1,3 mm
C.10	10	NLXFEM3Dstruct	Curve 1	Linear	Hexahedral	1/10	Integral	

Figure	Participant	Code	Curve	Mesh element			SIF calculation method	More information
				Order	type	target size (ratio to crack depth a)		
C.11	11	Abaqus	Curve 1	Linear	Hexahedral	1/5	Integral	
C.12	12	Abaqus	Curve 1	Linear	Hexahedral	1/20	Displacement	
C.13	13	Abaqus	Curve 1	Linear	Hexahedral	1/5	Integral	
C.14	14	Abaqus	Curve 1	Linear	Hexahedral	1/20	Integral	
C.15	15	Abaqus	Curve 1	Linear	Hexahedral	1/5	Integral	
C.16	16	Abaqus	Curve 1	Linear	Hexahedral	1/4	Integral	
			Curve 2			1/8		
			Curve 3			1/16		
		Abaqus (FEM)	Curve 4			1/4		
C.17	17	Abaqus	Curve 1	Linear	Hexahedral	1/33	Integral	
		Abaqus (FEM)	Curve 2					
		Theory of Raju-Newman	Curve 3					
C.18	18	Abaqus	Curve 1	Linear	Hexahedral	1/5	Integral	Results present average of 5 integration domains / Crack plane on element face
			Curve 2			1/3		Results present average of 5 integration domains / Crack plane in middle of element
			Curve 3			3/20		Results present average of 5 integration domains / Crack plane in middle of element
C.19	18	Abaqus	Curve 1	Linear	Hexahedral	1/5	Integral	Integration domain 1 (domain not specified, but increasing from 1 to 5) / Crack plane on element face
			Curve 2					Integration domain 2 (domain not specified, but increasing from 1 to 5) / Crack plane on element face
			Curve 3					Integration domain 3 (domain not specified, but increasing from 1 to 5) / Crack plane on element face
			Curve 4					Integration domain 4 (domain not specified, but increasing from 1 to 5) / Crack plane on element face
			Curve 5					Integration domain 5 (domain not specified, but increasing from 1 to 5) / Crack plane on element face
			Curve 6					Resuls present average of the 5 integration domains / Crack plane on element face

Figure	Participant	Code	Curve	Mesh element			SIF calculation method	More information
				Order	type	target size (ratio to crack depth a)		
C.20	18	Abaqus	Curve 1	Linear	Hexahedral	1/3	Integral	Integration domain 1 (domain not specified, but increasing from 1 to 5) / Crack plane in middle of element
			Curve 2					Integration domain 2 (domain not specified, but increasing from 1 to 5) / Crack plane in middle of element
			Curve 3					Integration domain 3 (domain not specified, but increasing from 1 to 5) / Crack plane in middle of element
			Curve 4					Integration domain 4 (domain not specified, but increasing from 1 to 5) / Crack plane in middle of element
			Curve 5					Integration domain 5 (domain not specified, but increasing from 1 to 5) / Crack plane in middle of element
			Curve 6					Results present average of the 5 integration domains / Crack plane in middle of element
C.21	18	Abaqus	Curve 1	Linear	Hexahedral	3/20	Integral	Integration domain 1 (domain not specified, but increasing from 1 to 5) / Crack plane in middle of element
			Curve 2					Integration domain 2 (domain not specified, but increasing from 1 to 5) / Crack plane in middle of element
			Curve 3					Integration domain 3 (domain not specified, but increasing from 1 to 5) / Crack plane in middle of element
			Curve 4					Integration domain 4 (domain not specified, but increasing from 1 to 5) / Crack plane in middle of element
			Curve 5					Integration domain 5 (domain not specified, but increasing from 1 to 5) / Crack plane in middle of element
			Curve 6					Results present average of the 5 integration domains / Crack plane in middle of element

Figure C.2. Participant 1 – Benchmark A2

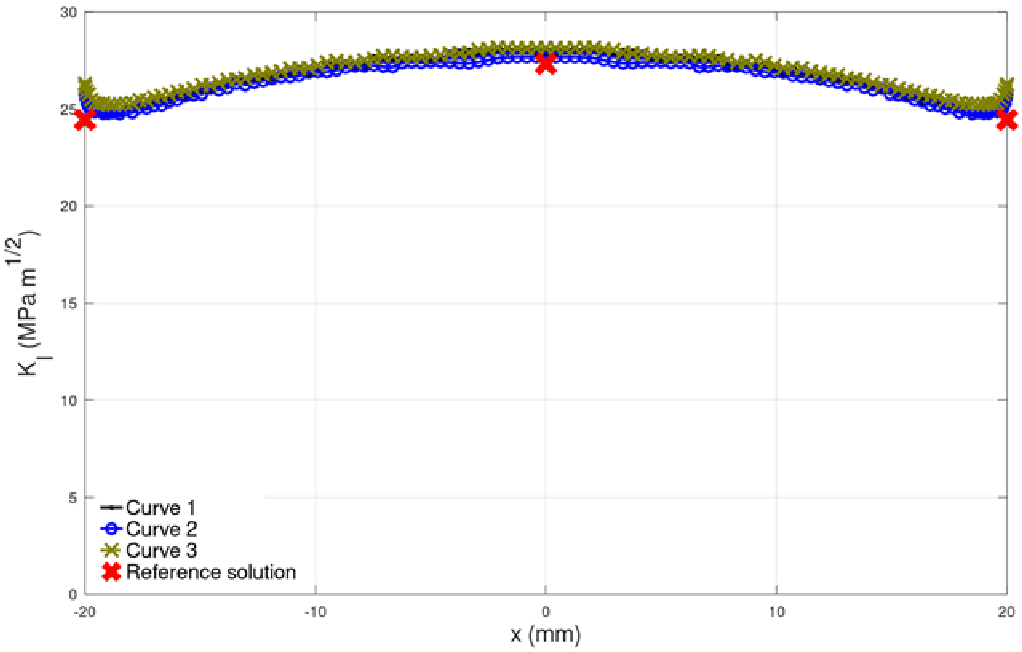

Figure C.3. Participant 2 – Benchmark A2

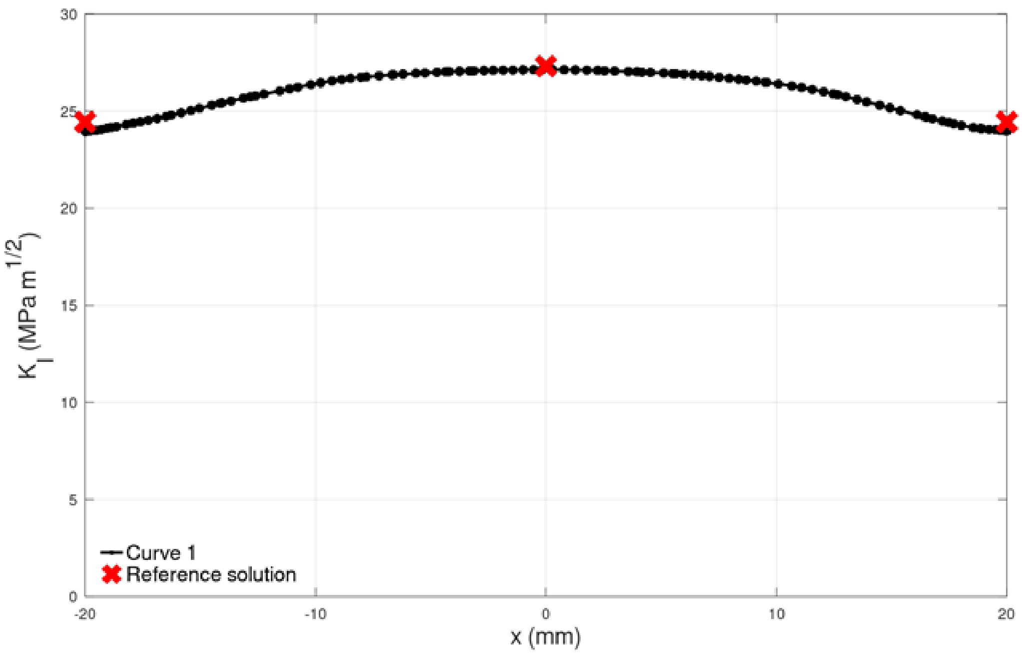

Figure C.4. Participant 3 – Benchmark A2

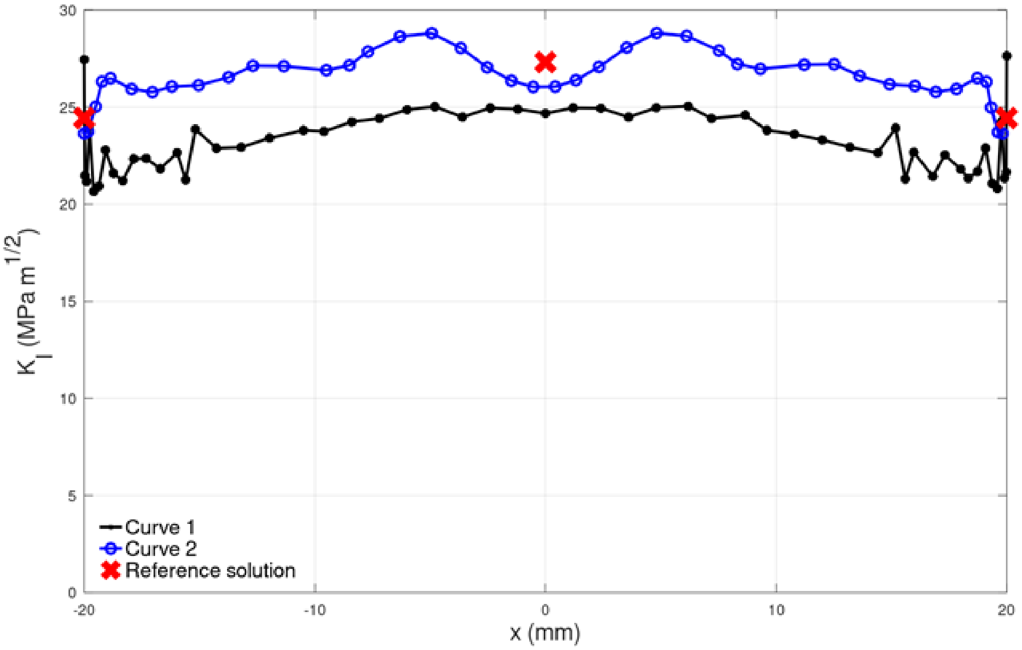

Figure C.5. Participant 4 – Benchmark A2

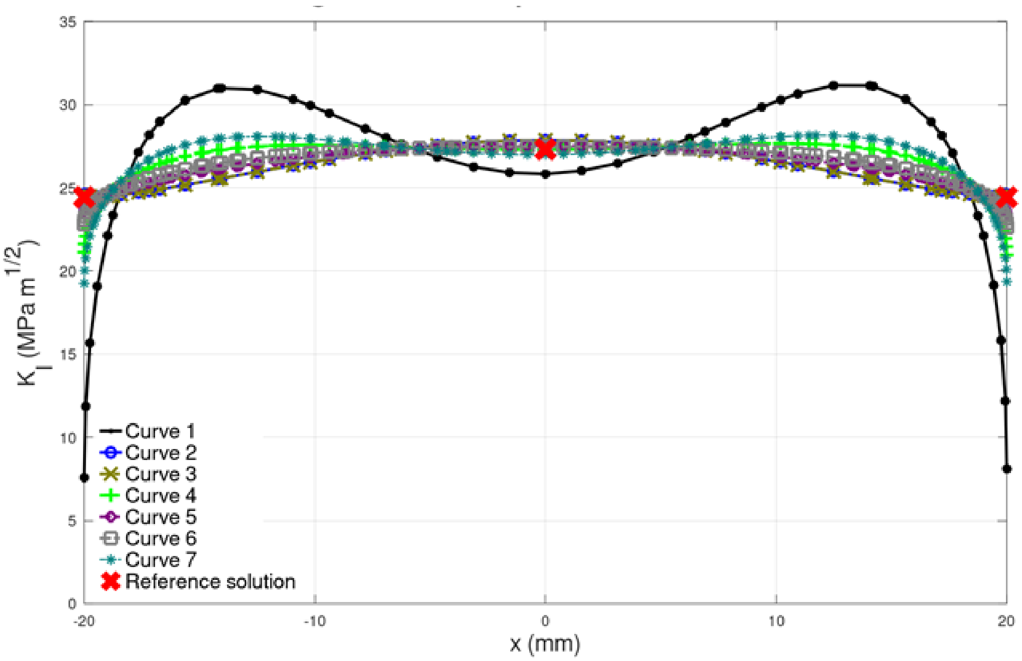

Figure C.6. Participant 5 – Benchmark A2

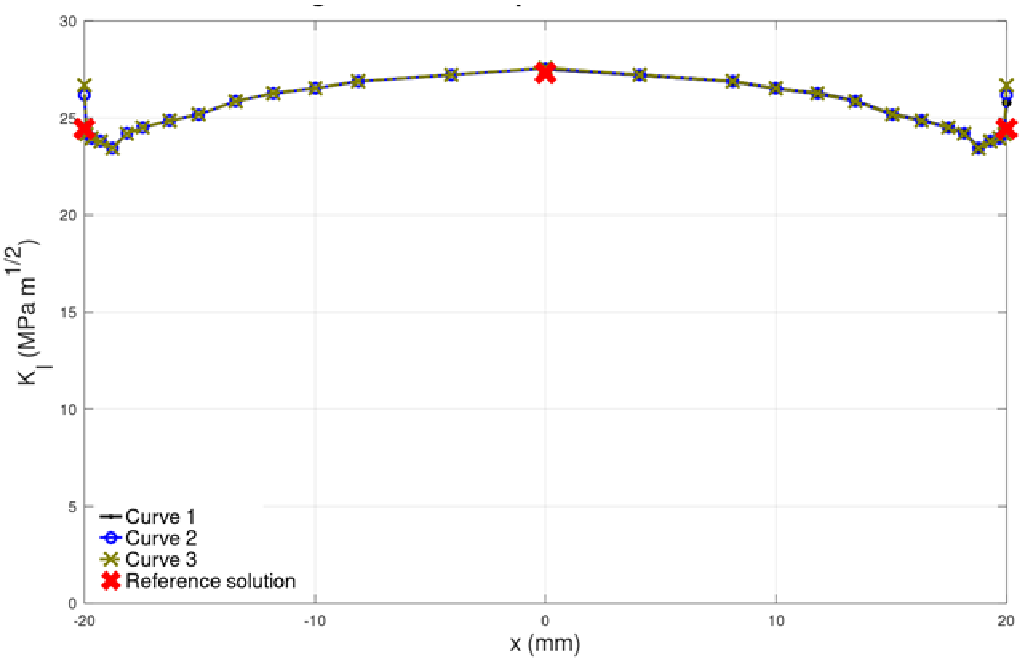

Figure C.7. Participant 6 – Benchmark A2

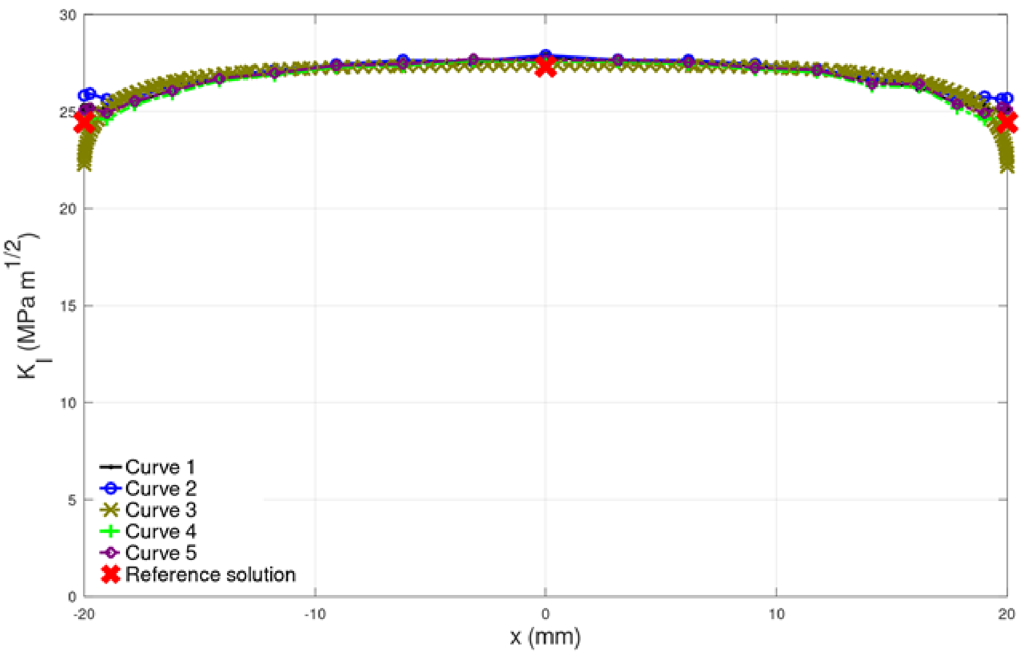

Figure C.8. Participant 7 – Benchmark A2

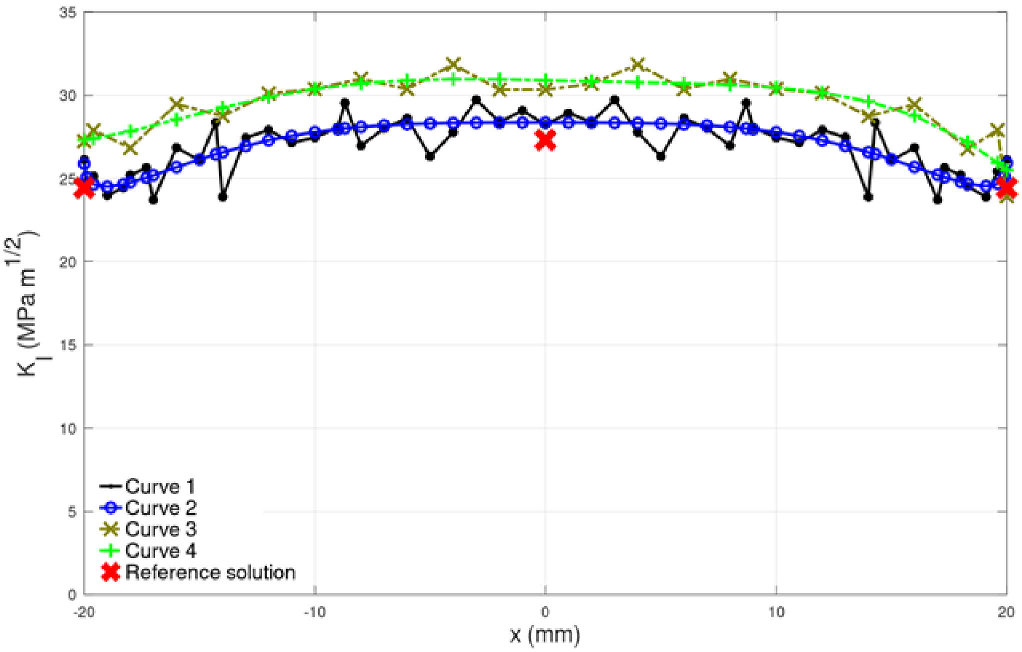

Figure C.9. Participant 8 – Benchmark A2

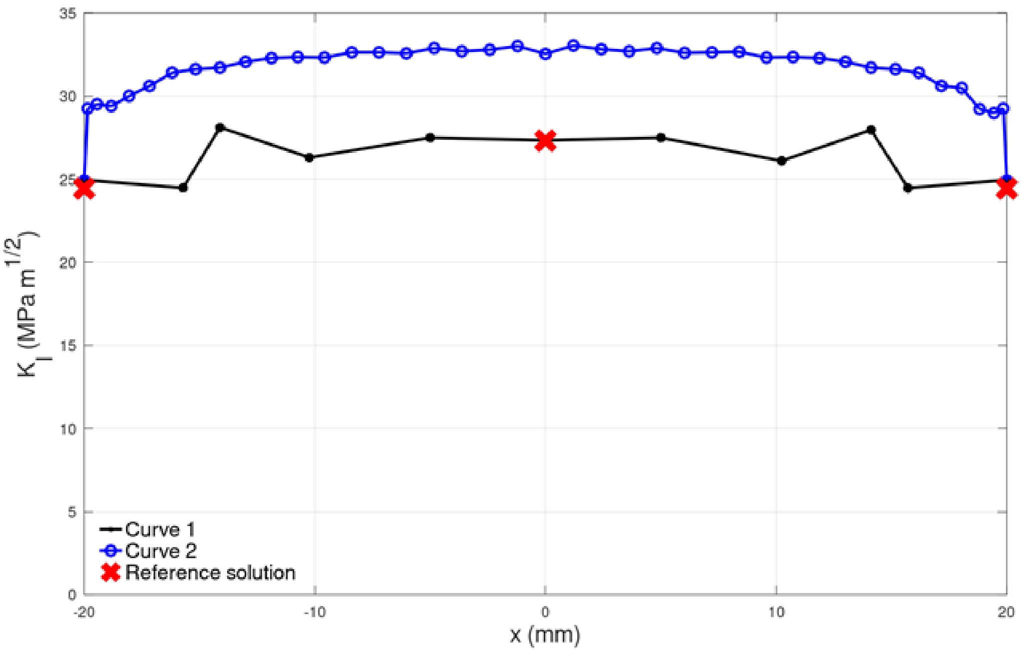

Figure C.10. Participant 9 – Benchmark A2

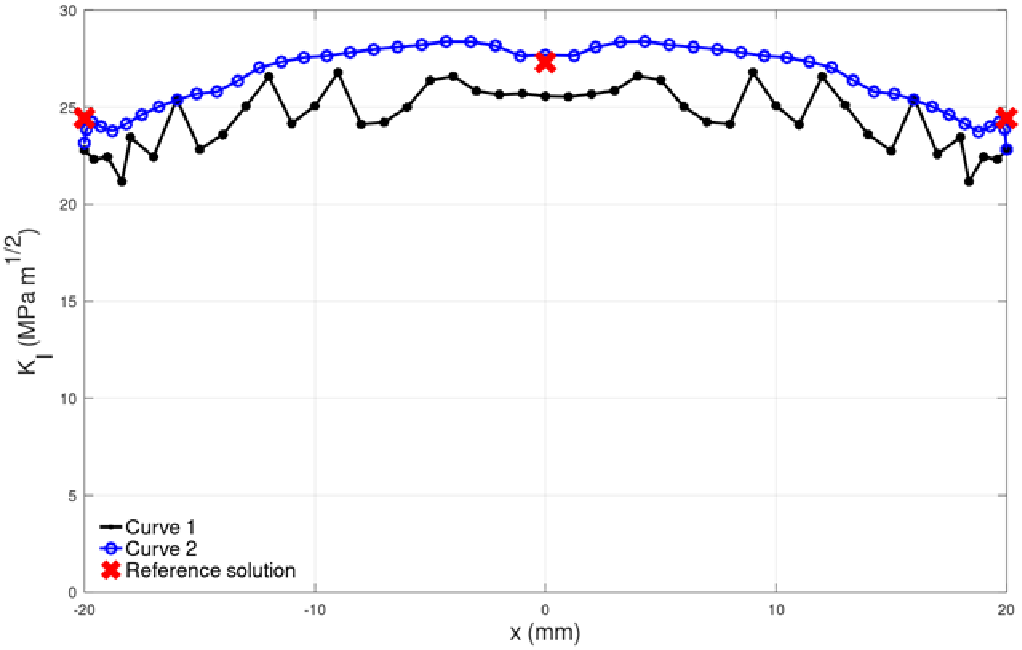

Figure C.11. Participant 10 – Benchmark A2

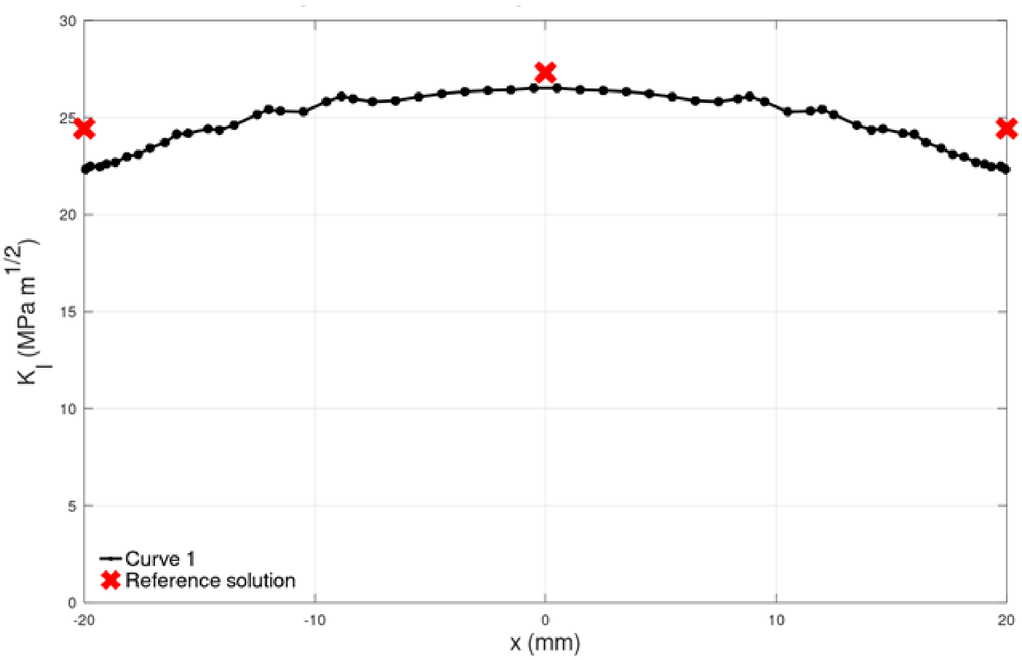

Figure C.12. Participant 11 – Benchmark A2

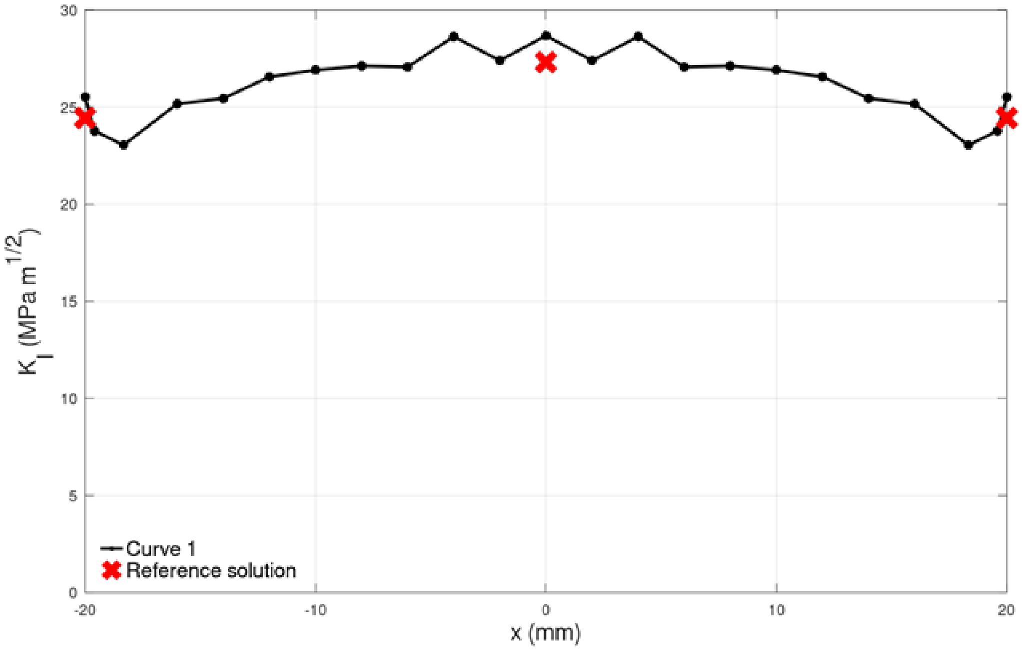

Figure C.13. Participant 12 – Benchmark A2

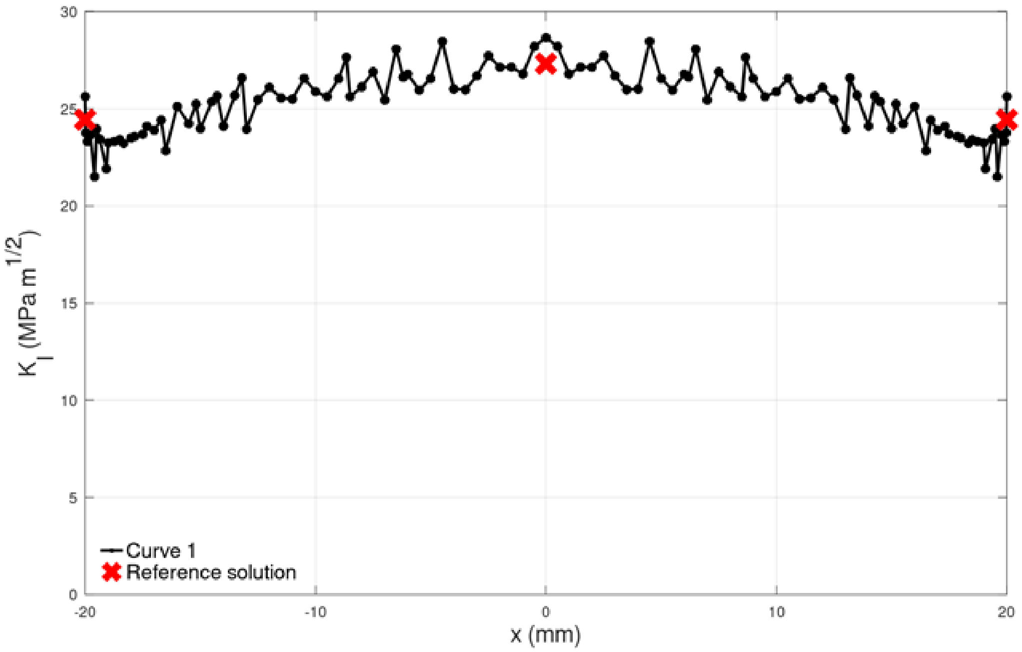

Figure C.14. Participant 13 – Benchmark A2

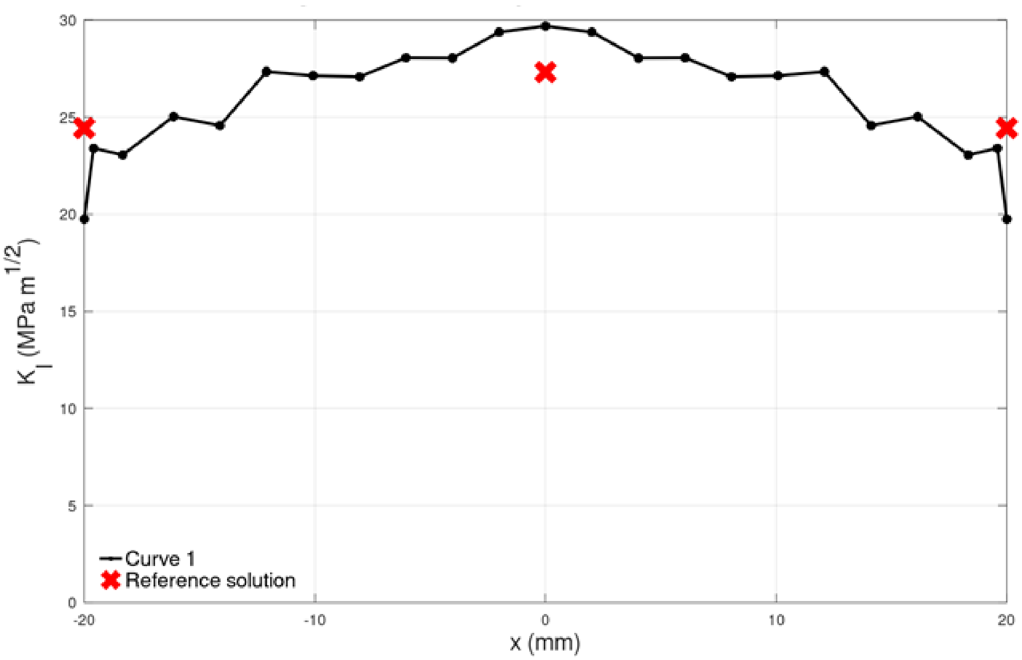

Figure C.15. Participant 14 – Benchmark A2

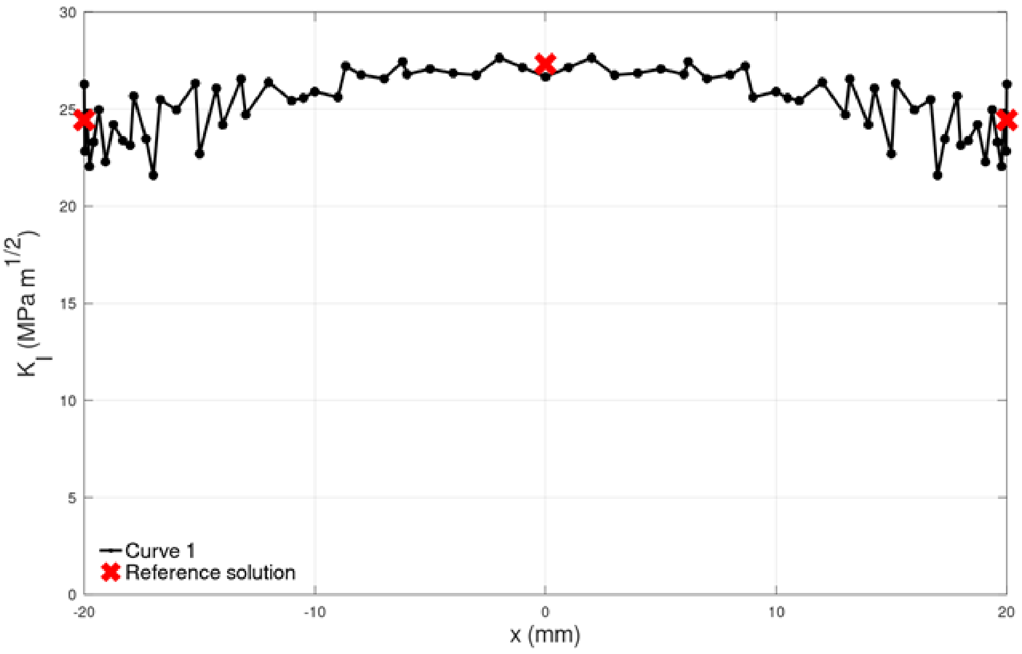

Figure C.16. Participant 15 – Benchmark A2

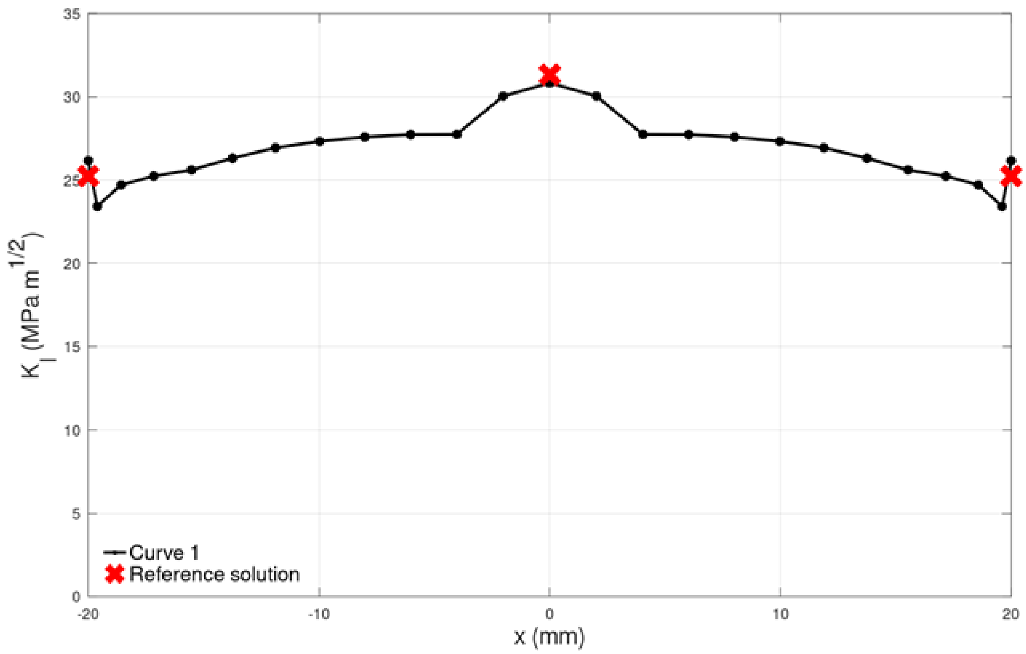

Figure C.17. Participant 16 – Benchmark A2

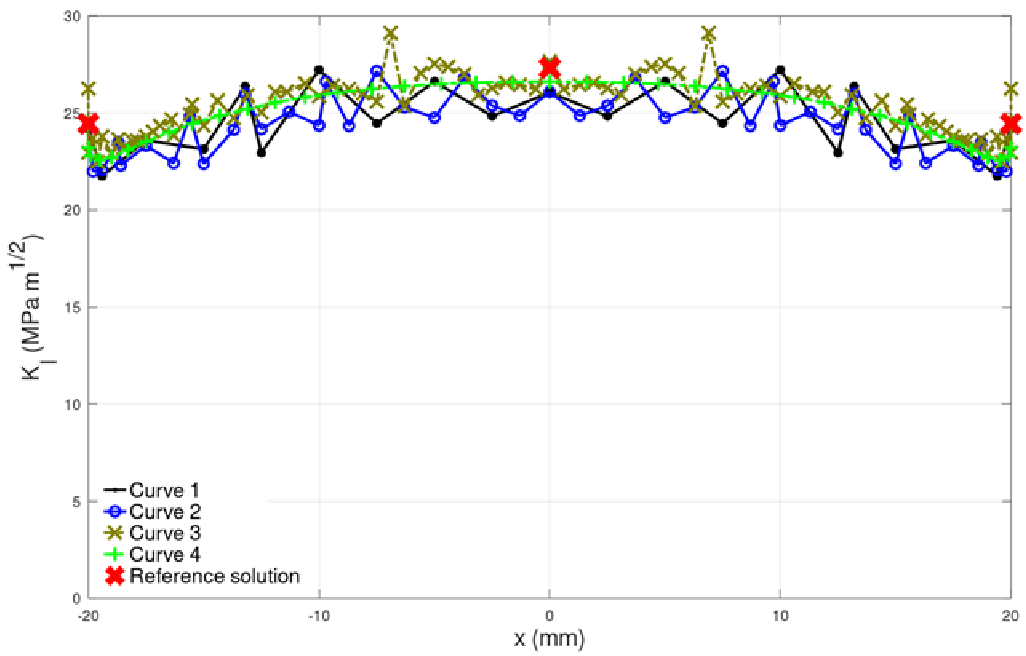

Figure C.18. Participant 17 – Benchmark A2

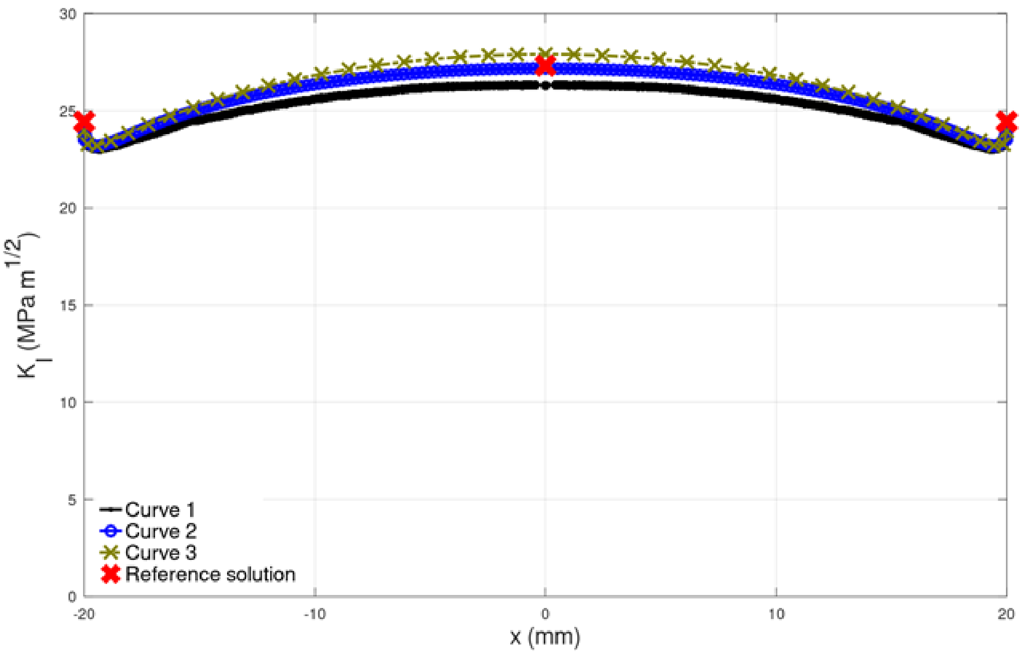

Figure C.19. Participant 18 – Benchmark A2

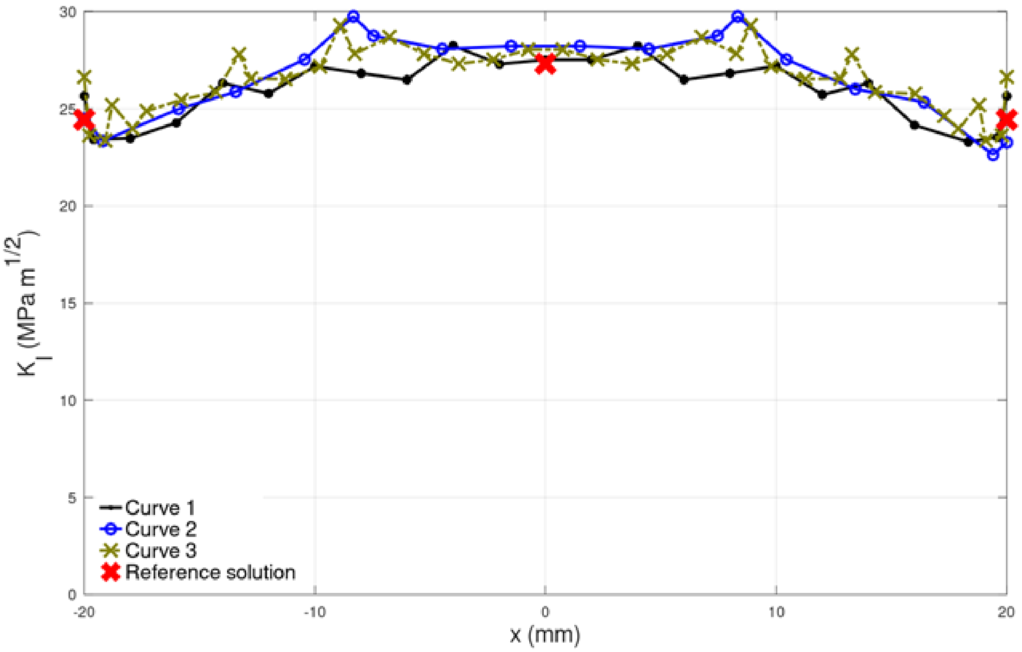

Figure C.20. Participant 18 – Benchmark A2 – Mesh 1

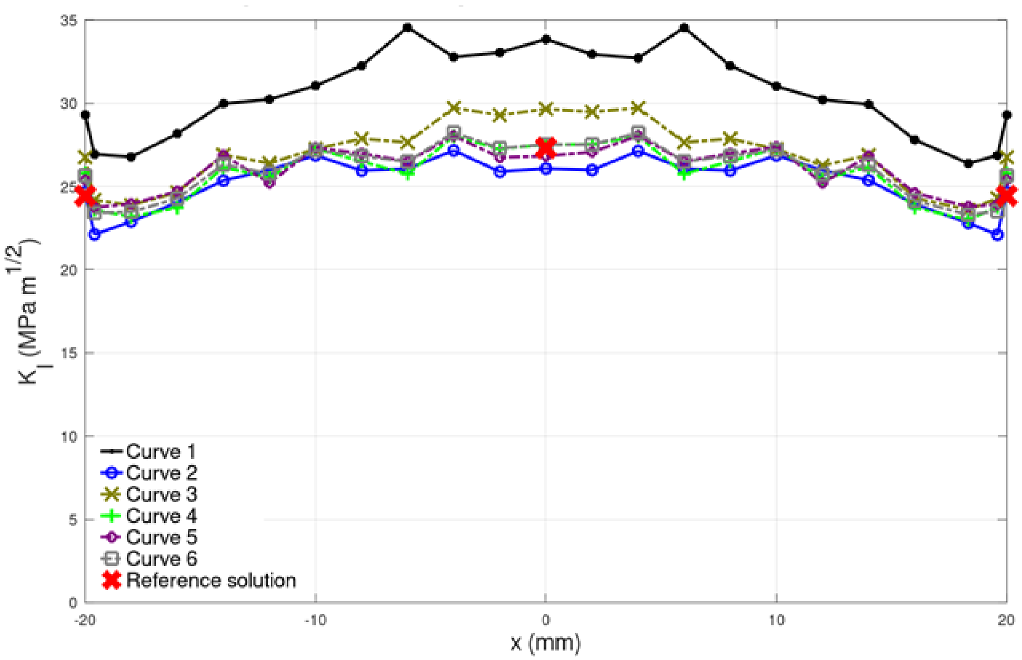

Figure C.21. Participant 18 – Benchmark A2 – Mesh 2

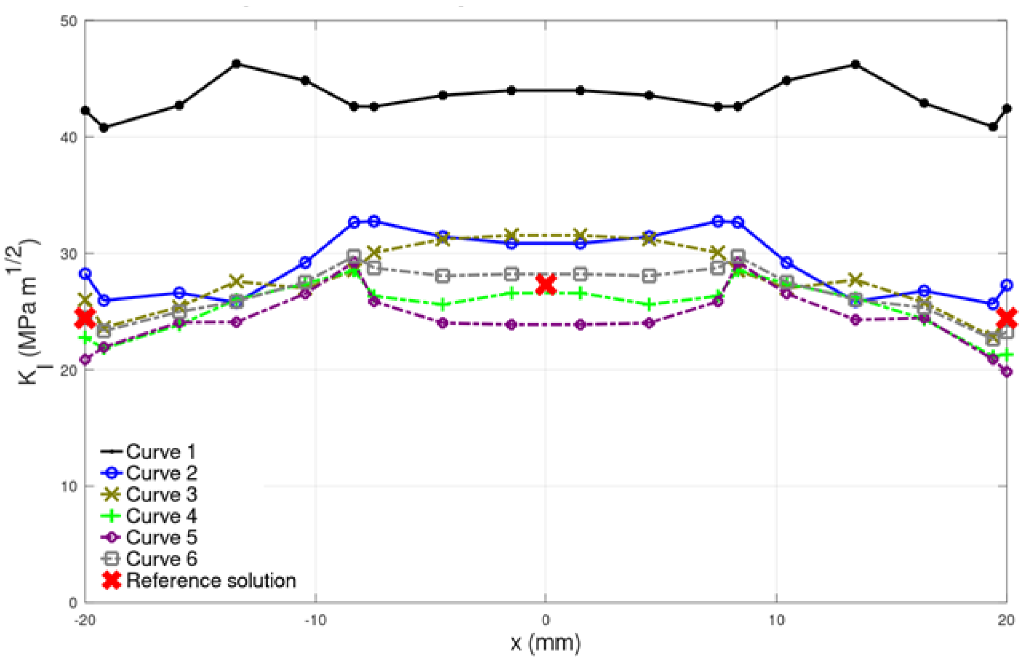

Figure C.22. Participant 18 – Benchmark A2 – Mesh 3

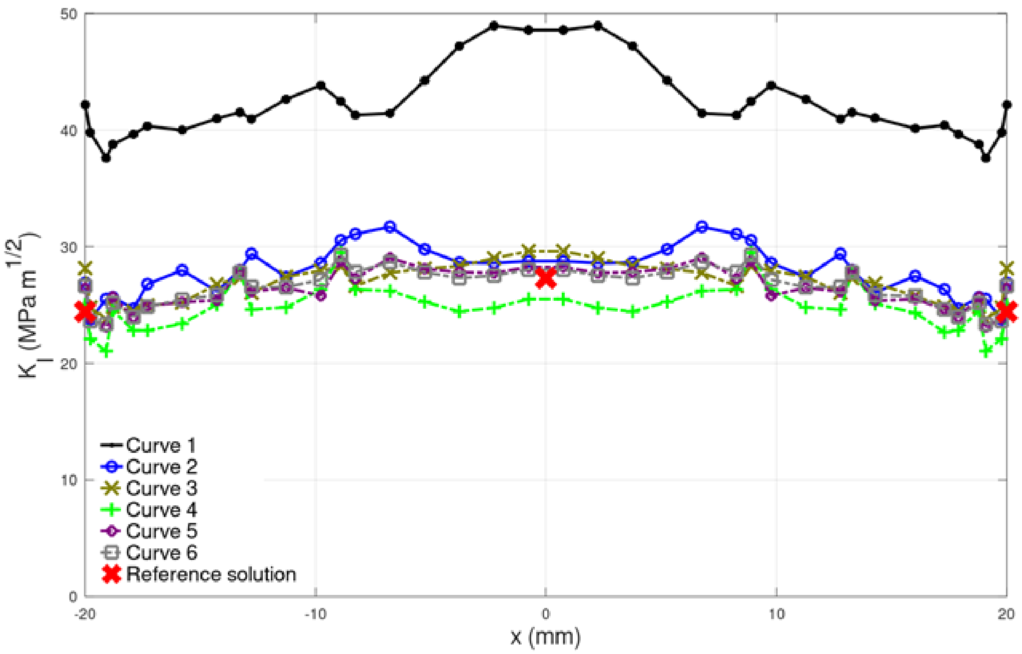

Annex D. Resulting graphs for benchmark A3

Figure D.1. Summary data for all participants on benchmark A3

Figure	Participant	Code	Curve	Mesh element: Order	Mesh element: type	Mesh element: target size (ratio to crack depth a)	SIF calculation method	More information
D.1	2	Morfeo crack	Curve 1	Quadratic	Tetrahedral	1/10	Integral	
D.2	3	Ansys	Curve 1	Linear	Hexahedral	1/10	Integral	
D.3	4	Code-Aster	Curve 1	Quadratic	Tetrahedral	1/5	Displacement	
			Curve 2			1/5	Integral	
			Curve 3			1/10	Displacement	
D.4	5	Systus	Curve 1	Quadratic	Hexahedral	1/10	Integral	Integration domain: R_{min} = 0,5 mm; R_{max} = 2 mm / XY and YZ symmetry used
			Curve 2					Integration domain: R_{min} = 0,5 mm; R_{max} = 3 mm / XY and YZ symmetry used
			Curve 3					Integration domain: R_{min} = 0,5 mm; R_{max} = 4 mm / XY and YZ symmetry used
D.5	6	Code-Aster	Curve 1	Quadratic	Hexahedral	1/20		Geometrical crack-tip enrichment / 5 refinement steps (XQ5HG mesh)
		Code-Aster (FEM)	Curve 2		Tetrahedral	1/25		Zcrack integral method
D.6	7	Abaqus	Curve 1	Linear	Hexahedral	1/10	Integral	
			Curve 2					Curve 2 is a polynomial fit (degree 6) of the data points from Curve 1
D.7	8	Abaqus	Curve 1	Linear	Hexahedral	1/2	Integral	
			Curve 2			1/6 to 1/14		
D.8	9	Abaqus	Curve 1	Linear	Hexahedral	1/10	Integral	
D.9	10	NLXFEM3Dheat + NLXFEM3Dstruct	Curve 1	Linear	Hexahedral	1/10	Integral	
D.10	11	Abaqus	Curve 1	Linear	Hexahedral	1/5	Integral	
D.11	12	Abaqus	Curve 1	Linear	Hexahedral	1/20	Displacement	
D.12	13	Abaqus	Curve 1	Linear	Hexahedral	1/5	Integral	
D.13	14	Abaqus	Curve 1	Linear	Hexahedral	1/12,5	Integral	
D.14	15	Abaqus	Curve 1	Linear	Hexahedral	1/5	Integral	Results are evaluated at 60 s in stead of 120 s
D.15	16	Abaqus	Curve 1	Linear	Hexahedral	1/4	Integral	
			Curve 2			1/8		
			Curve 3			1/16		

Figure	Participant	Code	Curve	Mesh element			SIF calculation method	More information
				Order	type	target size (ratio to crack depth a)		
D.16	18	Abaqus	Curve 1	Linear	Hexahedral	1/5	Integral	Integration domain 1 (domain not specified, but increasing from 1 to 5) / Crack plane on element face
			Curve 2					Integration domain 2 (domain not specified, but increasing from 1 to 5) / Crack plane on element face
			Curve 3					Integration domain 3 (domain not specified, but increasing from 1 to 5) / Crack plane on element face
			Curve 4					Integration domain 4 (domain not specified, but increasing from 1 to 5) / Crack plane on element face
			Curve 5					Integration domain 5 (domain not specified, but increasing from 1 to 5) / Crack plane on element face
			Curve 6					Results present average of the 5 integration domains / Crack plane on element face
D.17	4, 5, 6, 7, 8, 9, 10, 11, 12, 14, 16, 18	Multiple codes	Curve 1	This figure plots KI as function of time at point A of the crack, obtained by several participants by calculation or theory. For the details of the calculations, see above				Results obtained by participant 4, by X-FEM calculation (mesh a/5)
			Curve 2					Results obtained by participant 4, by X-FEM calculation (mesh a/10)
			Curve 3					Results obtained by participant 6, by theory
			Curve 4					Results obtained by participant 6, by X-FEM calculation
			Curve 5					Results obtained by participant 5, by theory
			Curve 6					Results obtained by participant 5, by X-FEM calculation
			Curve 7					Results obtained by participant 7, by X-FEM calculation
			Curve 8					Results obtained by participant 8, by X-FEM calculation
			Curve 9					Results obtained by participant 9, by X-FEM calculation
			Curve 10					Results obtained by participant 10, by theory
			Curve 11					Results obtained by participant 10, by X-FEM calculation
			Curve 12					Results obtained by participant 11, by X-FEM calculation
			Curve 13					Results obtained by participant 12, by X-FEM calculation
			Curve 14					Results obtained by participant 14, by X-FEM calculation
			Curve 15					Results obtained by participant 18, by X-FEM calculation
			Curve 16					Results obtained by participant 16, by X-FEM calculation (Mesh a/4)
			Curve 17					Results obtained by participant 16, by X-FEM calculation (Mesh a/8)
			Curve 18					Results obtained by participant 16, by X-FEM calculation (Mesh a/16)

Figure D.2. Participant 2 – Benchmark A3

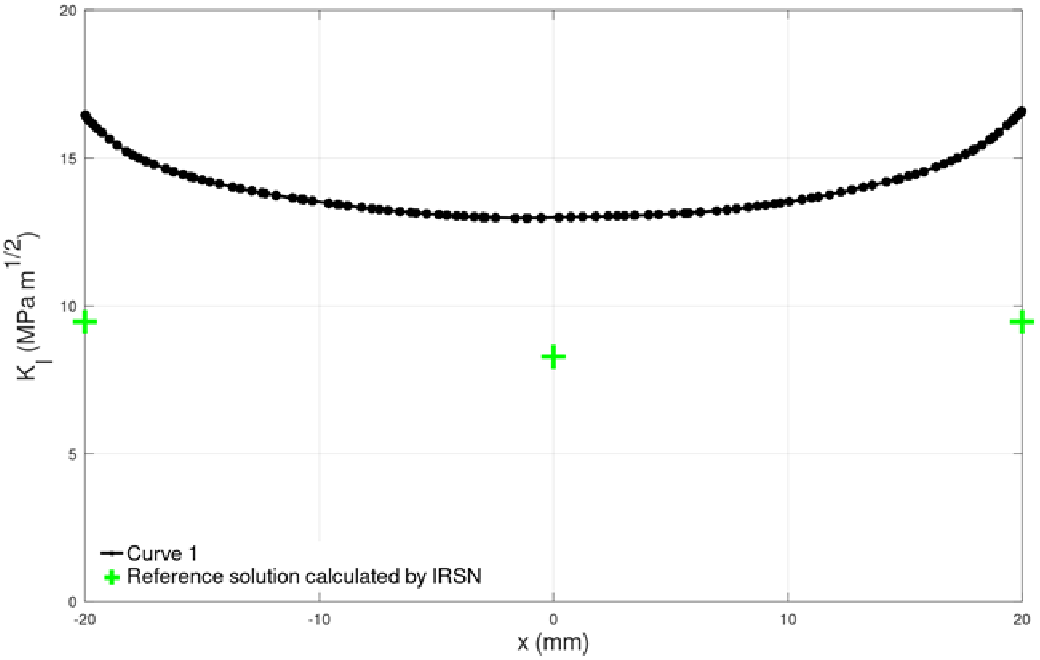

Figure D.3. Participant 3 – Benchmark A3

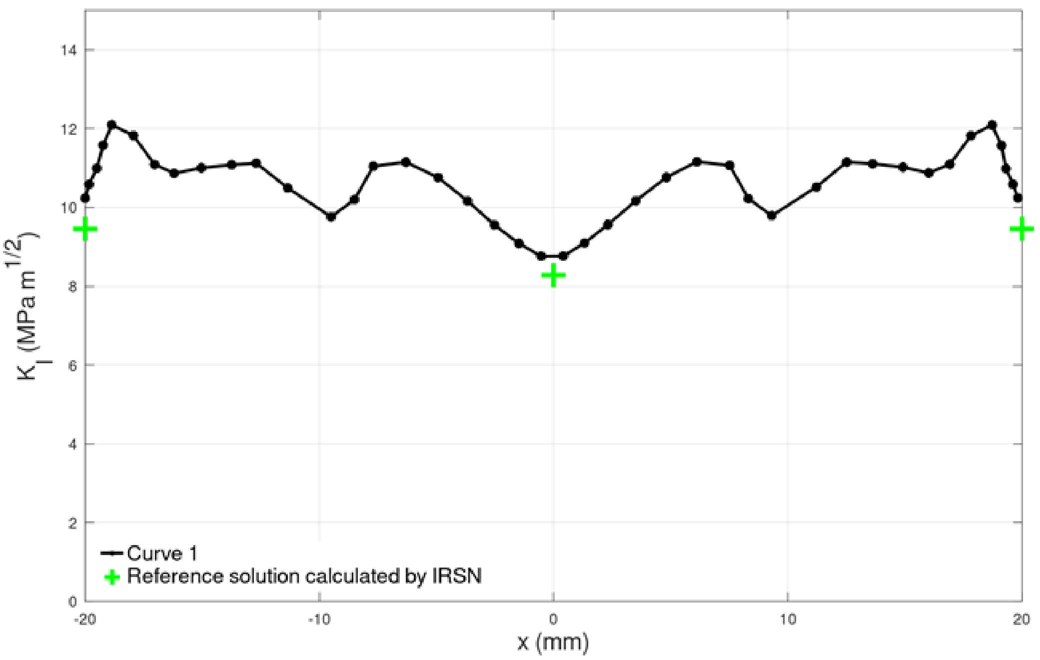

Figure D.4. Participant 4 – Benchmark A3

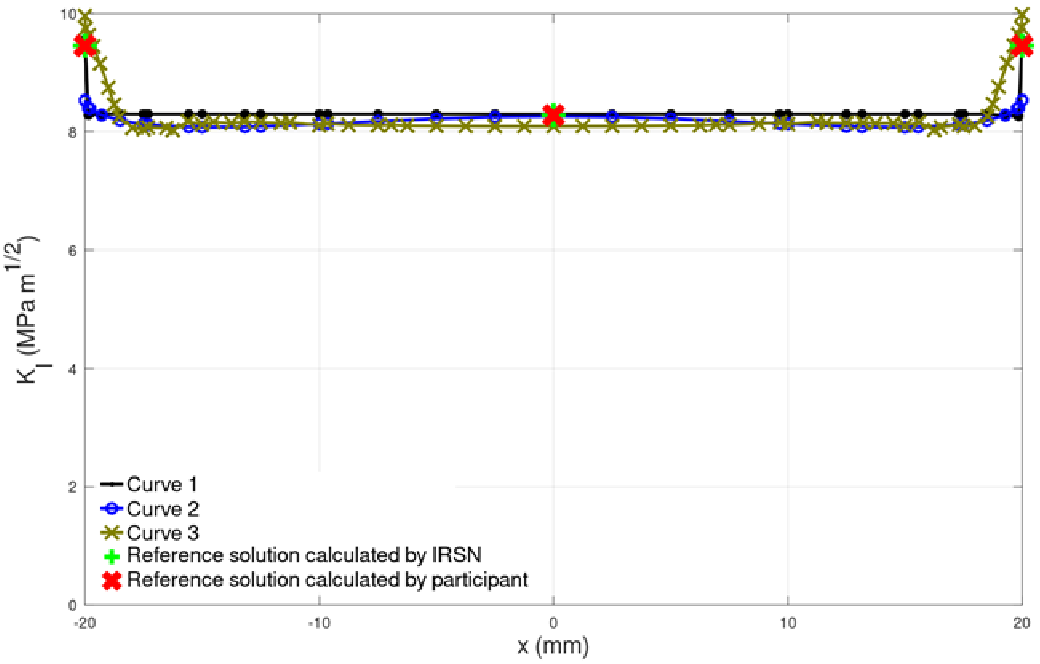

Figure D.5. Participant 5 – Benchmark A3

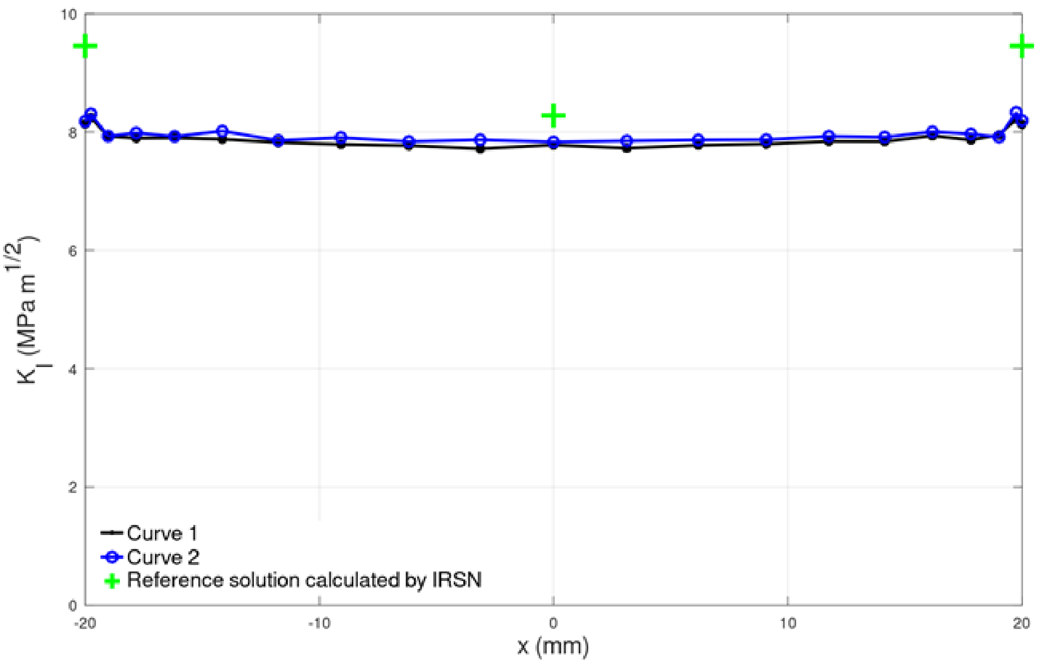

Figure D.6. Participant 6 – Benchmark A3

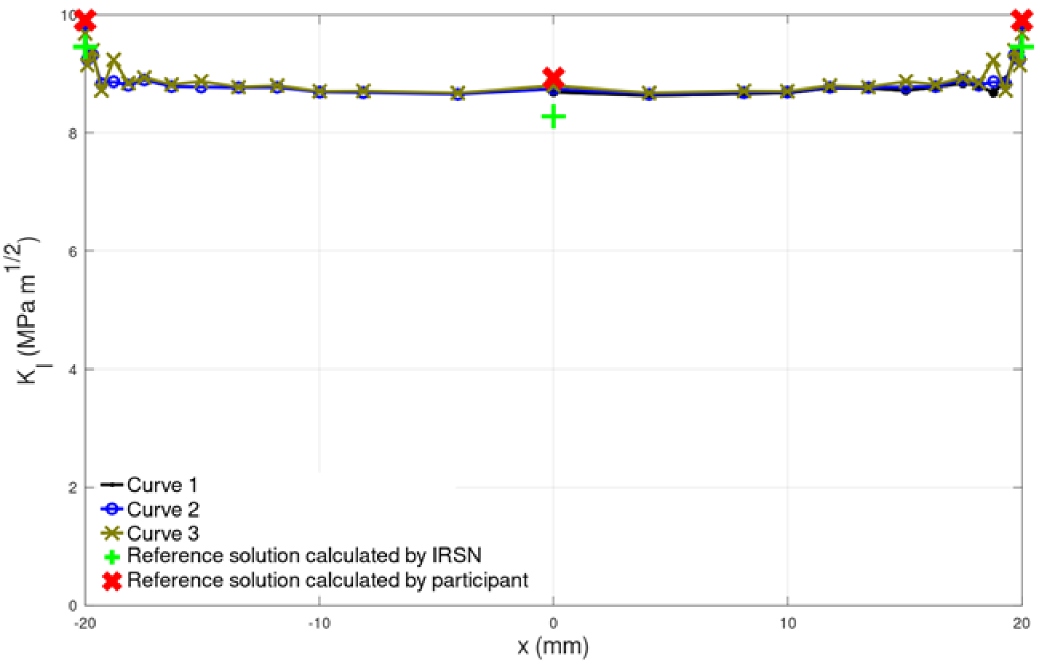

Figure D.7. Participant 7 – Benchmark A3

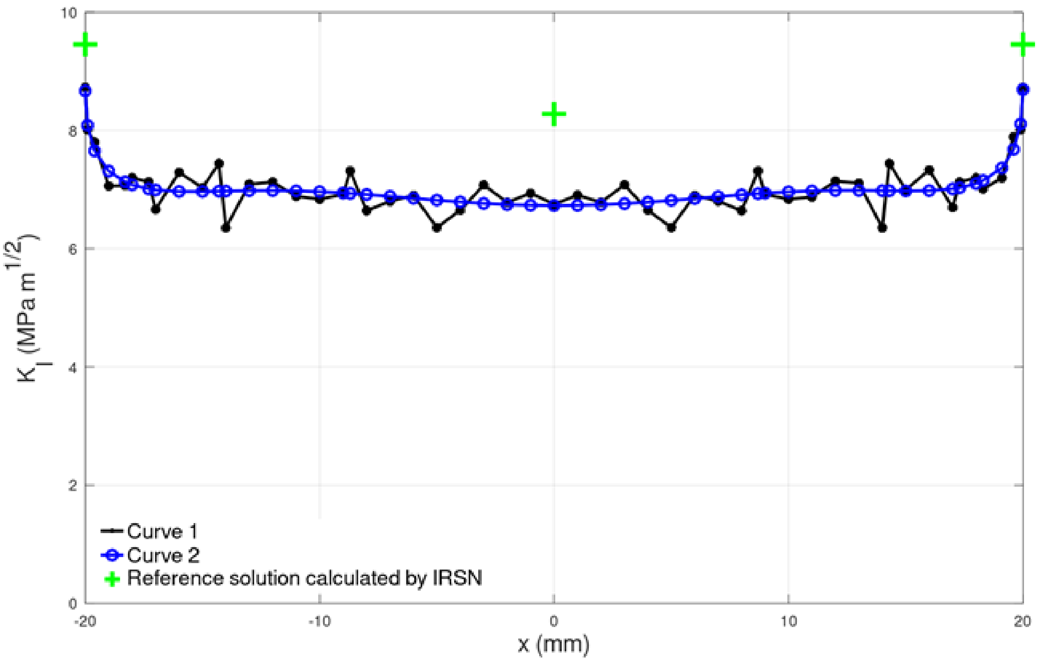

Figure D.8. Participant 8 – Benchmark A3

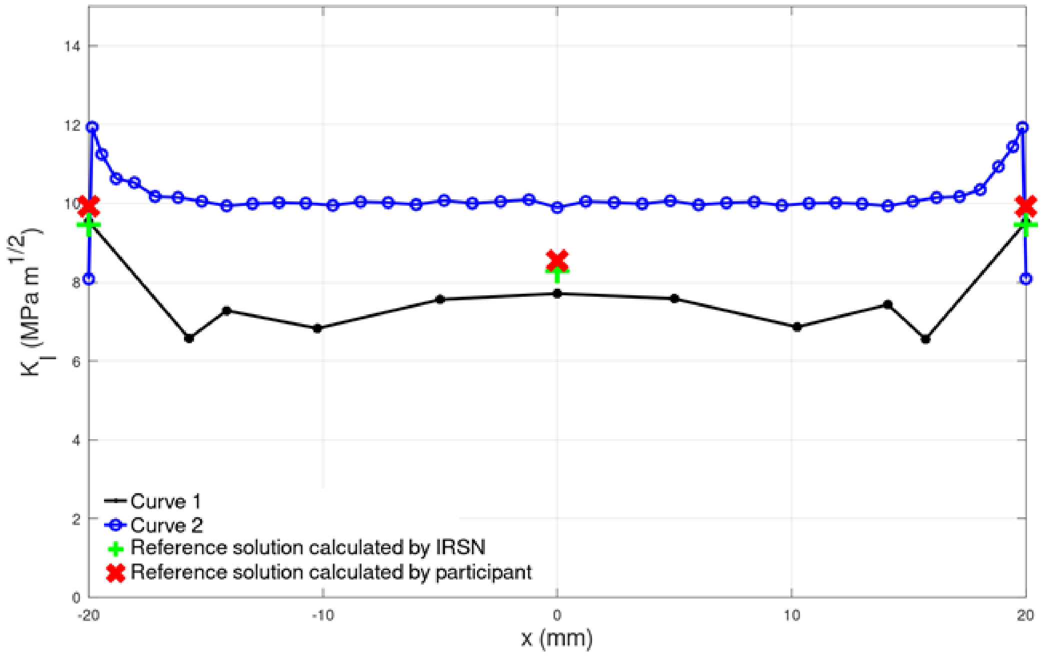

Figure D.9. Participant 9 – Benchmark A3

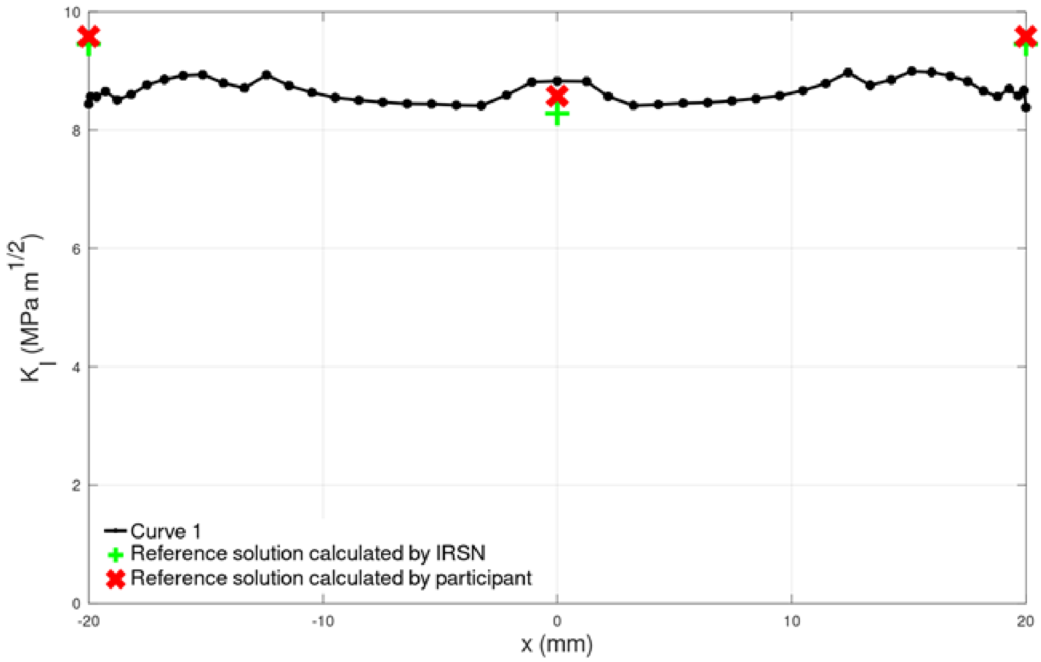

Figure D.10. Participant 10 – Benchmark A3

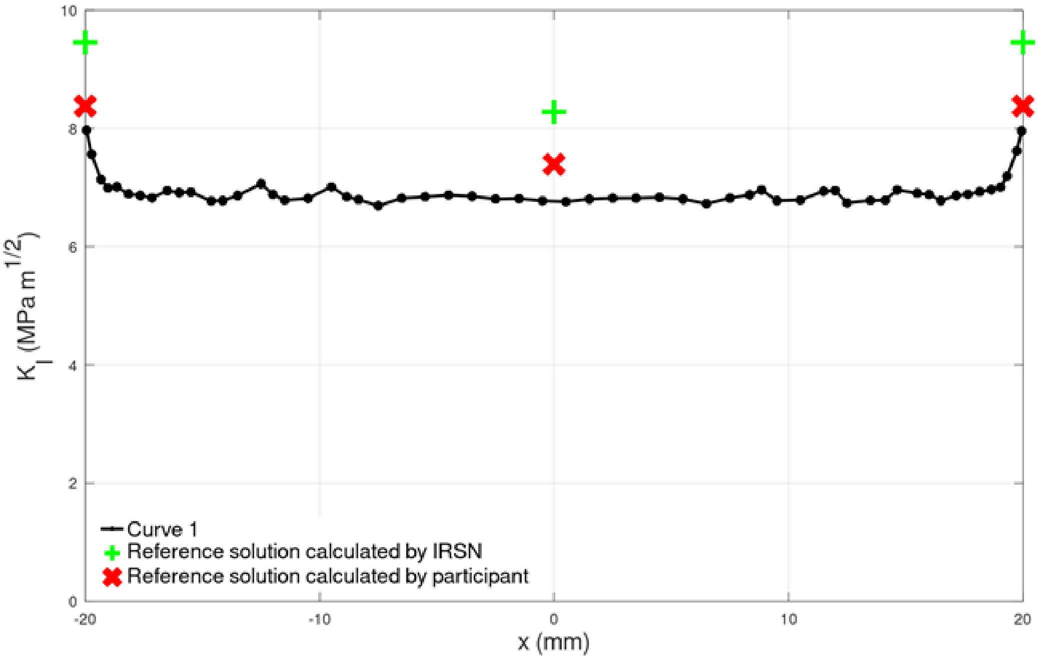

Figure D.11. Participant 11 – Benchmark A3

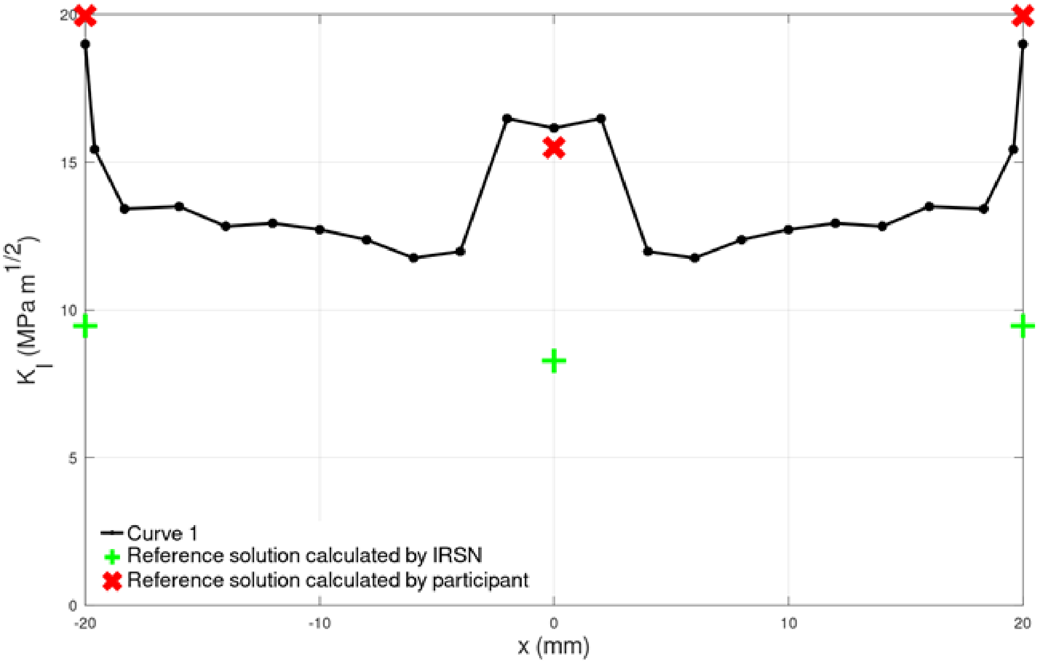

Figure D.12. Participant 12 – Benchmark A3

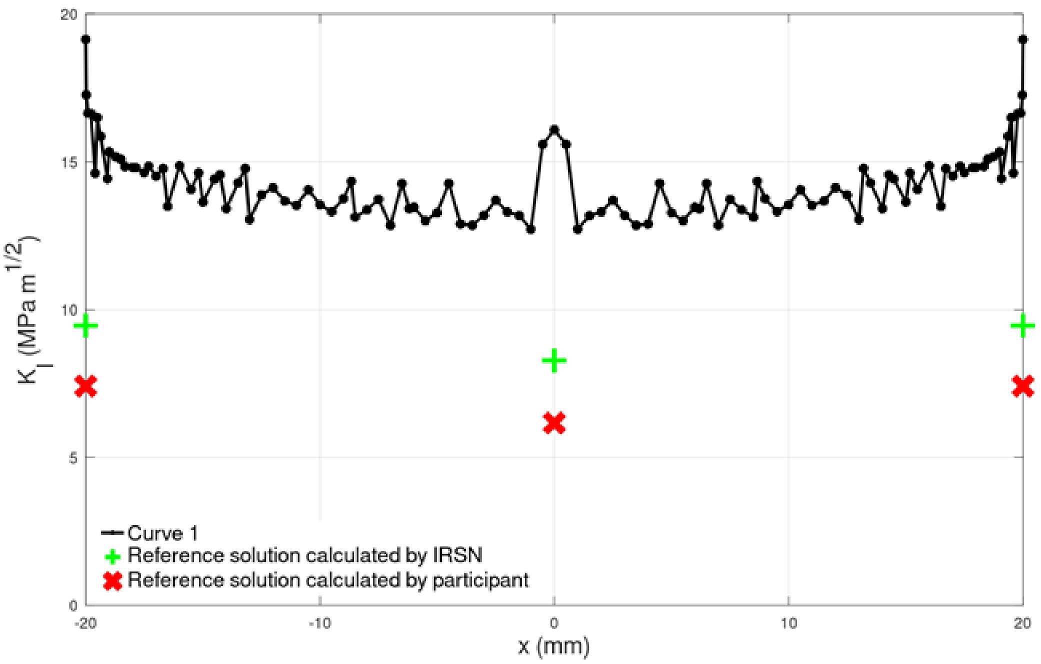

Figure D.13. Participant 13 – Benchmark A3

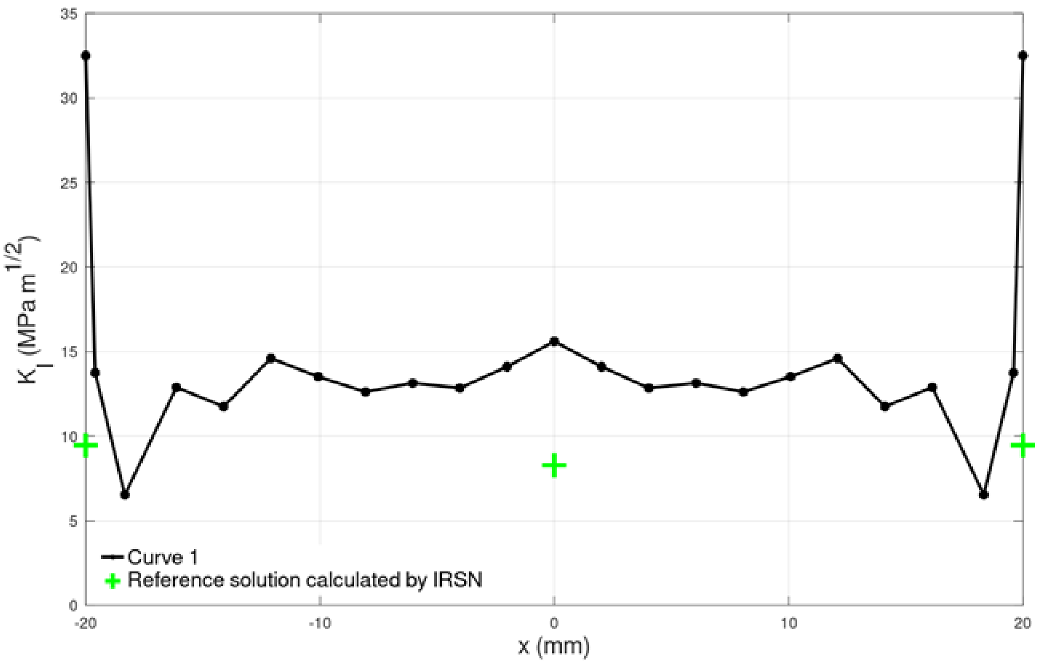

Figure D.14. Participant 14 – Benchmark A3

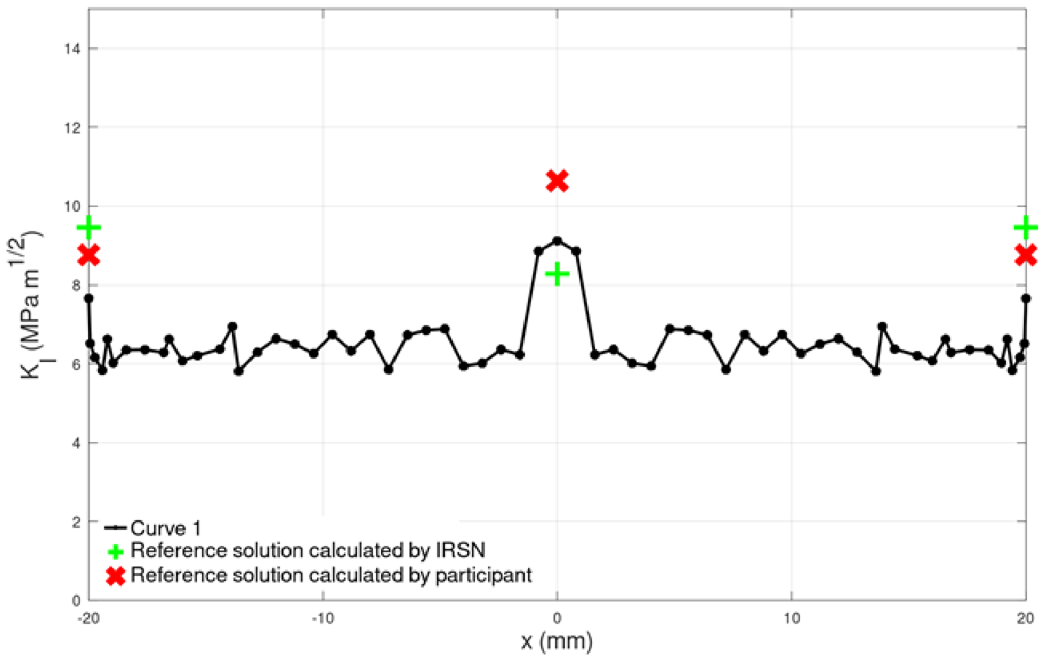

Figure D.15. Participant 15 – Benchmark A3

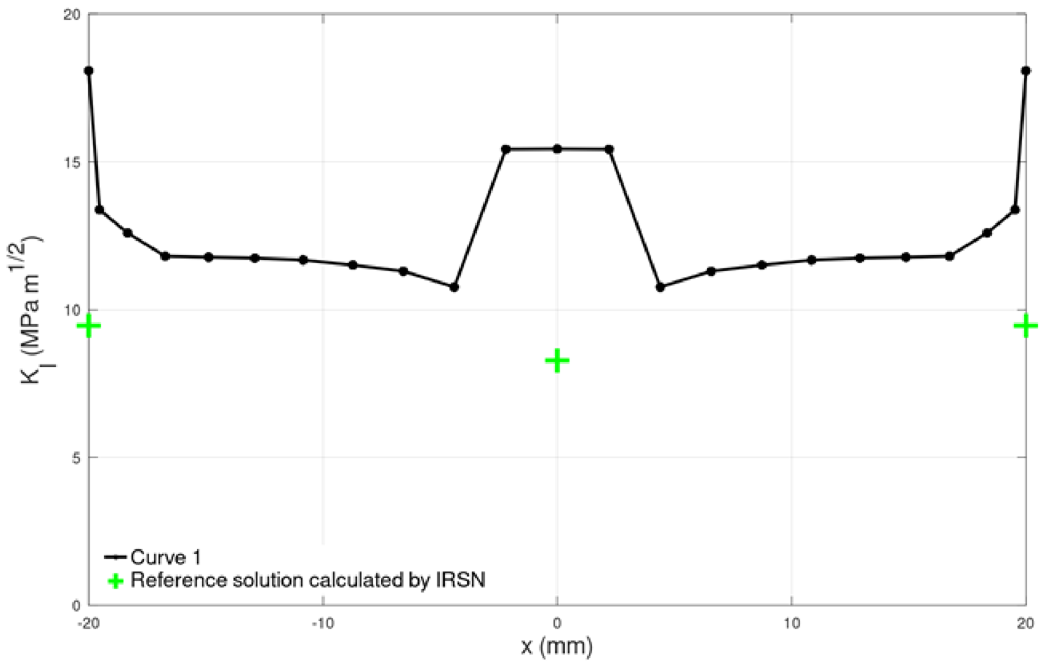

Figure D.16. Participant 16 – Benchmark A3

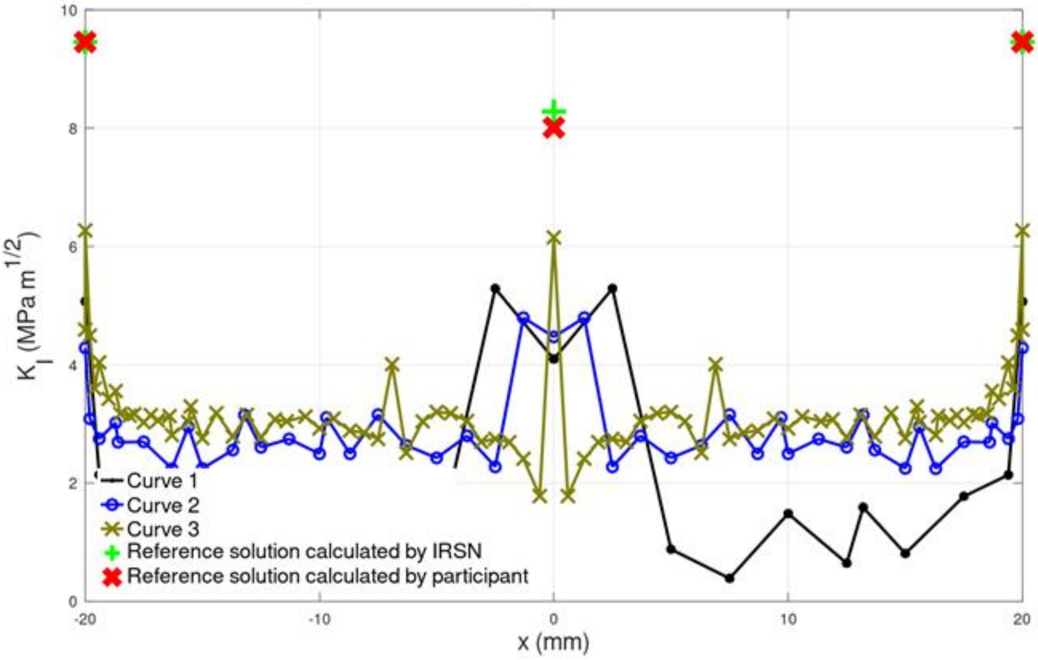

Figure D.17. Participant 18 – Benchmark A3

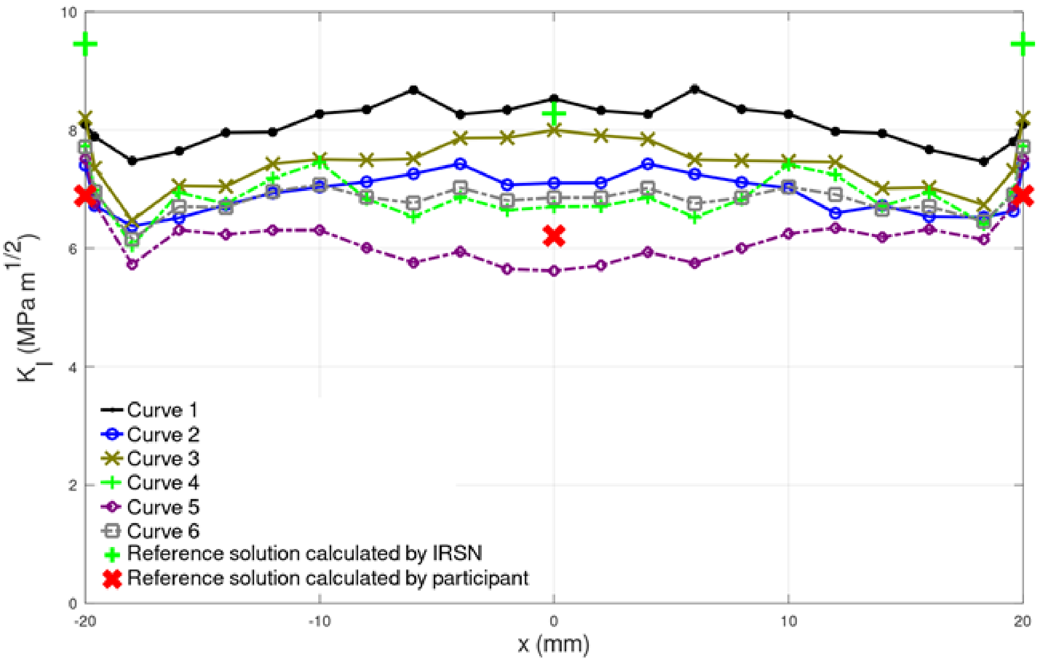

Figure D.18. K_I as function of time at point A

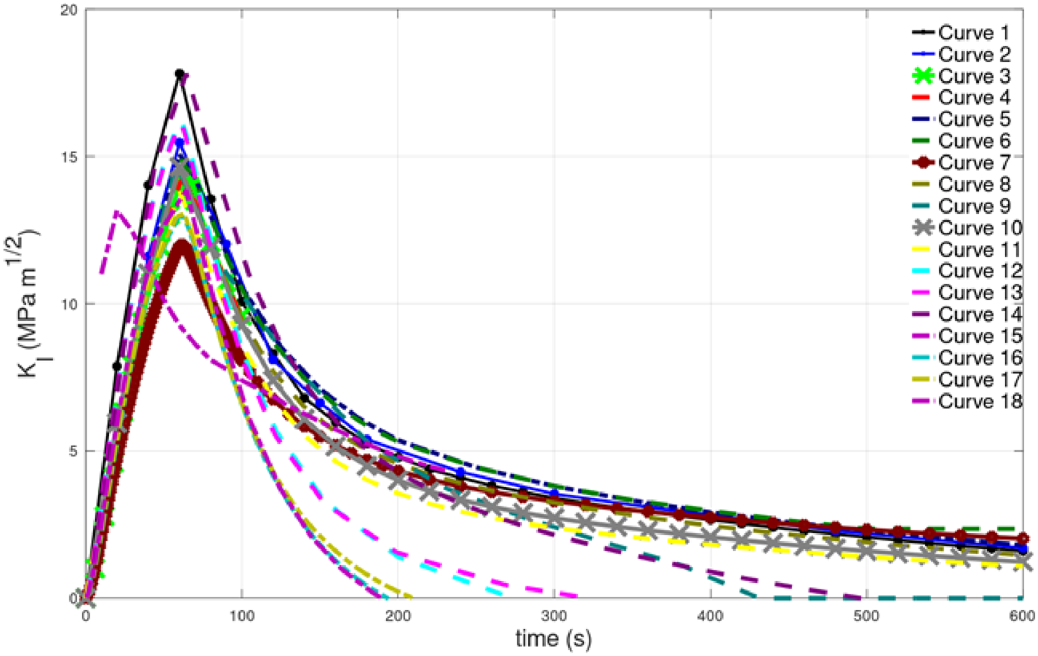

Annex E. Resulting graphs for benchmark B

Figure E.1. Summary data for all participants on benchmark B

Figure	Participant	Code	Curve	Mesh element			SIF calculation method	SIF	More information
				Order	type	target size (ratio to crack depth a)			
E.1	2	Morfeo crack	Curve 1	Quadratic	Tetrahedral	1/10	Integral	K_I	
E.2	2	Morfeo crack	Curve 1	Quadratic	Tetrahedral	1/10	Integral	K_{II}	
E.3	2	Morfeo crack	Curve 1	Quadratic	Tetrahedral	1/10	Integral	K_{III}	
E.4	3	Abaqus	Curve 1	Linear	Hexahedral	1/10	Integral	K_{II}	
		Ansys	Curve 2	Linear	Hexahedral	1/10			
E.5	3	Abaqus	Curve 1	Linear	Hexahedral	1/10	Integral	K_{III}	
		Ansys	Curve 2	Linear	Hexahedral	1/10			
E.6	4	Code-Aster	Curve 1	Quadratic	Tetrahedral	1/10	Displacement	K_I	
E.7	4	Code-Aster	Curve 1	Quadratic	Tetrahedral	1/10	Displacement	K_{II}	
E.8	4	Code-Aster	Curve 1	Quadratic	Tetrahedral	1/10	Displacement	K_{III}	
E.9	5	Systus	Curve 1	Quadratic	Hexahedral	1/5	Integral	K_I	Integration domain: R_{min} = 0,5 mm; R_{max} = 2 mm
			Curve 2						Integration domain: R_{min} = 0,5 mm; R_{max} = 2 mm
			Curve 3						Integration domain: R_{min} = 0,5 mm; R_{max} = 2 mm
		Systus (FEM)	Curve 4			1/10	Displacement		
E.10	5	Systus	Curve 1	Quadratic	Hexahedral	1/5	Integral	K_{II}	Integration domain: R_{min} = 0,5 mm; R_{max} = 2 mm
			Curve 2						Integration domain: R_{min} = 0,5 mm; R_{max} = 2 mm
			Curve 3						Integration domain: R_{min} = 0,5 mm; R_{max} = 2 mm
		Systus (FEM)	Curve 4			1/10	Displacement		
E.11	5	Systus	Curve 1	Quadratic	Hexahedral	1/5	Integral	K_{III}	Integration domain: R_{min} = 0,5 mm; R_{max} = 2 mm
			Curve 2						Integration domain: R_{min} = 0,5 mm; R_{max} = 2 mm
			Curve 3						Integration domain: R_{min} = 0,5 mm; R_{max} = 2 mm
		Systus (FEM)	Curve 4			1/10	Displacement		
E.12	6	Code-Aster (FEM)	Curve 1	Quadratic	Tetrahedral	1/10	Integral	K_{II}	
E.13	6	Code-Aster (FEM)	Curve 1	Quadratic	Tetrahedral	1/10	Integral	K_{III}	
E.14	7	Abaqus	Curve 1	Linear	Hexahedral	1/5	Integral	K_I	
			Curve 2			polynomial fit			Curve 2 is a polynomial fit (degree 6) of the data points from Curve 1
			Curve 3			2/5	Integral		
			Curve 4			polynomial fit			Curve 4 is a polynomial fit (degree 6) of the data points from Curve 3
E.15	7	Abaqus	Curve 1	Linear	Hexahedral	1/5	Integral	K_{II}	
			Curve 2			polynomial fit			Curve 2 is a polynomial fit (degree 6) of the data points from Curve 1
			Curve 3			2/5	Integral		
			Curve 4			polynomial fit			Curve 4 is a polynomial fit (degree 6) of the data points from Curve 3

Figure	Participant	Code	Curve	Mesh element			SIF calculation method	SIF	More information
				Order	type	target size (ratio to crack depth a)			
E.16	7	Abaqus	Curve 1	Linear	Hexahedral	1/5	Integral	K_{III}	
			Curve 2			polynomial fit			
			Curve 3			2/5	Integral		
			Curve 4			polynomial fit			
E.17	8	Abaqus	Curve 1	Linear	Hexahedral	2/5	Integral	K_I	
E.18	8	Abaqus	Curve 1	Linear	Hexahedral	2/5	Integral	K_{II}	
E.19	8	Abaqus	Curve 1	Linear	Hexahedral	2/5	Integral	K_{III}	
E.20	9	Abaqus	Curve 1	Linear	Hexahedral	1/5	Integral	K_I	Integration domain: R_{min} = 0,5 mm; R_{max} = 1,3 mm / Element size at crack tip varying from 1 mm to 2 mm
			Curve 2			1/10			Integration domain: R_{min} = 0,5 mm; R_{max} = 1,3 mm / Element size at crack tip varying from 0,5 mm to 0,8 mm
E.21	9	Abaqus	Curve 1	Linear	Hexahedral	1/5	Integral	K_{II}	Integration domain: R_{min} = 0,5 mm; R_{max} = 1,3 mm / Element size at crack tip varying from 1 mm to 2 mm
			Curve 2			1/10			Integration domain: R_{min} = 0,5 mm; R_{max} = 1,3 mm / Element size at crack tip varying from 0,5 mm to 0,8 mm
E.22	9	Abaqus	Curve 1	Linear	Hexahedral	1/5	Integral	K_{III}	Integration domain: R_{min} = 0,5 mm; R_{max} = 1,3 mm / Element size at crack tip varying from 1 mm to 2 mm
			Curve 2			1/10			Integration domain: R_{min} = 0,5 mm; R_{max} = 1,3 mm / Element size at crack tip varying from 0,5 mm to 0,8 mm
E.23	10	NLX-FEM3DStruct	Curve 1	Linear	Hexahedral	1/10	Integral	K_{II}	
E.24	10	NLX-FEM3DStruct	Curve 2	Linear	Hexahedral	1/10	Integral	K_{III}	
E.25	11	Abaqus	Curve 1	Linear	Hexahedral	1/5	Integral	K_I	
E.26	11	Abaqus	Curve 1	Linear	Hexahedral	1/5	Integral	K_{II}	
E.27	11	Abaqus	Curve 1	Linear	Hexahedral	1/5	Integral	K_{III}	
E.28	12	Abaqus	Curve 1	Linear	Hexahedral	1/10	Displacement	K_I	
E.29	12	Abaqus	Curve 1	Linear	Hexahedral	1/10	Displacement	K_{II}	
E.30	12	Abaqus	Curve 1	Linear	Hexahedral	1/10	Displacement	K_{III}	
E.31	13	Abaqus	Curve 1	Linear	Hexahedral	3/50	Integral	K_I	
E.32	13	Abaqus	Curve 1	Linear	Hexahedral	3/50	Integral	K_{II}	
E.33	13	Abaqus	Curve 1	Linear	Hexahedral	3/50	Integral	K_{III}	
E.34	14	Abaqus	Curve 1	Linear	Hexahedral	13/100	Integral	K_{II}	
E.35	14	Abaqus	Curve 1	Linear	Hexahedral	13/100	Integral	K_{III}	

Figure	Participant	Code	Curve	Mesh element			SIF calculation method	SIF	More information
				Order	type	target size (ratio to crack depth a)			
E.36	15	Abaqus	Curve 1	Linear	Hexahedral	1/10	Integral	K_I	
E.37	15	Abaqus	Curve 1	Linear	Hexahedral	1/10	Integral	K_{II}	
E.38	15	Abaqus	Curve 1	Linear	Hexahedral	1/10	Integral	K_{III}	
E.39	16	Abaqus	Curve 1	Linear	Hexahedral	1/50 (uniform)	Integral	K_I	
		Abaqus	Curve 2			1/50 (non-uniform)		K_I	
E.40	16	Abaqus	Curve 1	Linear	Hexahedral	1/50 (uniform)	Integral	K_{II}	
		Abaqus	Curve 2			1/50 (non-uniform)		K_{II}	
E.41	16	Abaqus	Curve 1	Linear	Hexahedral	1/50 (uniform)	Integral	K_{III}	
		Abaqus	Curve 2			1/50 (non-uniform)		K_{III}	
E.42	17	Abaqus	Curve 1	Linear	Hexahedral	3/50	Integral	K_{II}	
E.43	17	Abaqus	Curve 2	Linear	Hexahedral	3/50	Integral	K_{III}	
E.44	18	Abaqus	Curve 1	Linear	Hexahedral	2/5	Integral	K_{II}	Integration domain 1 (domain not specified, but increasing from 1 to 5) / Crack plane on element face
			Curve 2						Integration domain 2 (domain not specified, but increasing from 1 to 5) / Crack plane on element face
			Curve 3						Integration domain 3 (domain not specified, but increasing from 1 to 5) / Crack plane on element face
			Curve 4						Integration domain 4 (domain not specified, but increasing from 1 to 5) / Crack plane on element face
			Curve 5						Integration domain 5 (domain not specified, but increasing from 1 to 5) / Crack plane on element face
			Curve 6						Resuls present average of the 5 integration domains / Crack plane on element face

Figure	Participant	Code	Curve	Mesh element			SIF calculation method	SIF	More information
				Order	type	target size (ratio to crack depth a)			
E.45	18	Abaqus	Curve 1	Linear	Hexahedral	2/5	Integral	K_{III}	Integration domain 1 (domain not specified, but increasing from 1 to 5) / Crack plane on element face
			Curve 2						Integration domain 2 (domain not specified, but increasing from 1 to 5) / Crack plane on element face
			Curve 3						Integration domain 3 (domain not specified, but increasing from 1 to 5) / Crack plane on element face
			Curve 4						Integration domain 4 (domain not specified, but increasing from 1 to 5) / Crack plane on element face
			Curve 5						Integration domain 5 (domain not specified, but increasing from 1 to 5) / Crack plane on element face
			Curve 6						Resuls present average of the 5 integration domains / Crack plane on element face

Figure E.2. Participant 2 – Benchmark B – K_I

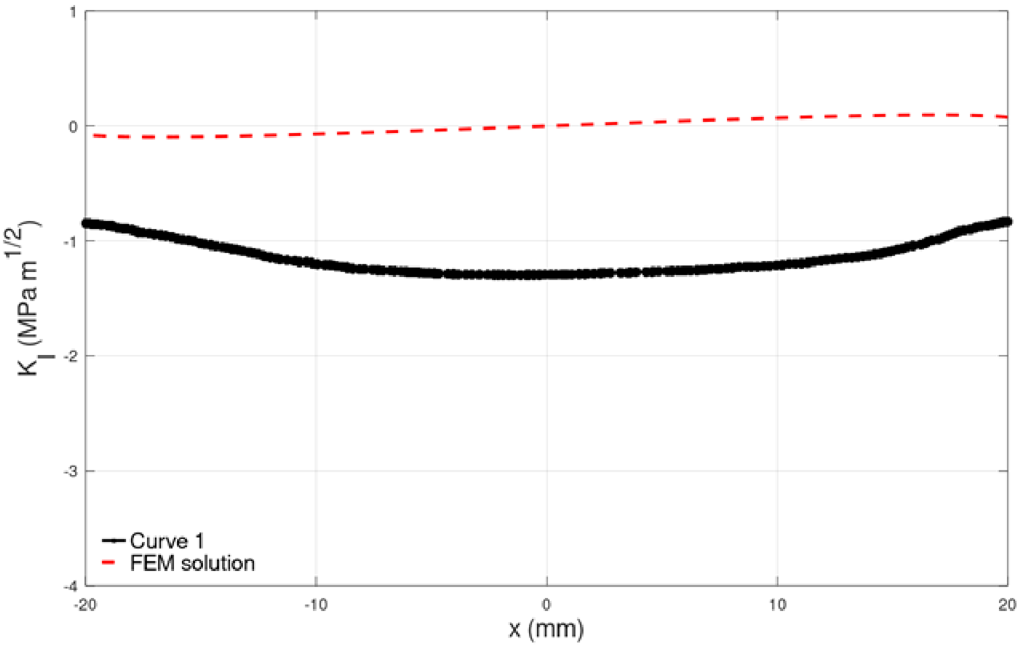

Figure E.3. Participant 2 – Benchmark B – K_{II}

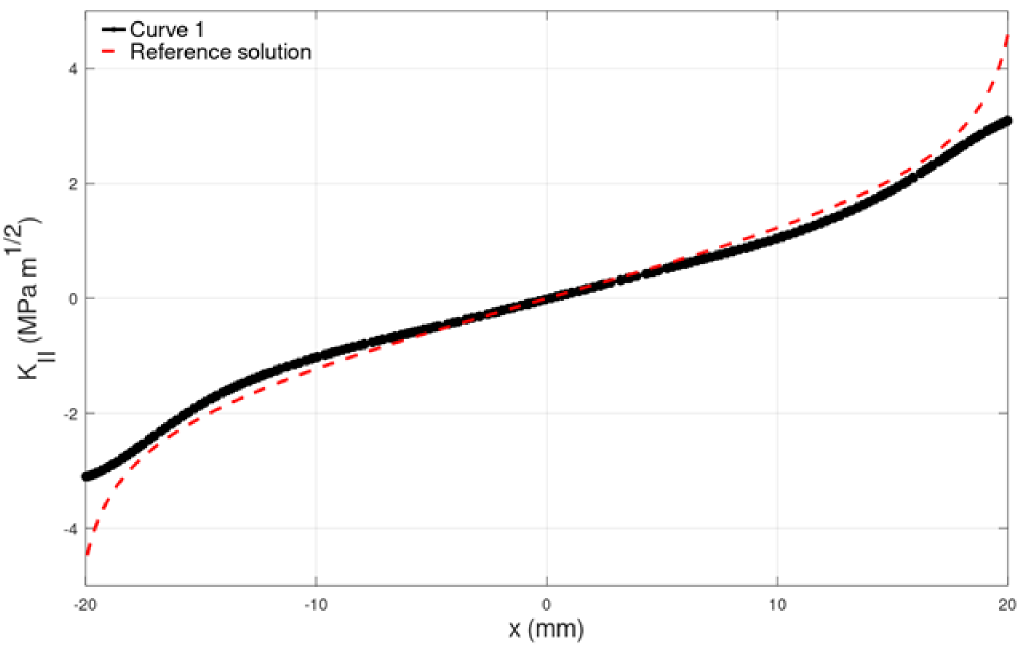

Figure E.4. Participant 2 – Benchmark B – K_{III}

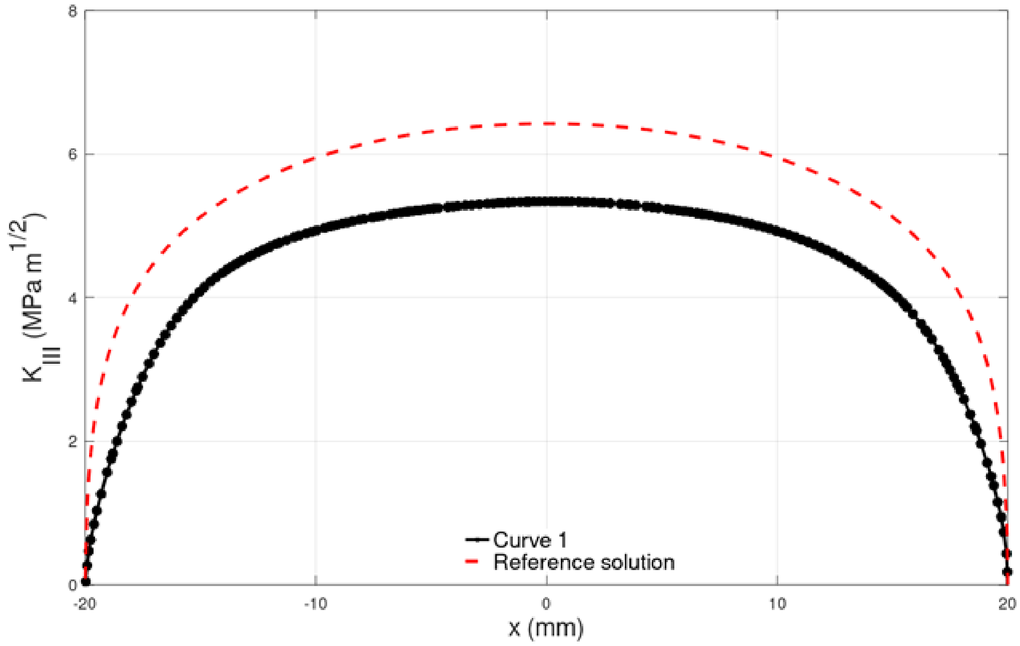

Figure E.5. Participant 3 – Benchmark B – K_{II}

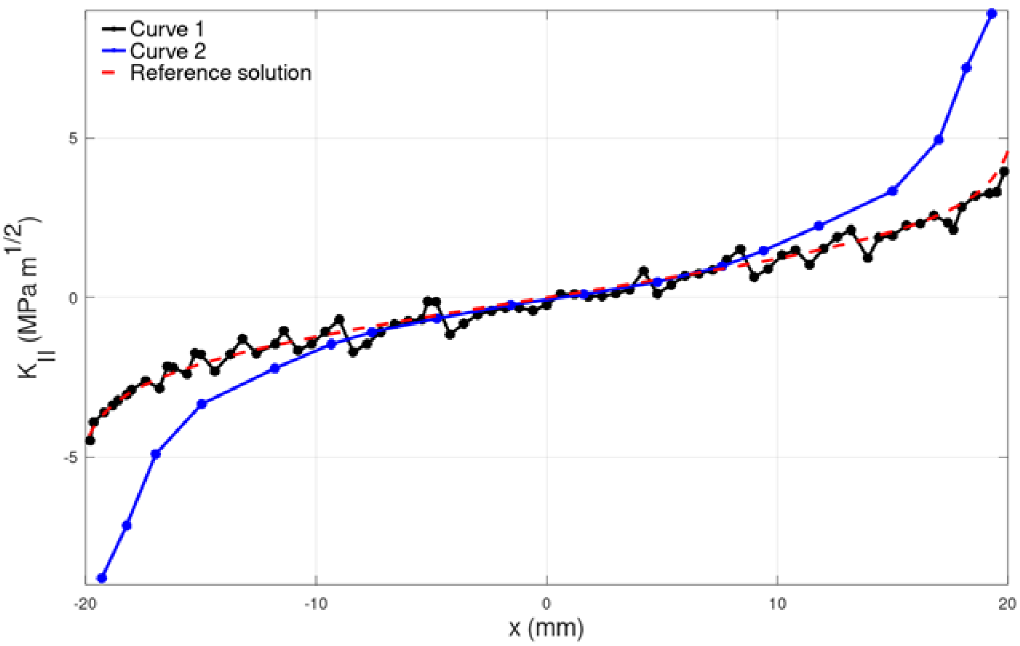

Figure E.6. Participant 3 – Benchmark B – K_{III}

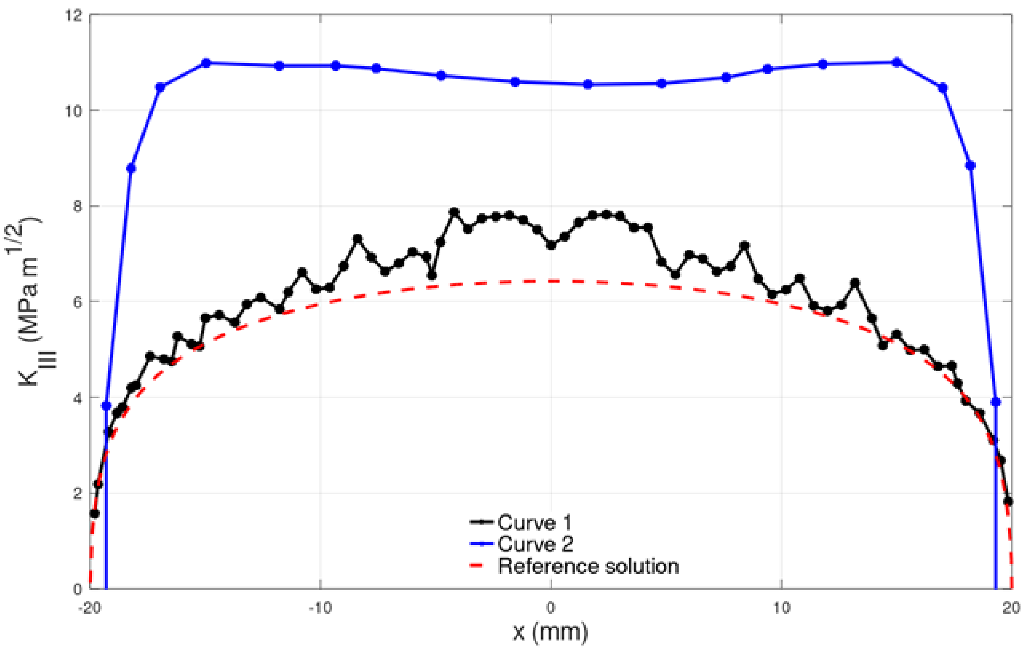

Figure E.7. Participant 4 – Benchmark B – K_I

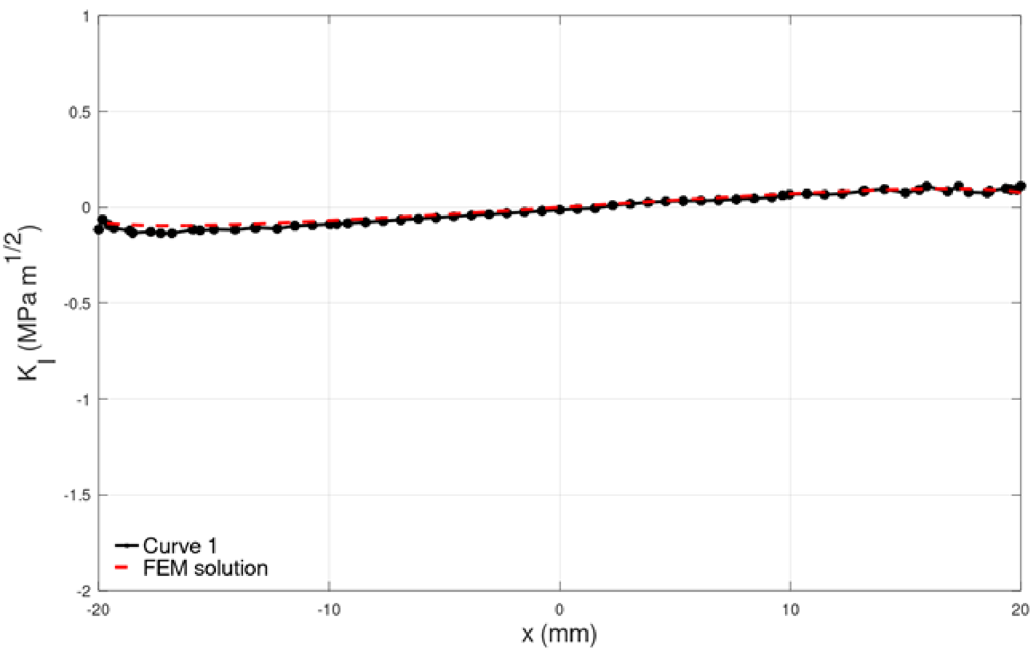

Figure E.8. Participant 4 – Benchmark B – K_{II}

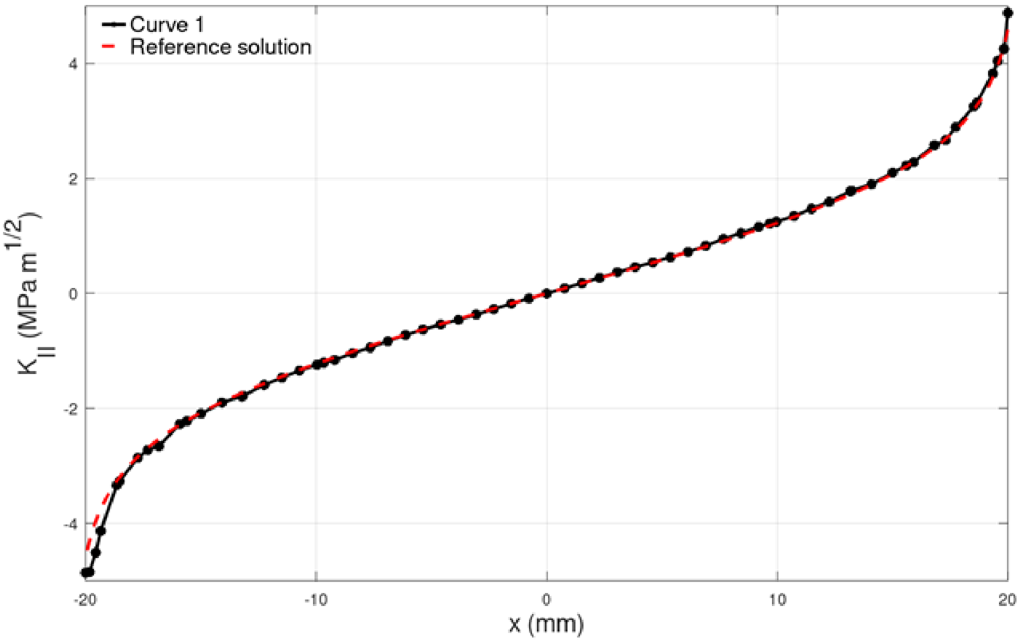

Figure E.9. Participant 4 – Benchmark B – K_{III}

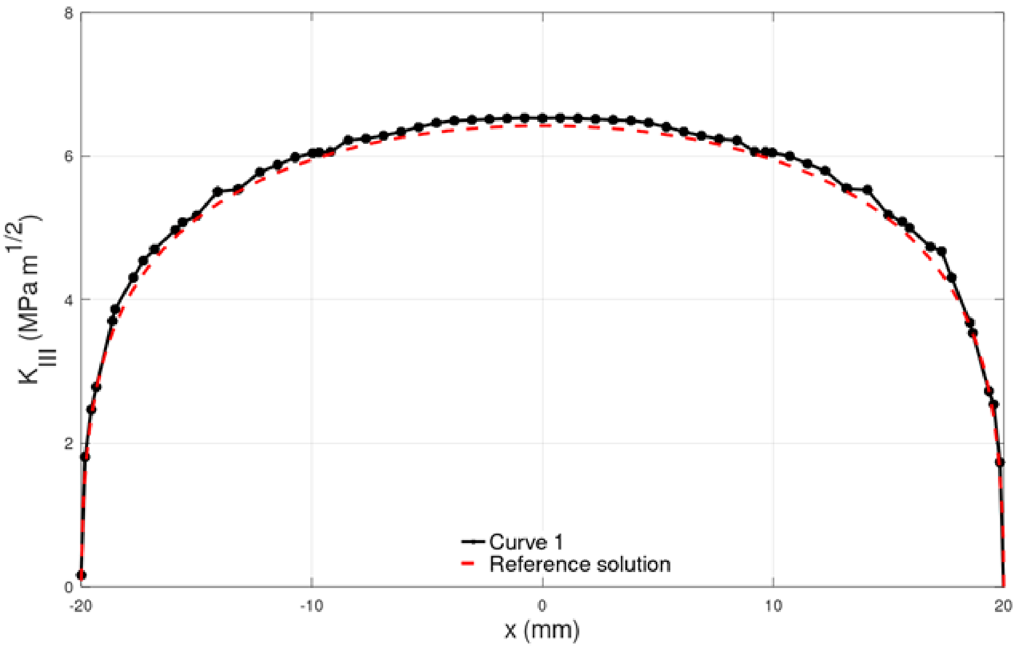

Figure E.10. Participant 5 – Benchmark B – K_I

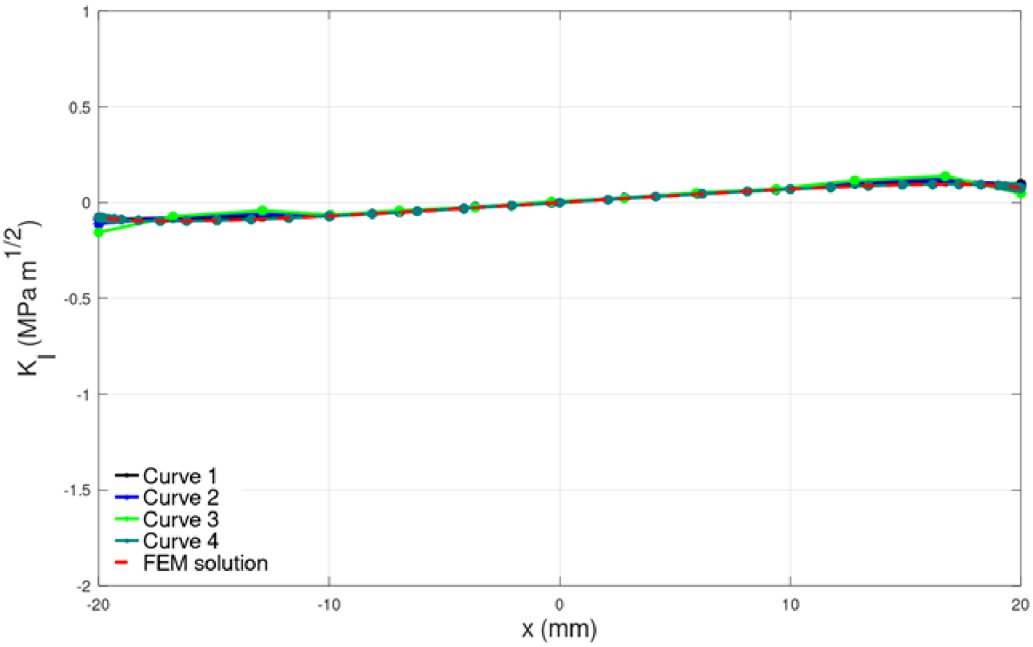

Figure E.11. Participant 5 – Benchmark B – K_{II}

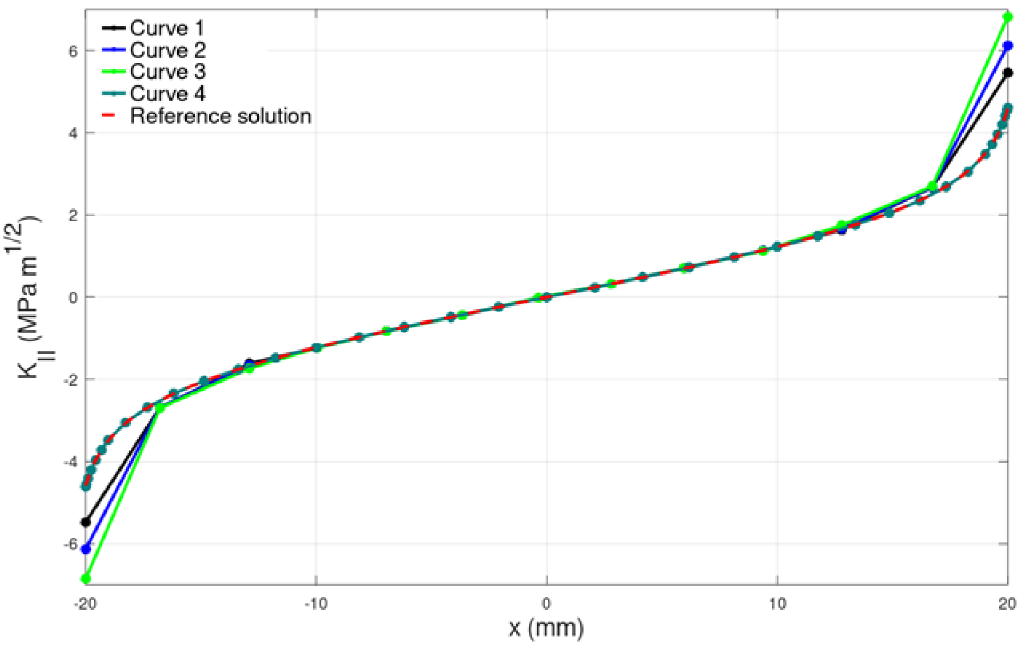

Figure E.12. Participant 5 – Benchmark B – K_{III}

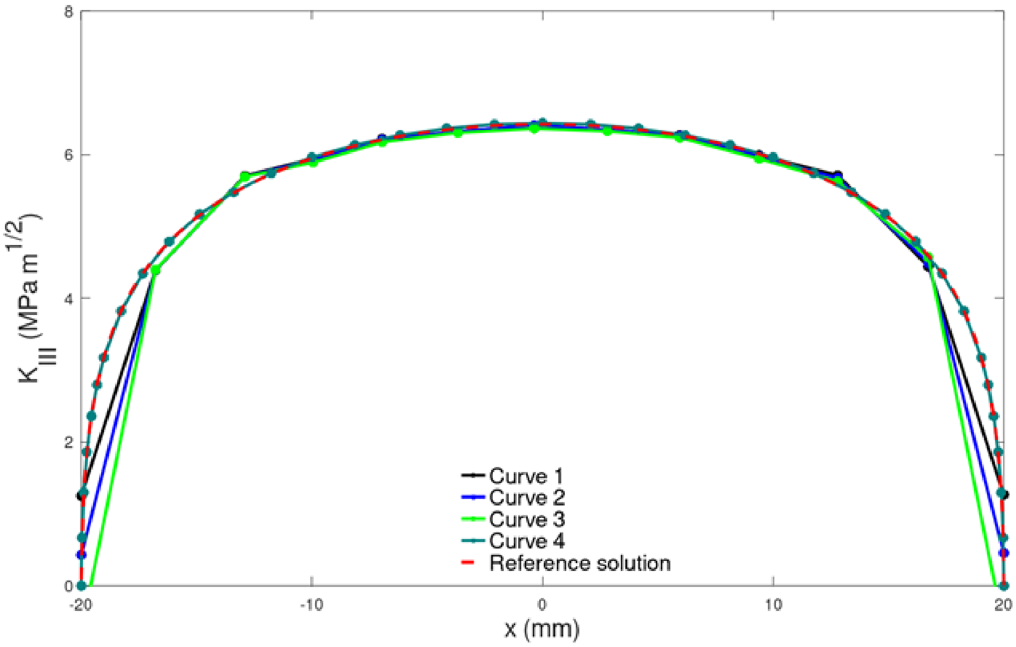

Figure E.13. Participant 6- Benchmark B – K_{II}

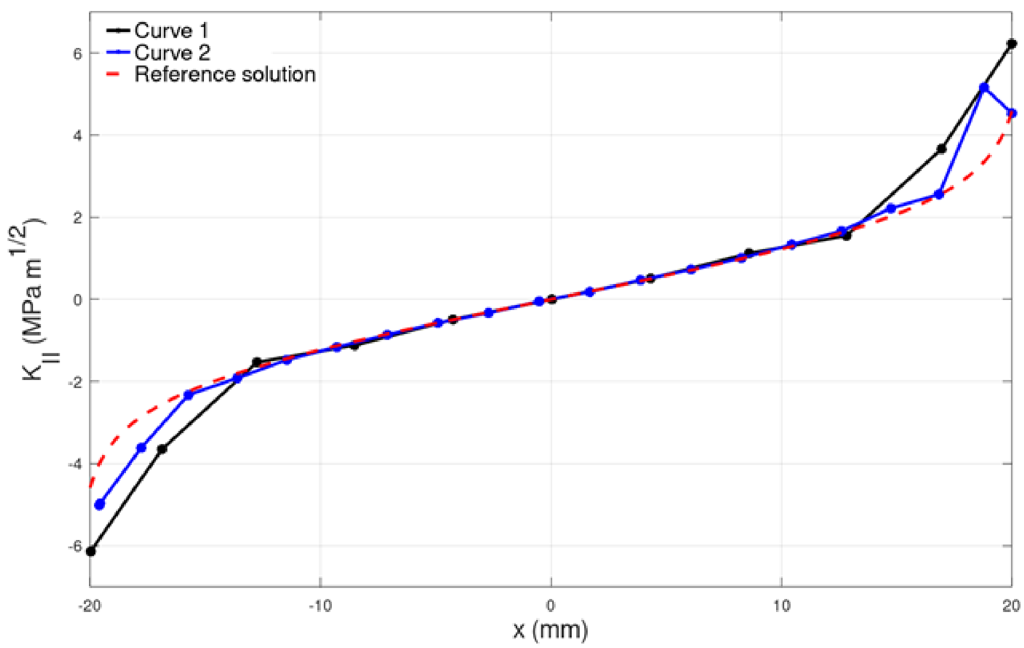

Figure E.14. Participant 6- Benchmark B – K_{III}

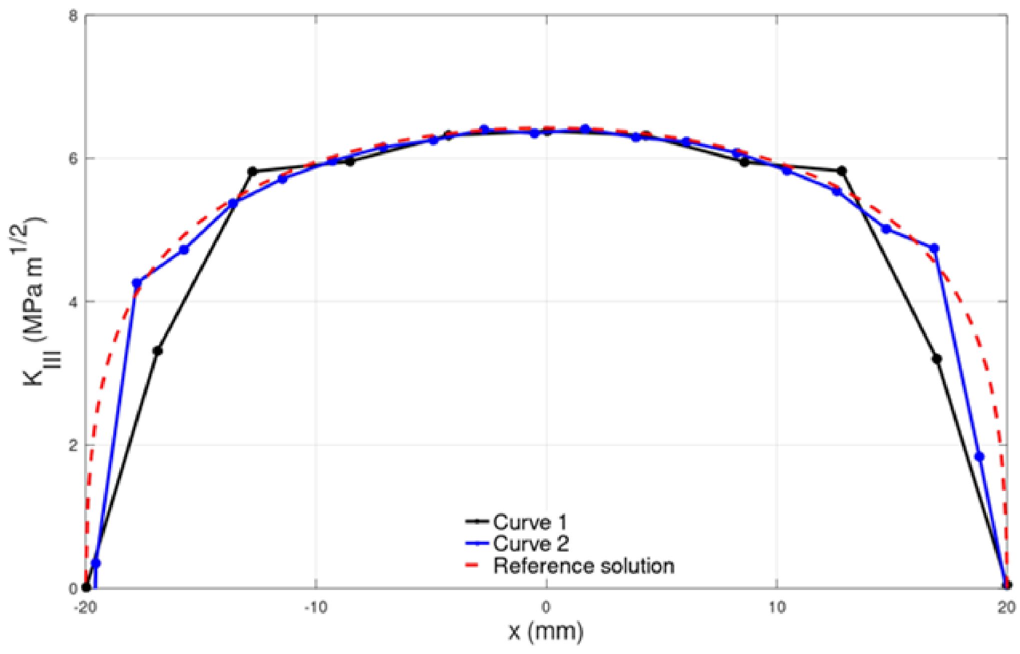

Figure E.15. Participant 7- Benchmark B – K_I

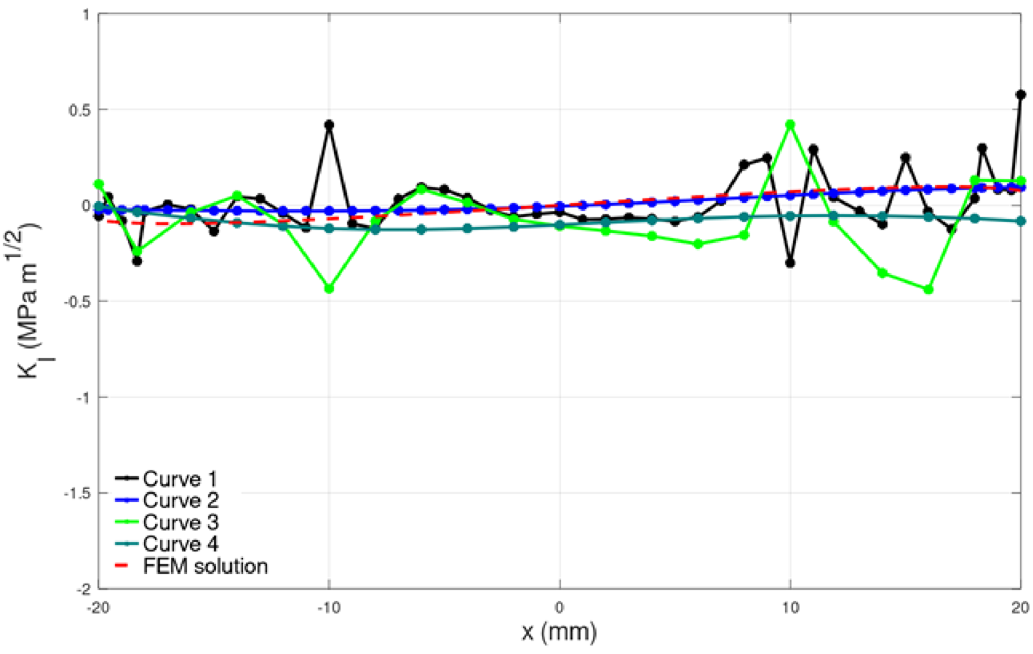

Figure E.16. Participant 7- Benchmark B – K_{II}

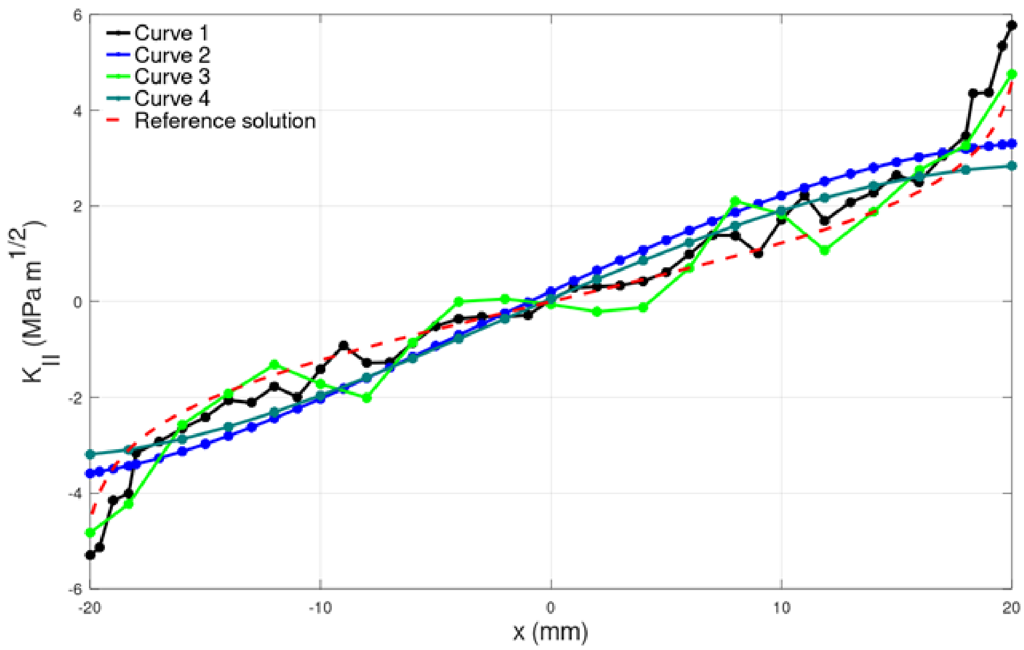

Figure E.17. Participant 7- Benchmark B – K_{III}

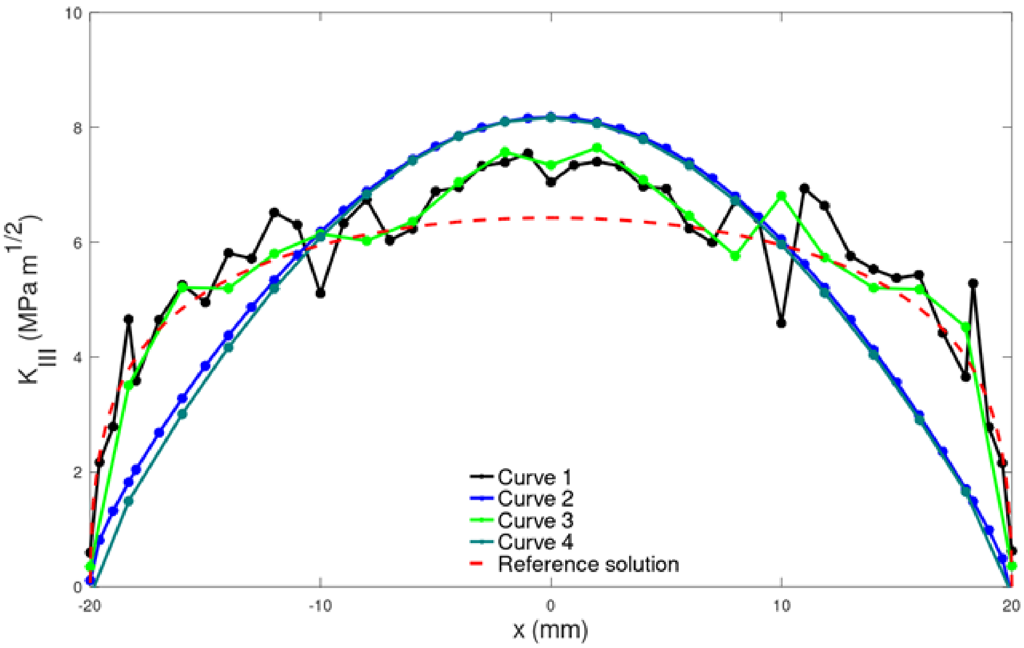

Figure E.18. Participant 8- Benchmark B – K_I

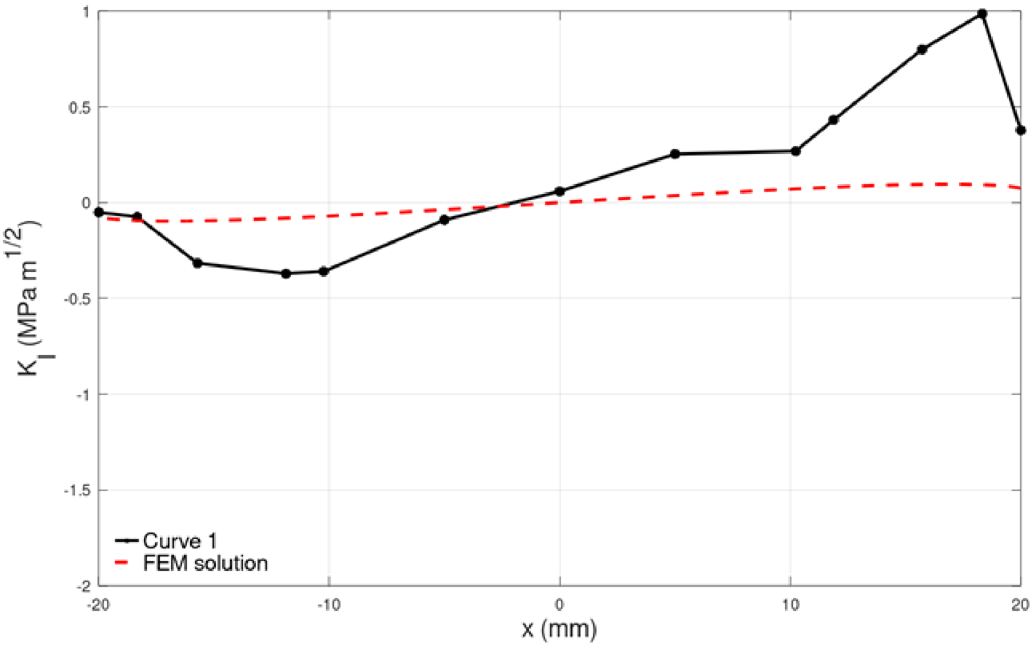

Figure E.19. Participant 8- Benchmark B – K_{II}

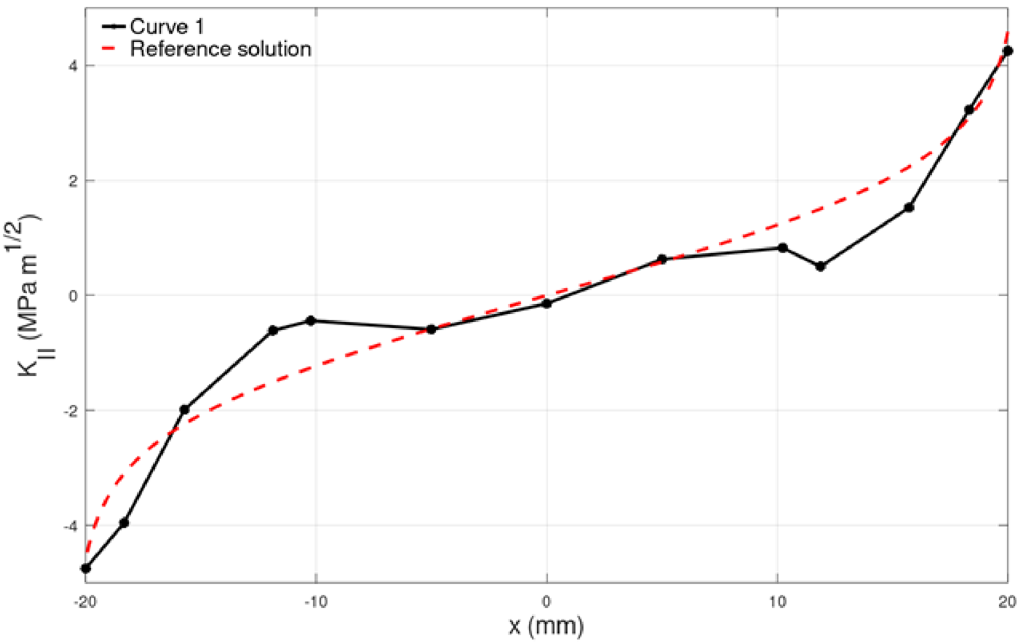

Figure E.20. Participant 8- Benchmark B – K_{III}

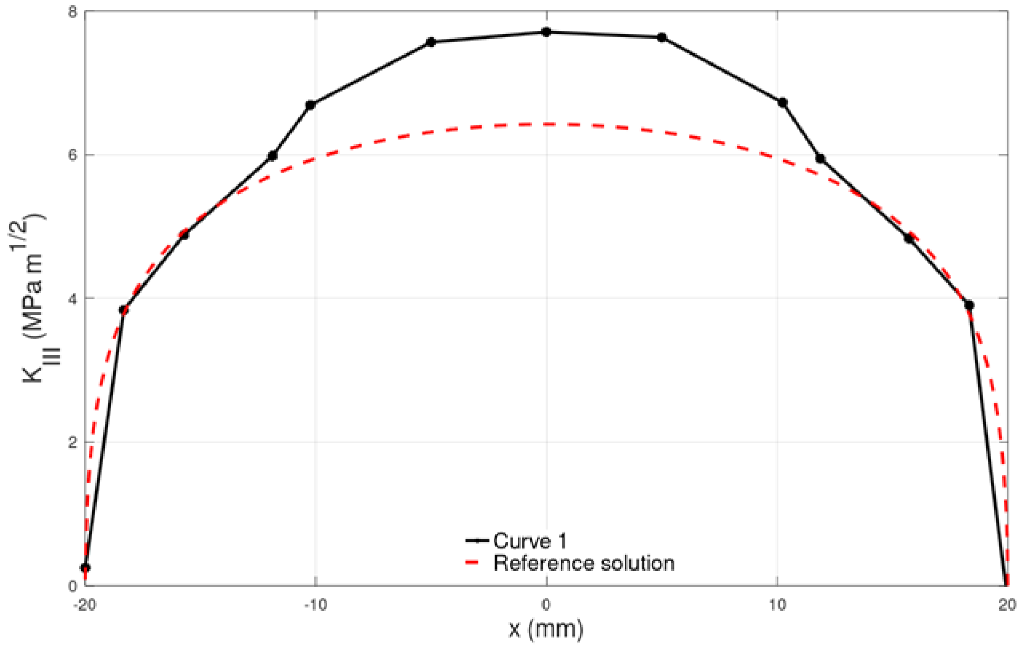

Figure E.21. Participant 9- Benchmark B – K_I

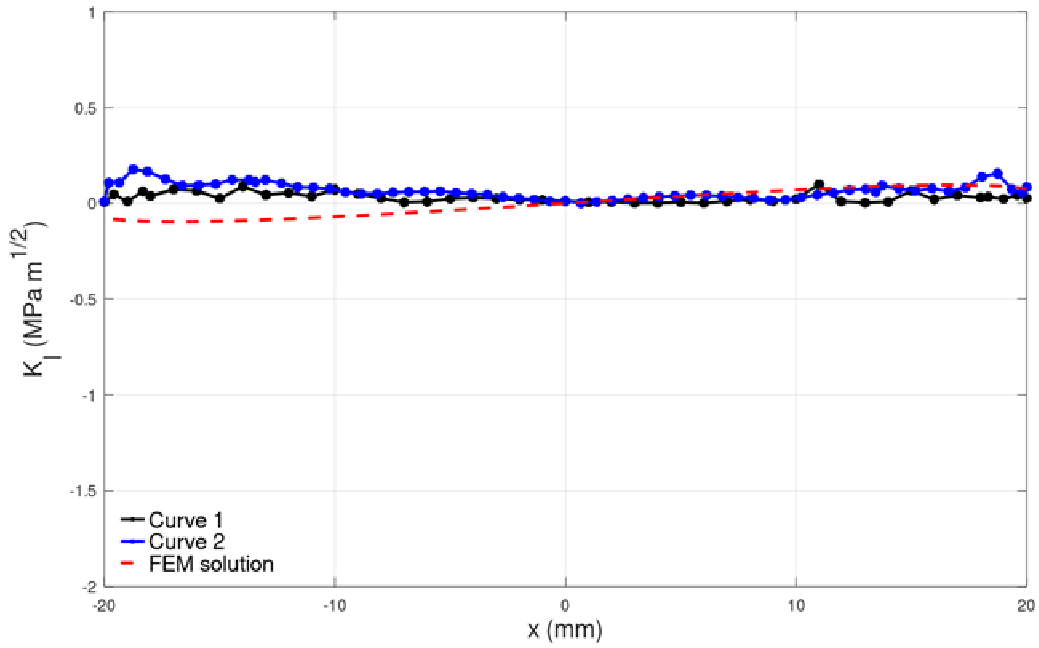

Figure E.22. Participant 9- Benchmark B – K_{II}

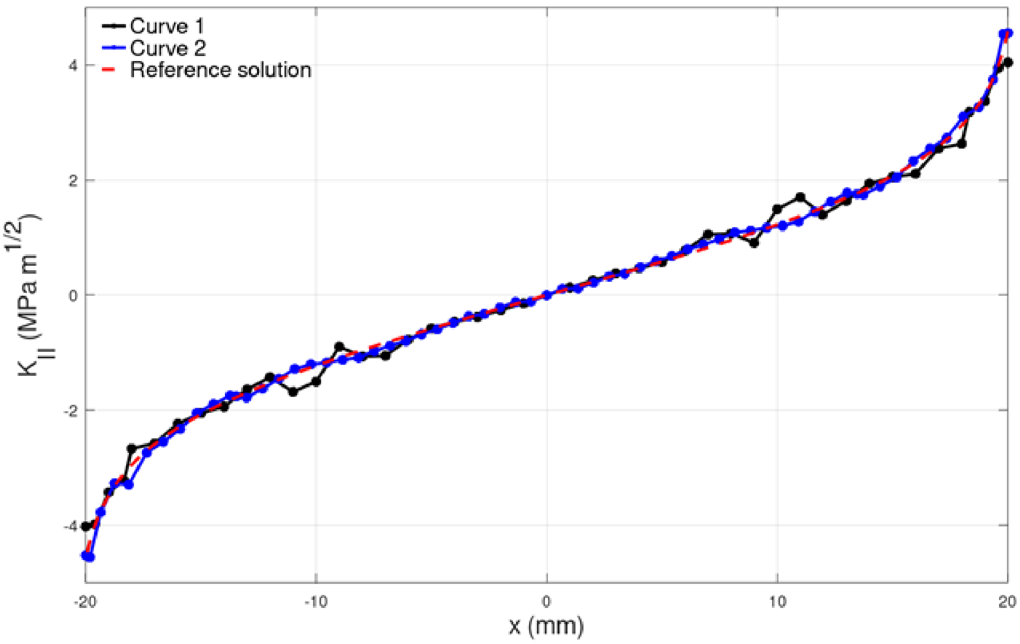

Figure E.23. Participant 9- Benchmark B – K_{III}

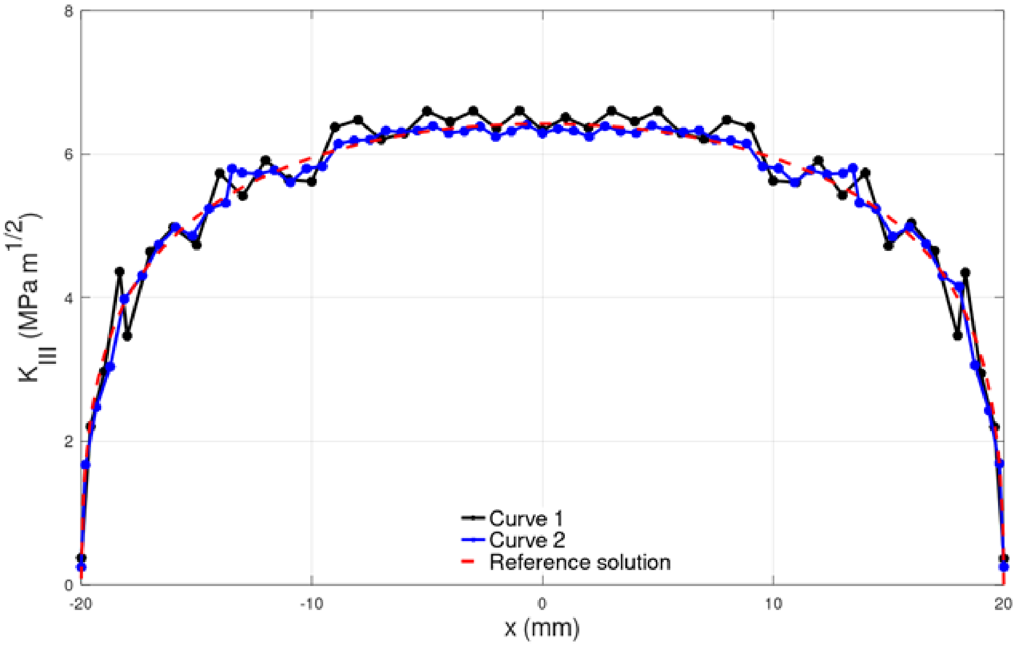

Figure E.24. Participant 10- Benchmark B – K_{II}

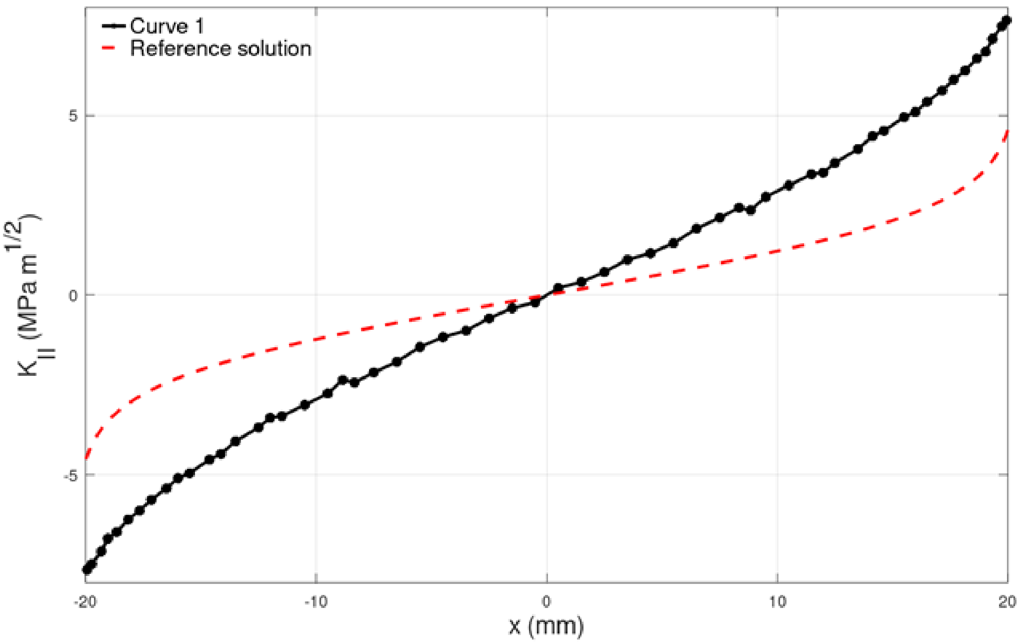

Figure E.25. Participant 10- Benchmark B – K_{III}

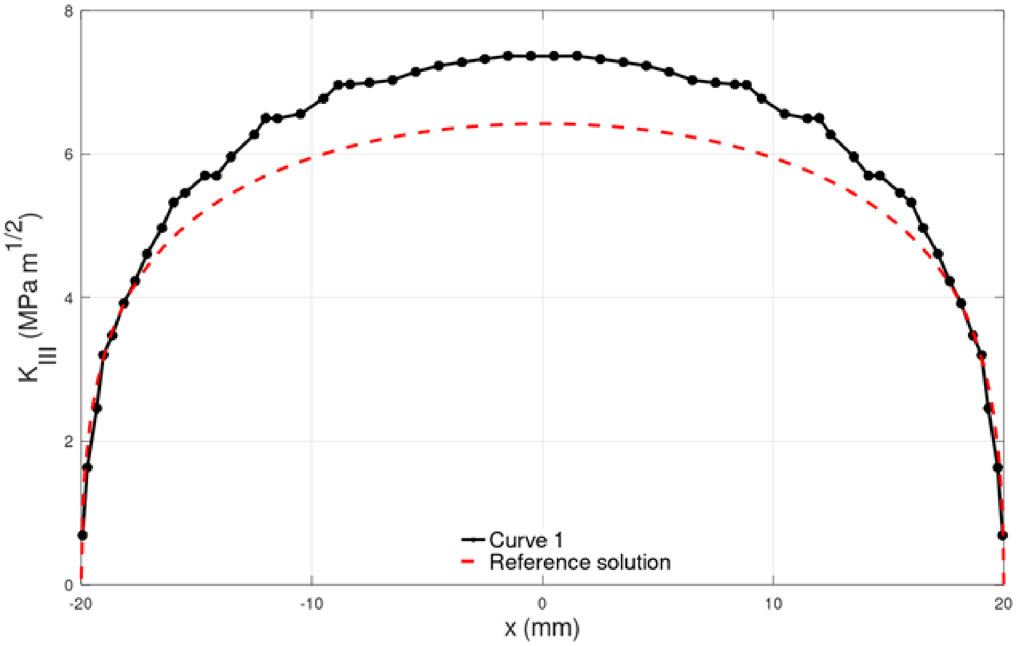

Figure E.26. Participant 11- Benchmark B – K_I

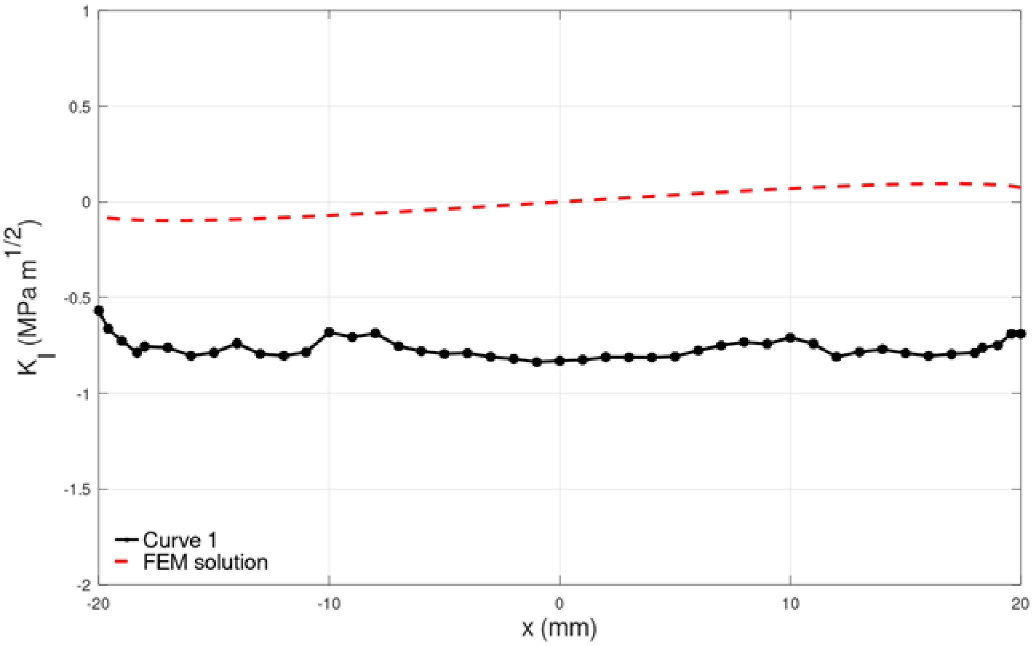

Figure E.27. Participant 11- Benchmark B – K_{II}

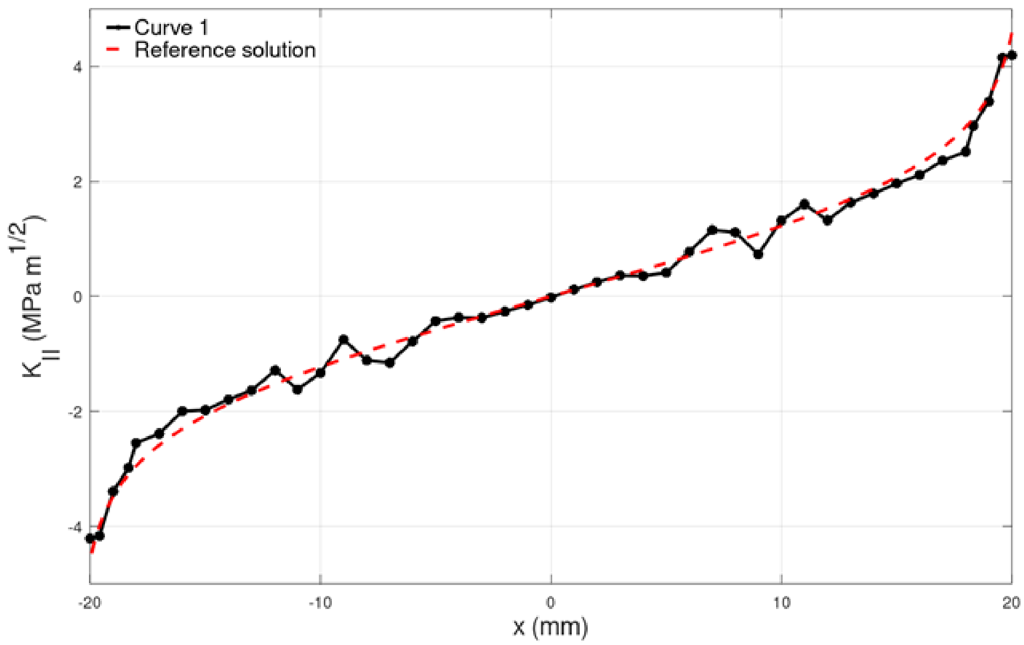

Figure E.28. Participant 11 – Benchmark B – K_{III}

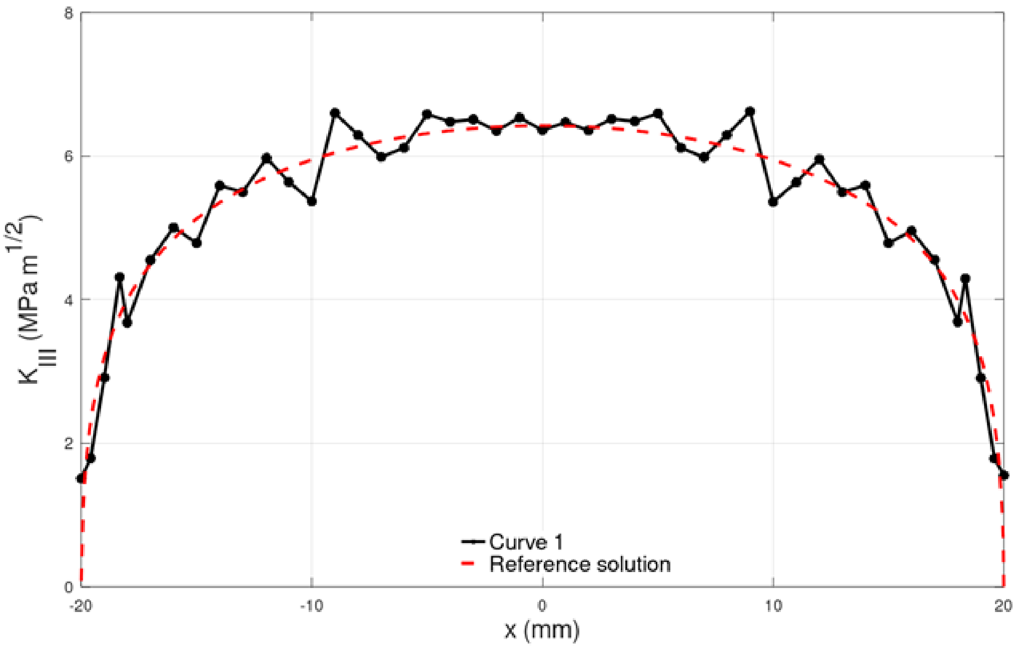

Figure E.29. Participant 12 – Benchmark B – K_I

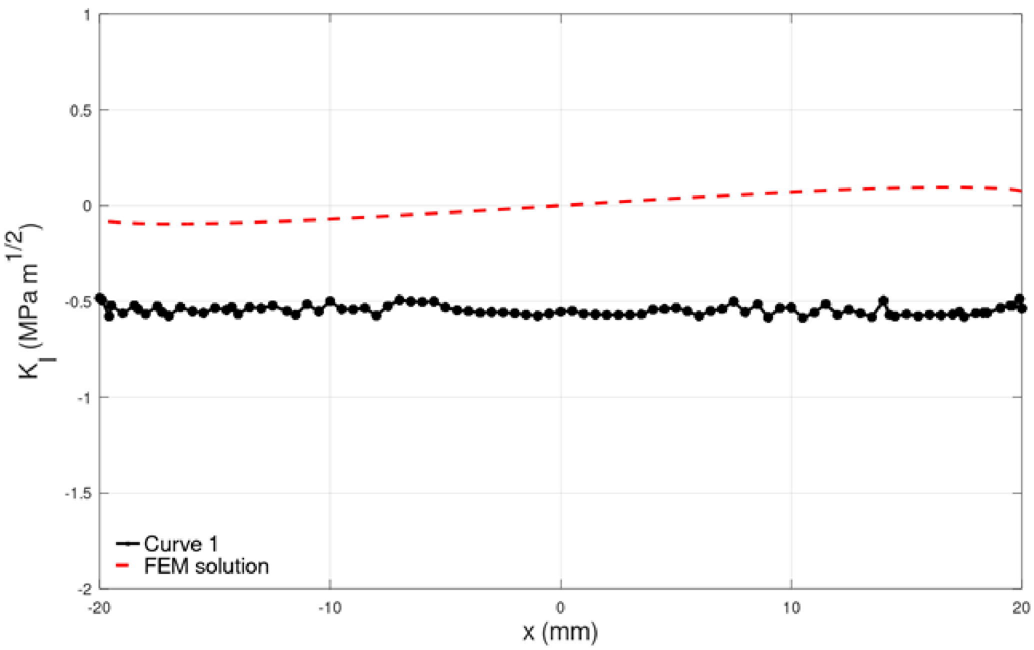

Figure E.30. Participant 12 – Benchmark B – K_{II}

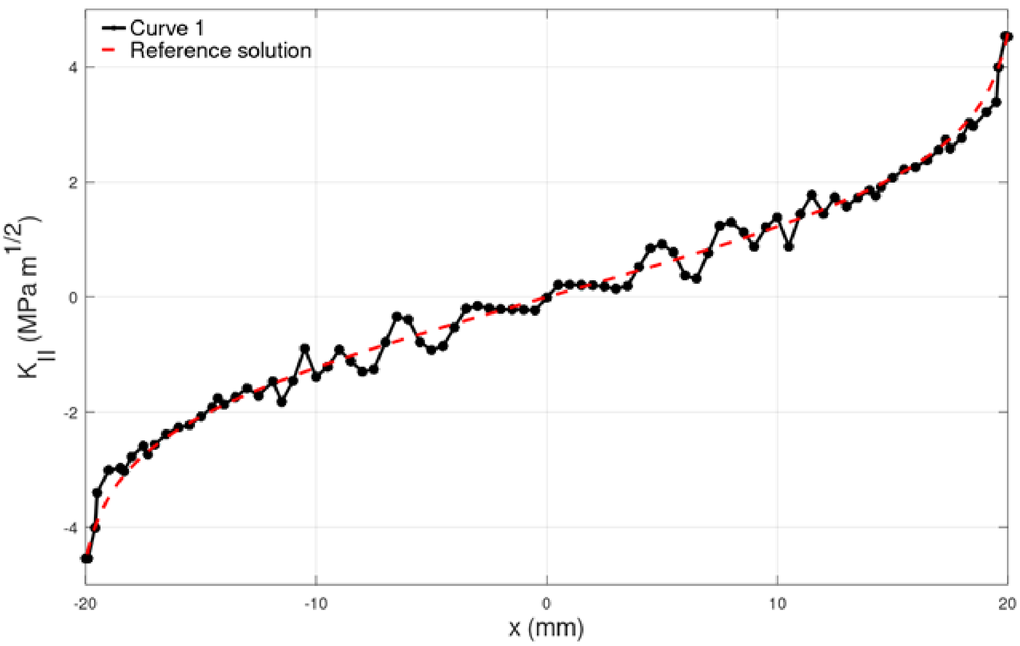

Figure E.31. Participant 12 – Benchmark B – K_{III}

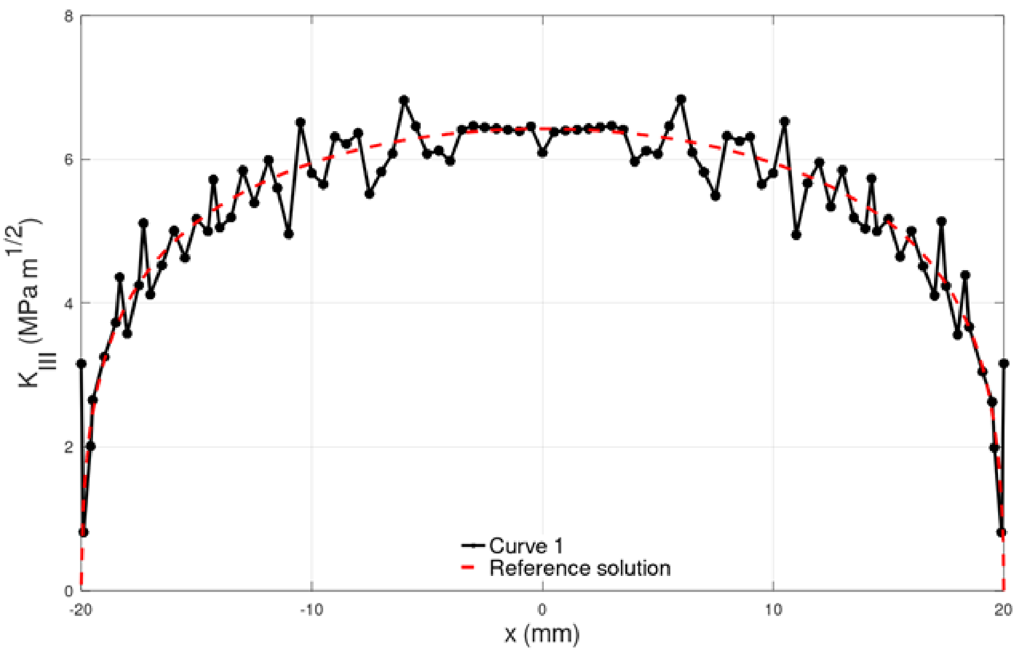

Figure E.32. Participant 13 – Benchmark B – K_I

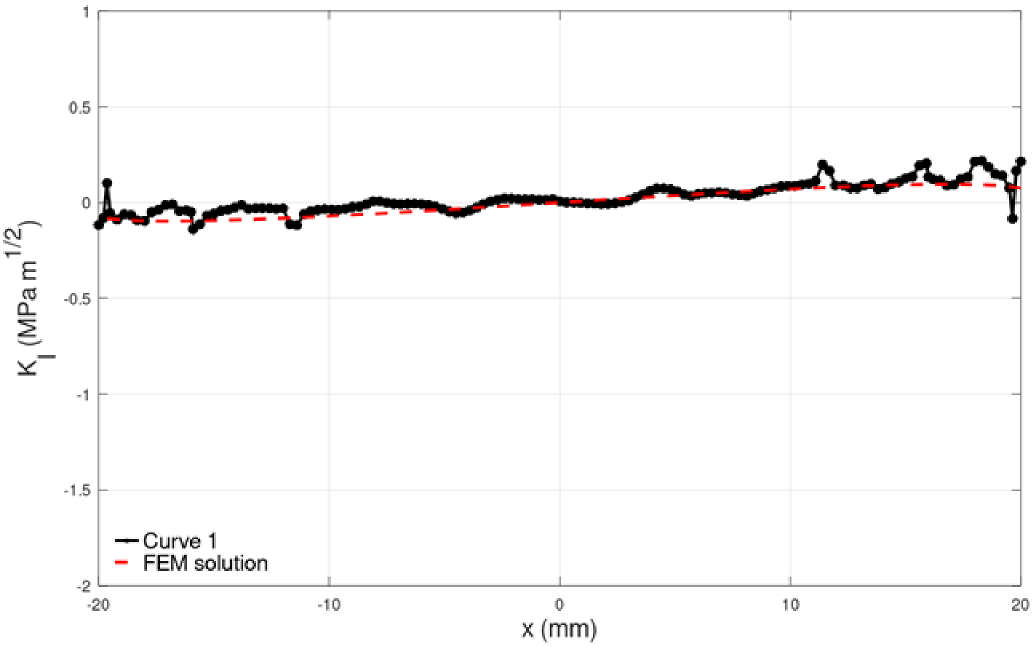

Figure E.33. Participant 13 – Benchmark B – K_{II}

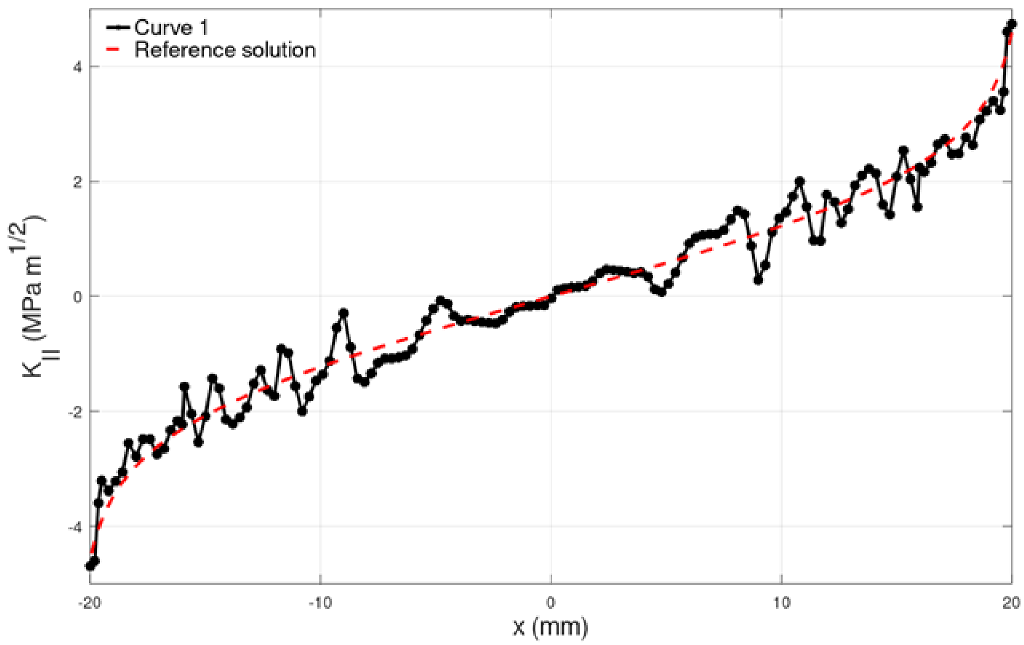

Figure E.34. Participant 13 – Benchmark B – K_{III}

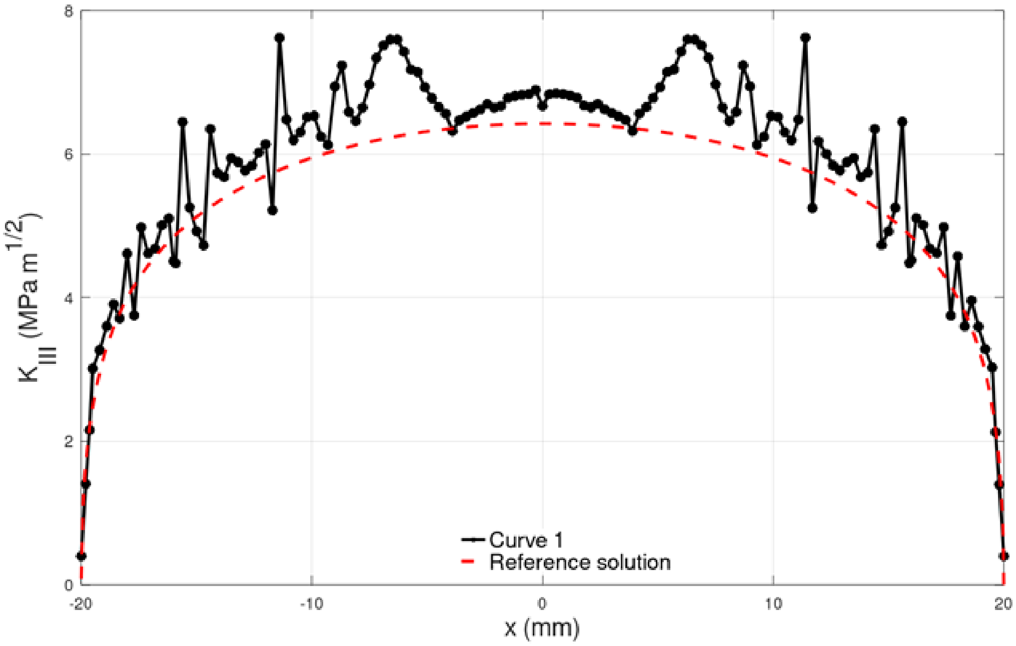

Figure E.35. Participant 14 – Benchmark B – K_{II}

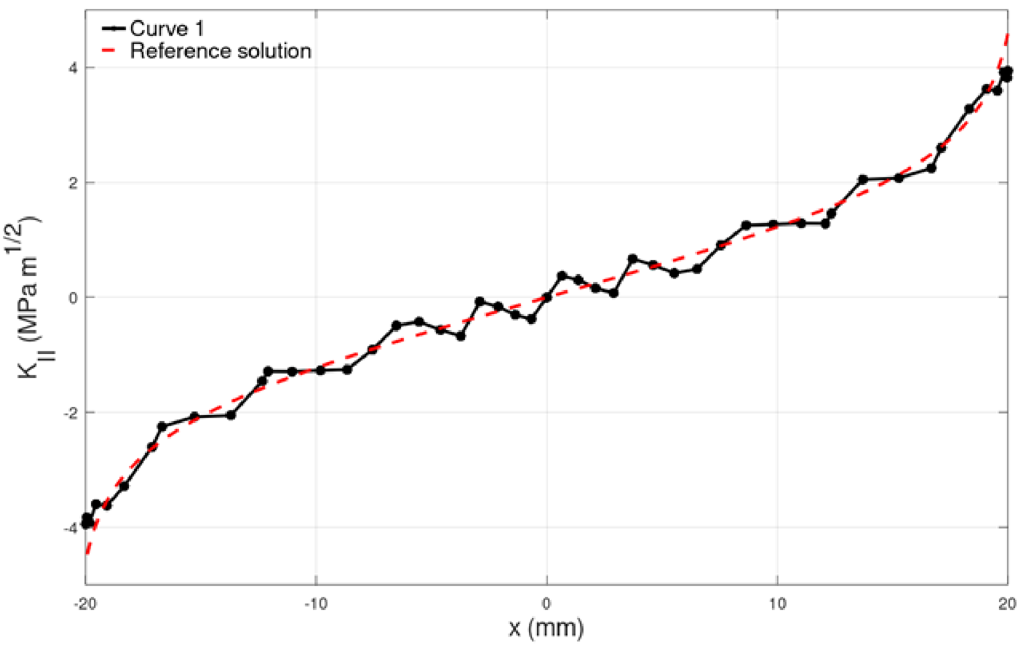

Figure E.36. Participant 14 – Benchmark B – K_{III}

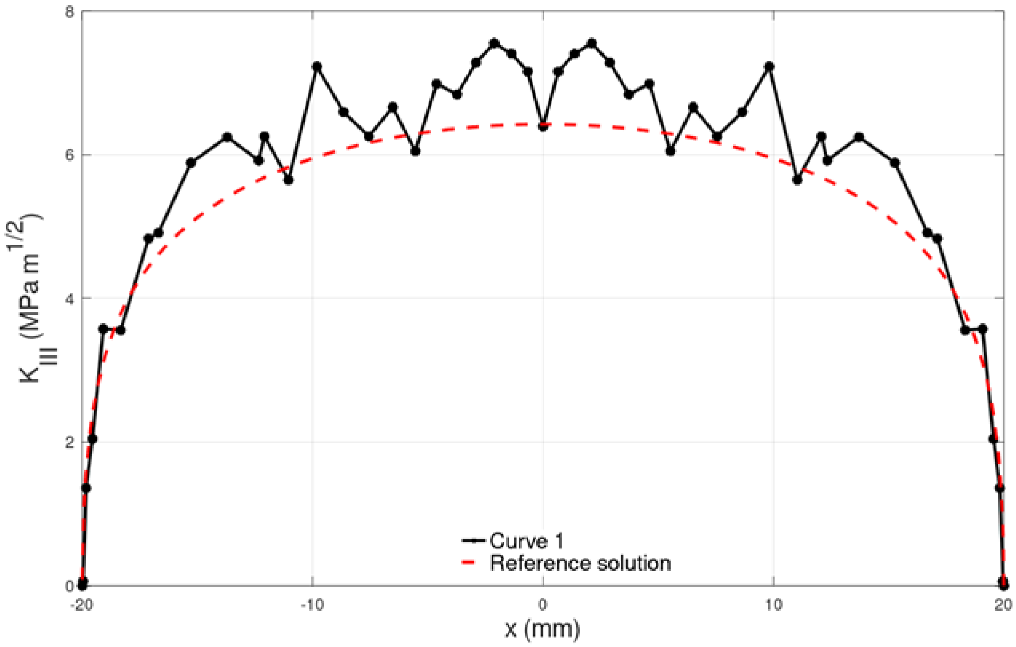

Figure E.37. Participant 15 – Benchmark B – K_I

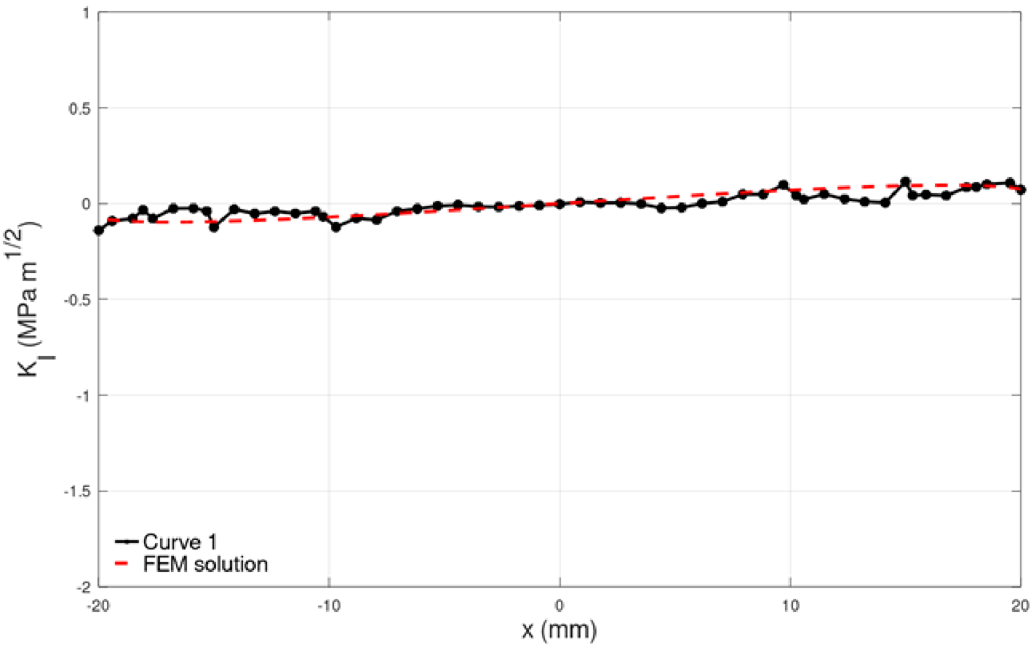

Figure E.38. Participant 15 – Benchmark B – K_{II}

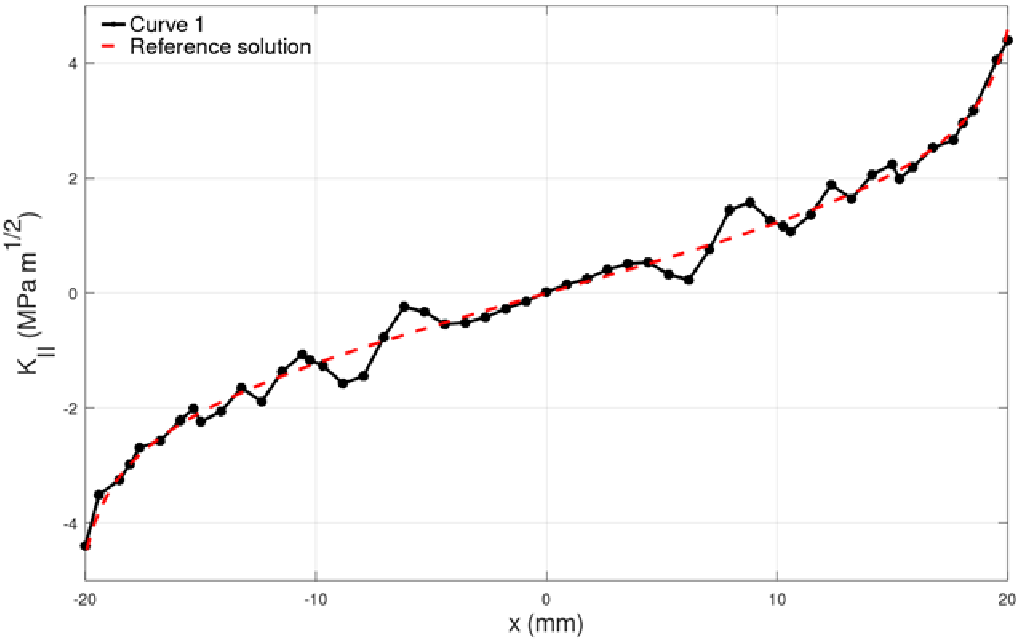

Figure E.39. Participant 15 – Benchmark B – K_{III}

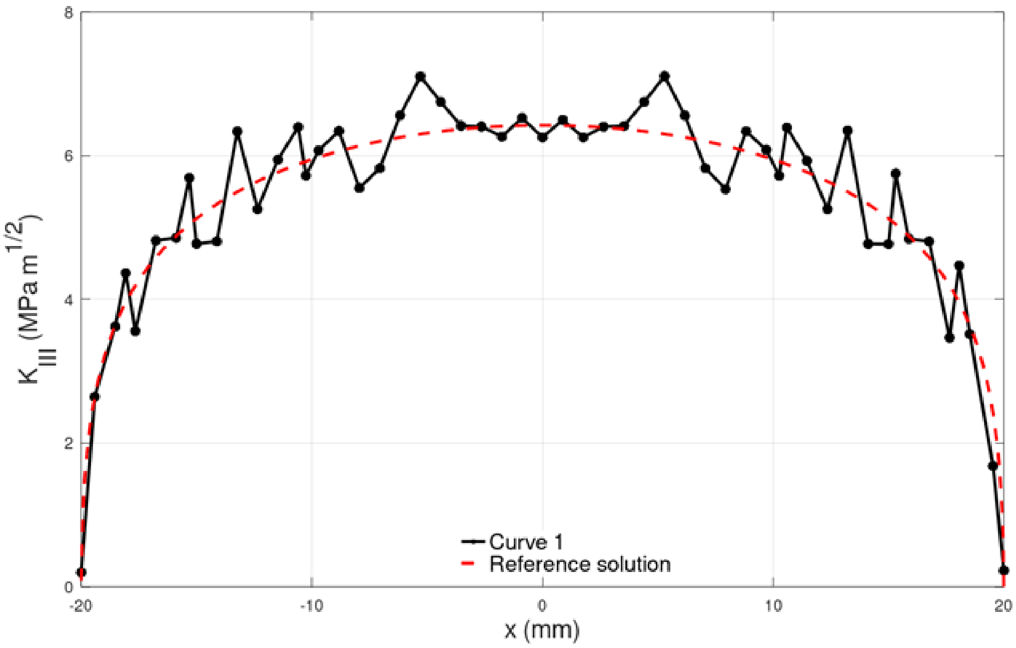

Figure E.40. Participant 16 – Benchmark B – K_I

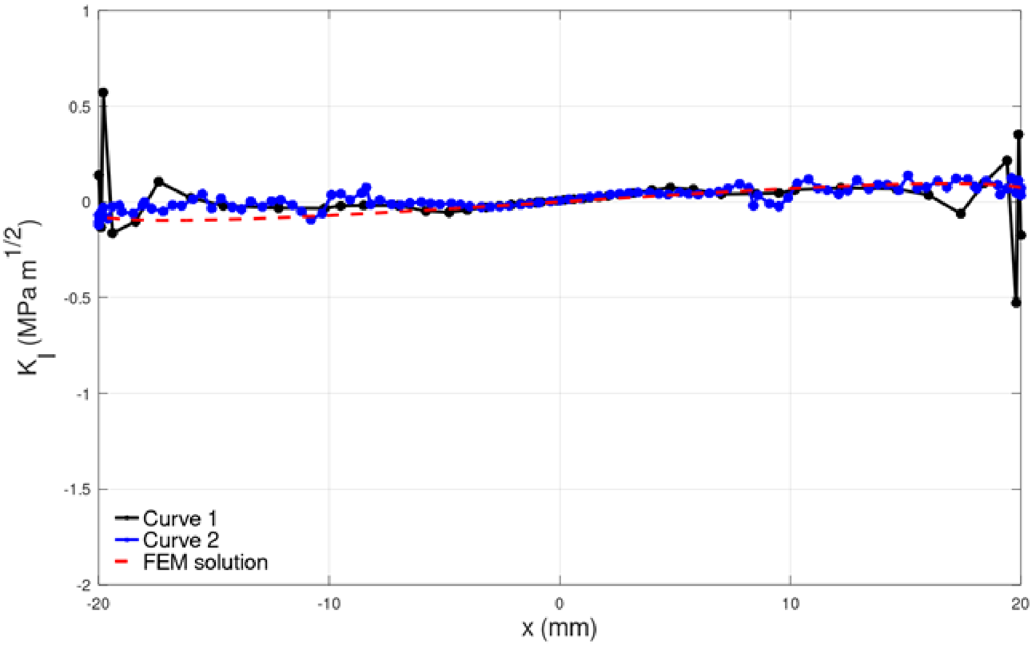

Figure E.41. Participant 16 – Benchmark B – K_{II}

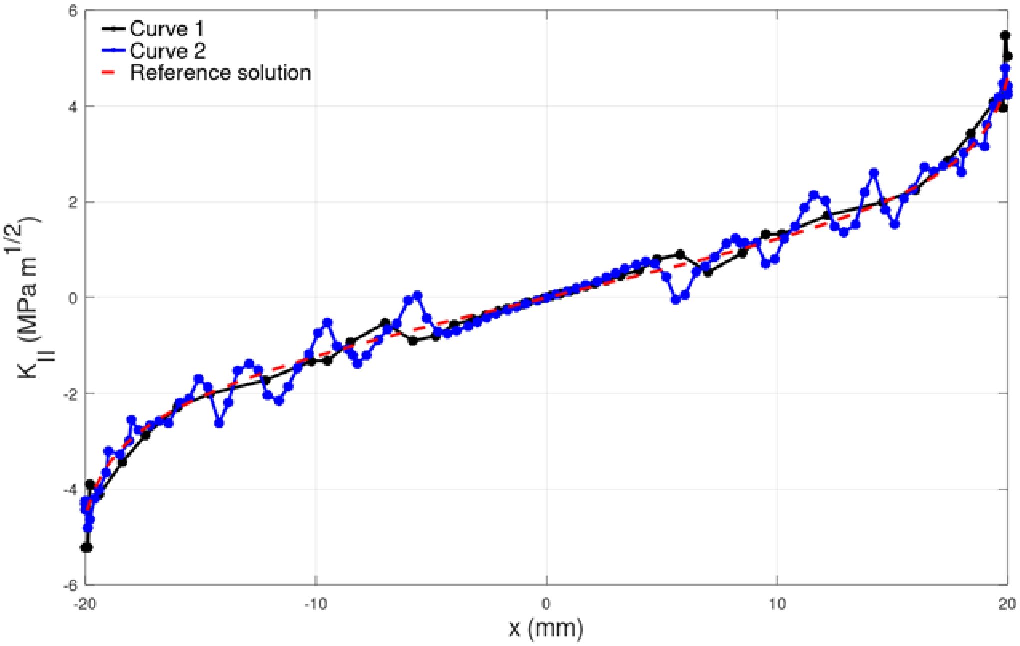

Figure E.42. Participant 16 – Benchmark B – K_{III}

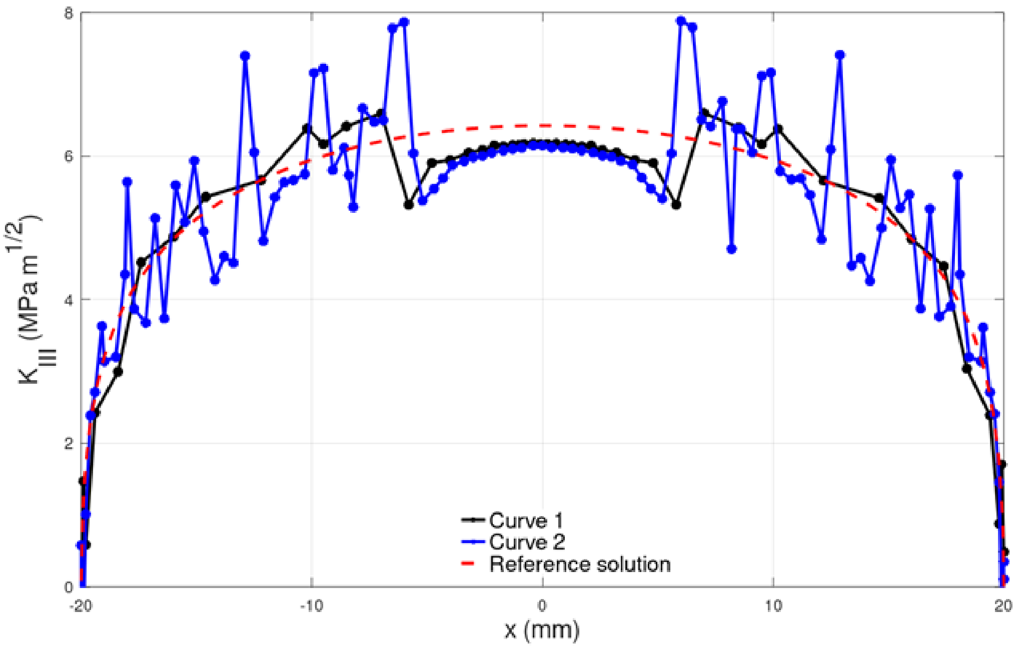

Figure E.43. Participant 17 – Benchmark B – K_{II}

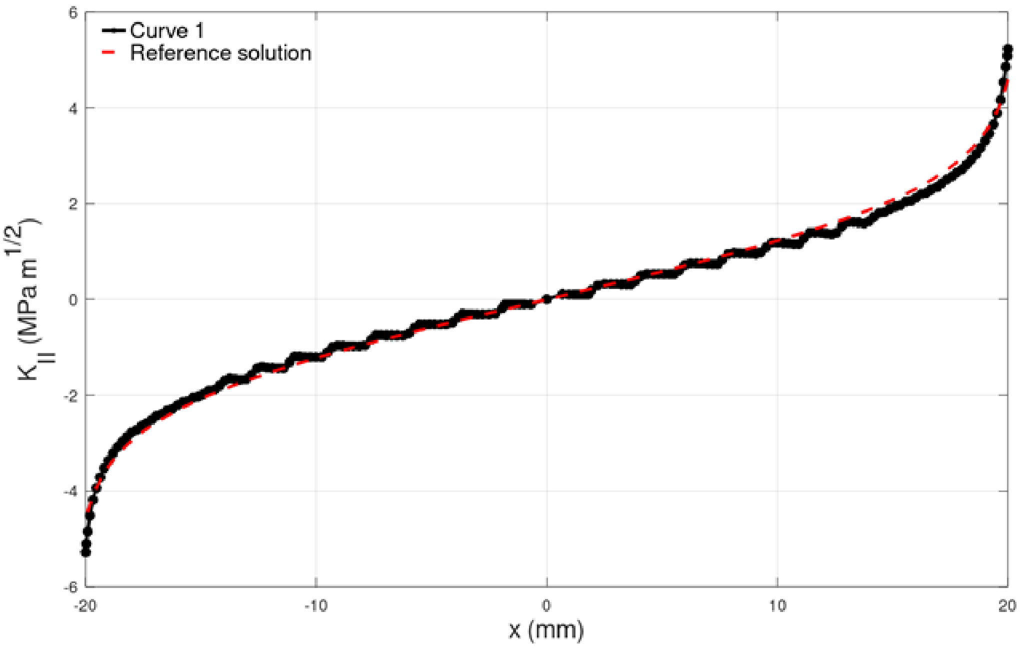

Figure E.44. Participant 17 – Benchmark B – K_{III}

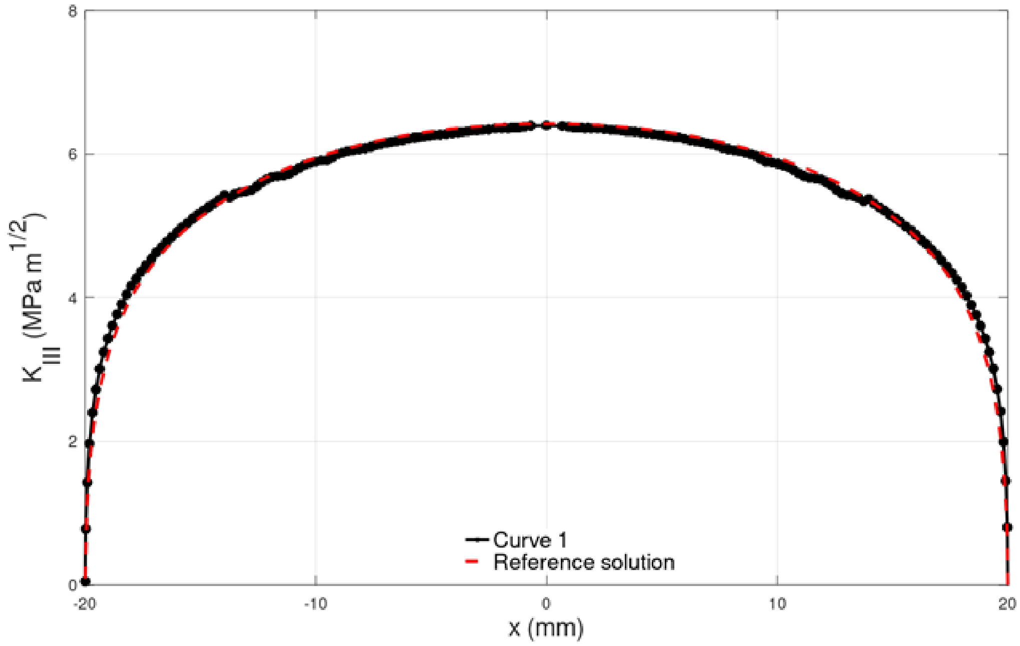

Figure E.45. Participant 18 – Benchmark B – K_{II}

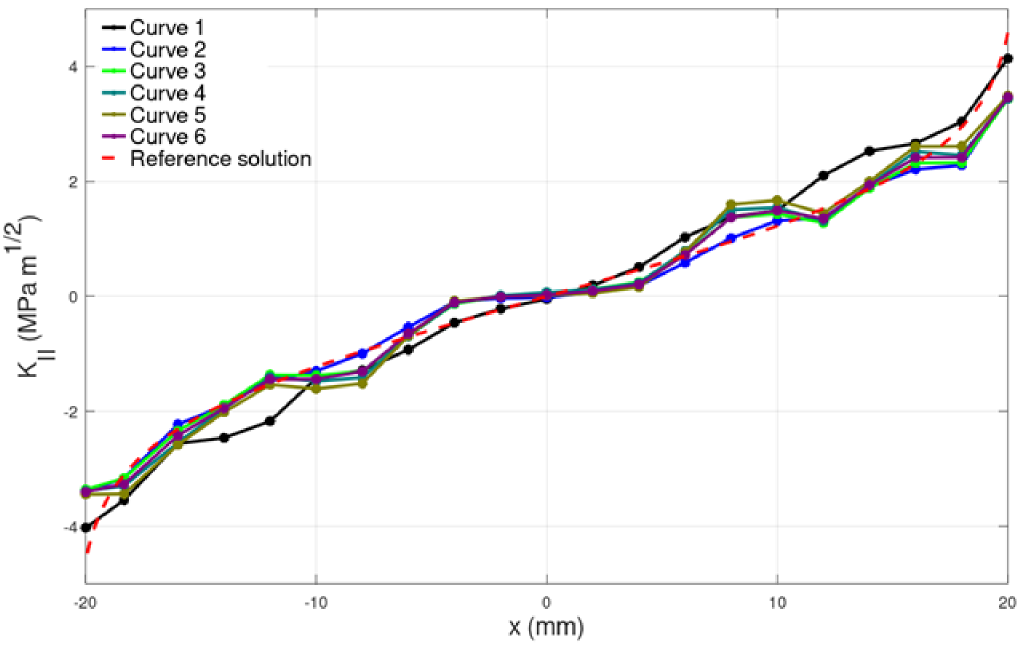

Figure E.46. Participant 18 – Benchmark B – K_{III}

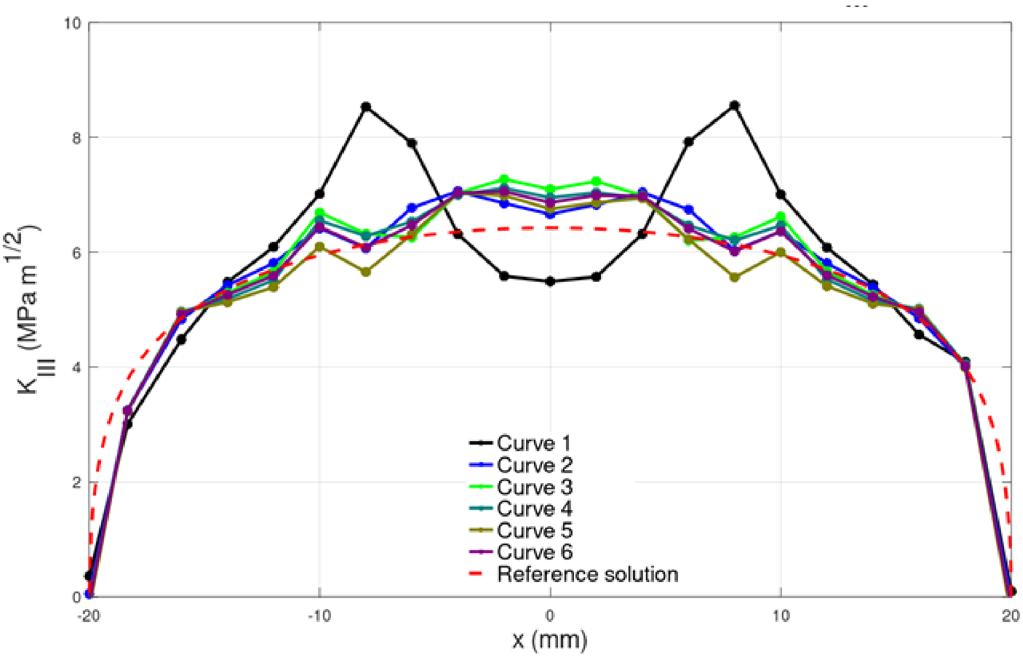

Annex F. Resulting graphs for benchmark C1

Figure F.1. Summary data for all participants on benchmark C1

Figure	Participant	Code	Curve	Mesh element			SIF calculation method	More information
				Order	type	target size (ratio to crack depth a)		
F.1	2	Morfeo crack	Curve 1	Linear + Quadratic	Tetrahedral	1/10	Integral	Mesh size at interface points C has been reduced to a/50 because of sharp edges
F.2	3	Ansys	Curve 1	Linear	Hexahedral	1/10	Integral	
F.3	5	Systus	Curve 1	Quadratic	Hexahedral	1/10	Integral	Integration domain: R_{min} = 0,5 mm; R_{max} = 2 mm / Results along crack front B-C invalid
			Curve 2					Integration domain: R_{min} = 0,5 mm; R_{max} = 3 mm / Results along crack front B-C invalid
			Curve 3					Integration domain: R_{min} = 0,5 mm; R_{max} = 4 mm / Results along crack front B-C invalid
F.4	6	Code-Aster (FEM)	Curve 1	Quadratic	Tetrahedral	1/25	Integral	
		Code-Aster	Curve 2	Quadratic	Hexahedral	1/25	?	
F.5	8	Abaqus	Curve 1	Linear	Hexahedral	1/8 to 1/10	Integral	
			Curve 2			1/10 to 1/20		
F.6	9	Abaqus	Curve 1	Linear	Hexahedral	1/10	Integral	
F.7	10	NLXFEM3Dheat + NLXFEM3Dstruct	Curve 1	Linear	Hexahedral	1/20	Integral	
F.8	11	Abaqus	Curve 1	Linear	Hexahedral	1/5	Integral	
F.9	12	Abaqus	Curve 1	Linear	Hexahedral	1/10	Displacement	
F.10	14	Abaqus	Curve 1	Linear	Hexahedral	1/10	Integral	
F.11	15	Abaqus	Curve 1	Linear	Hexahedral	1/10	Integral	
F.12	16	Abaqus	Curve 1	Linear	Hexahedral	1/28	Integral	
F.13	3, 6, 9, 10, 11, 12, 14, 16	Multiple codes	Curve 1	This figure plots K_I as function of time at point A of the crack, obtained by several participants by calculation or theory. For the details of the calculations, see above				Results obtained by participant 3, by X-FEM calculation
			Curve 2					Results obtained by participant 6, by theory
			Curve3					Results obtained by participant 6, by X-FEM calculation
			Curve 4					Results obtained by participant 9, by theory
			Curve 5					Results obtained by participant 9, by X-FEM calculation
			Curve 6					Results obtained by participant 10, by theory
			Curve 7					Results obtained by participant 10, by X-FEM calculation
			Curve 8					Results obtained by participant 11, by X-FEM calculation
			Curve 9					Results obtained by participant 12, by X-FEM calculation
			Curve 10					Results obtained by participant 14, by X-FEM calculation
			Curve 11					Results obtained by participant 16, by X-FEM calculation

Figure F.2. Participant 2 – Benchmark C1

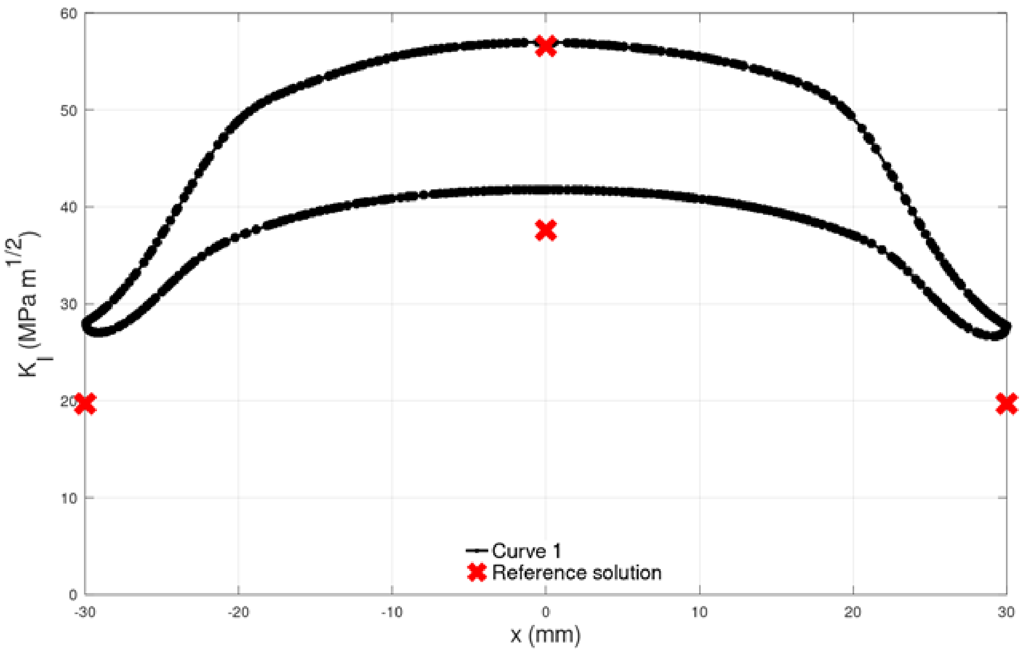

Figure F.3. Participant 3 – Benchmark C1

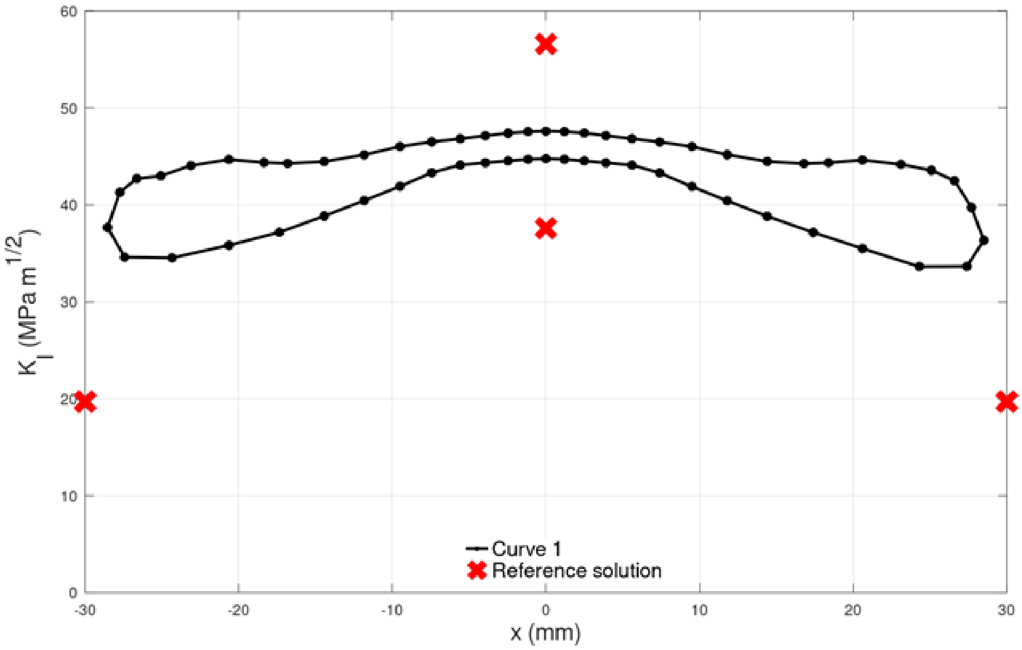

Figure F.4. Participant 5 – Benchmark C1

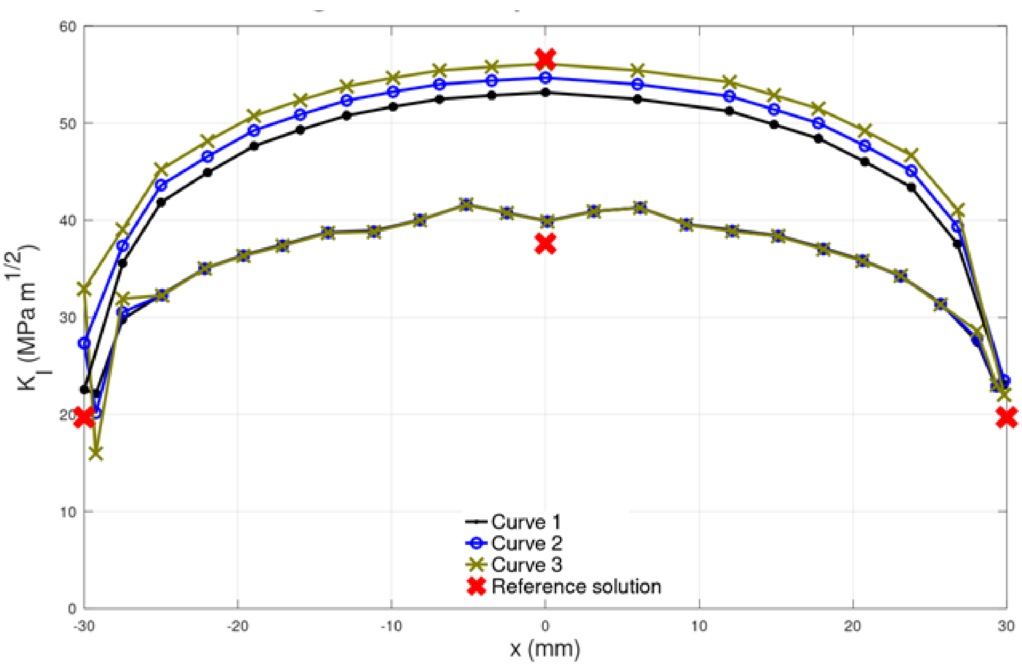

Figure F.5. Participant 6 – Benchmark C1

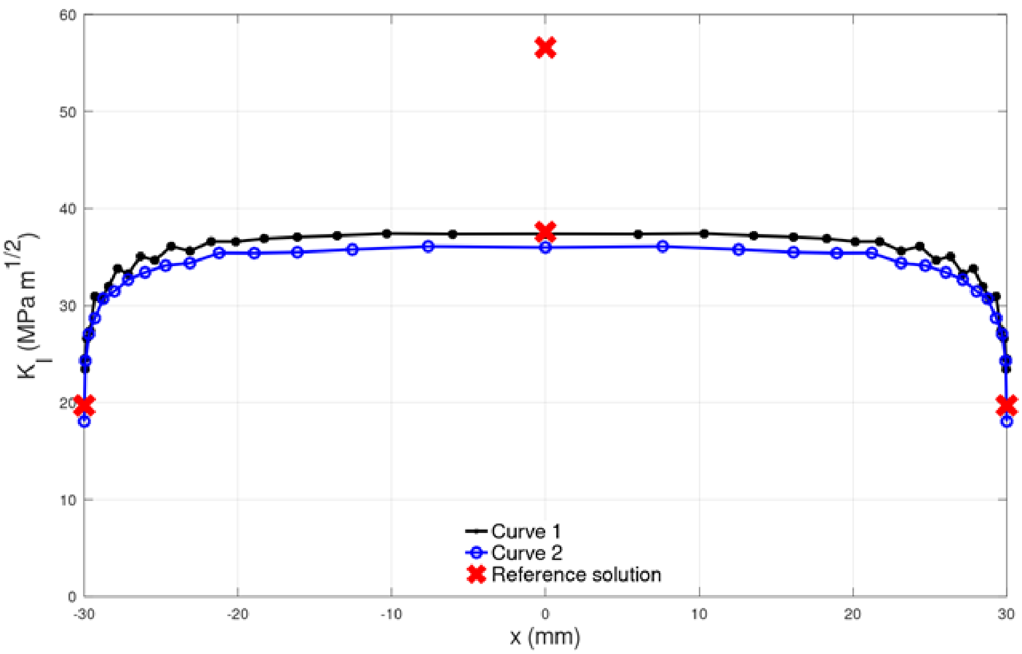

Figure F.6. Participant 8 – Benchmark C1

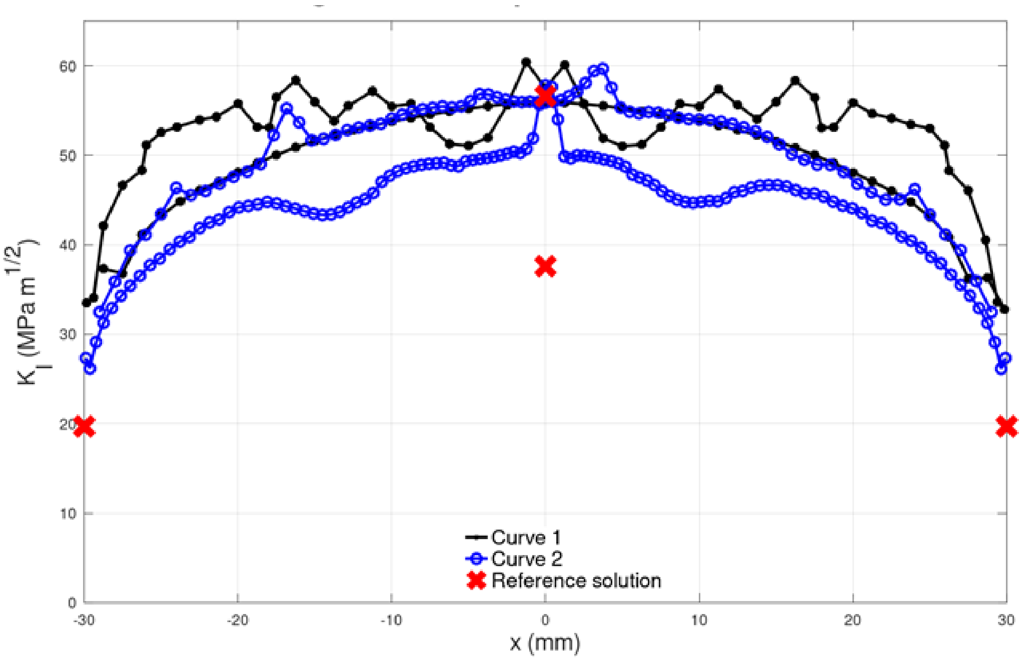

Figure F.7. Participant 9 – Benchmark C1

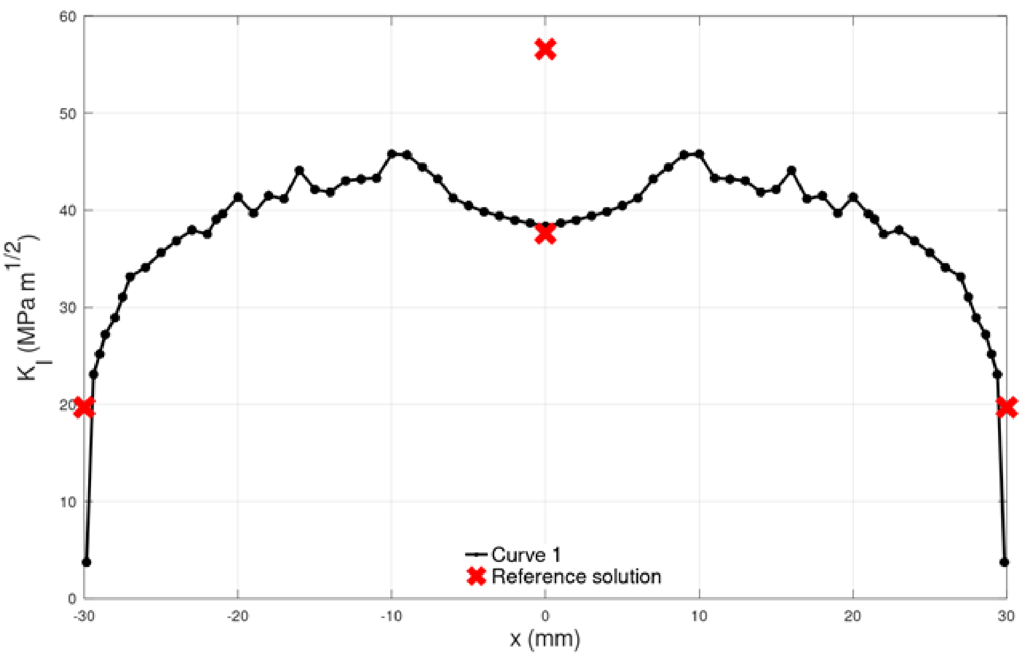

Figure F.8. Participant 10 – Benchmark C1

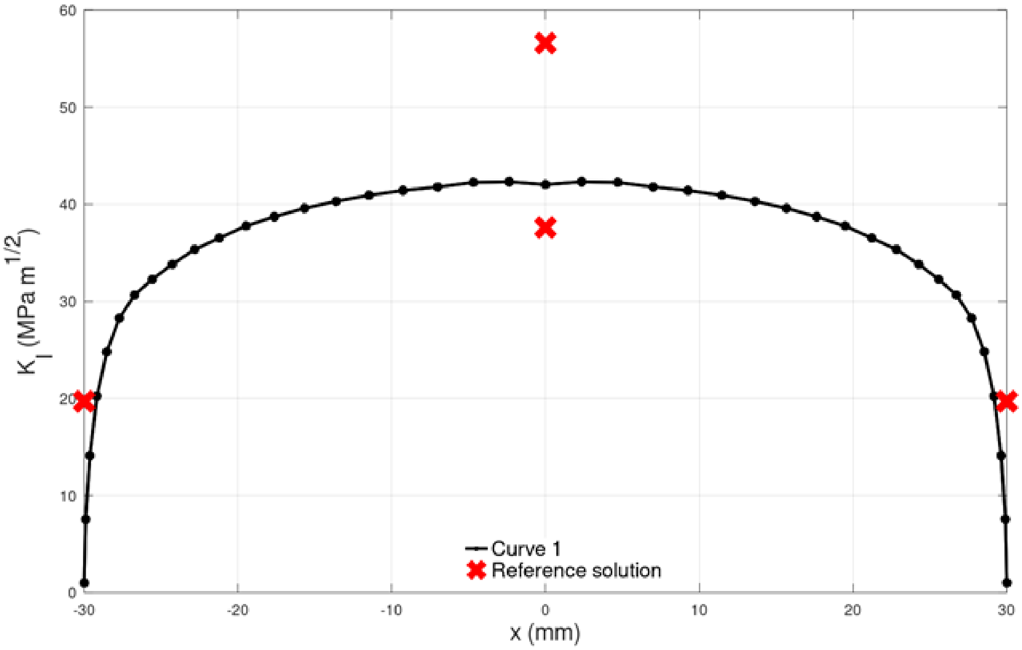

Figure F.9. Participant 11 – Benchmark C1

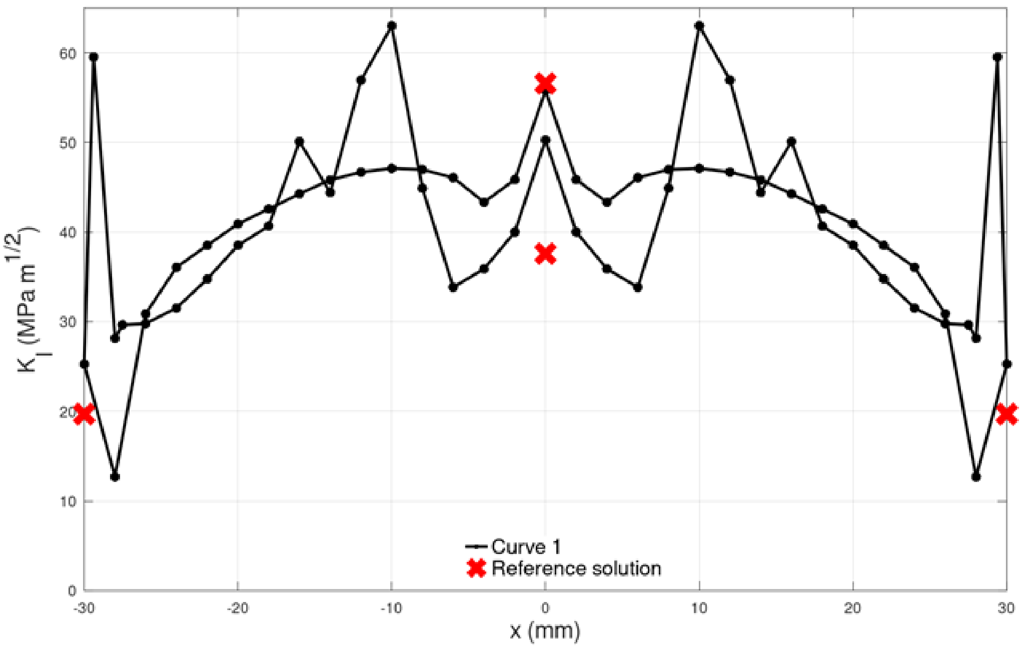

Figure F.10. Participant 12 – Benchmark C1

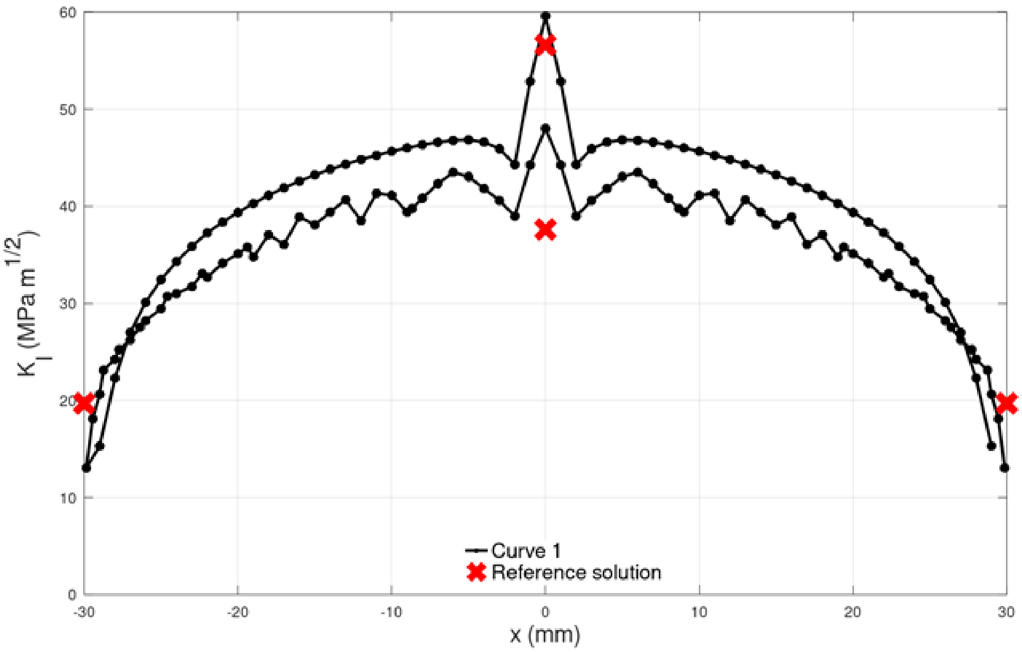

Figure F.11. Participant 14 – Benchmark C1

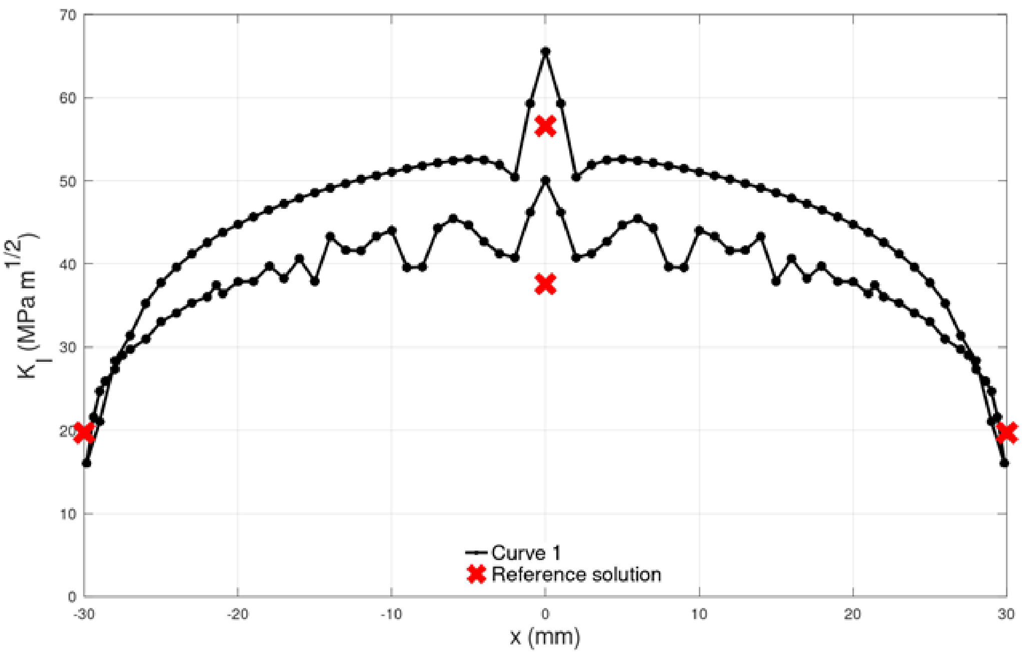

Figure F.12. Participant 15 – Benchmark C1

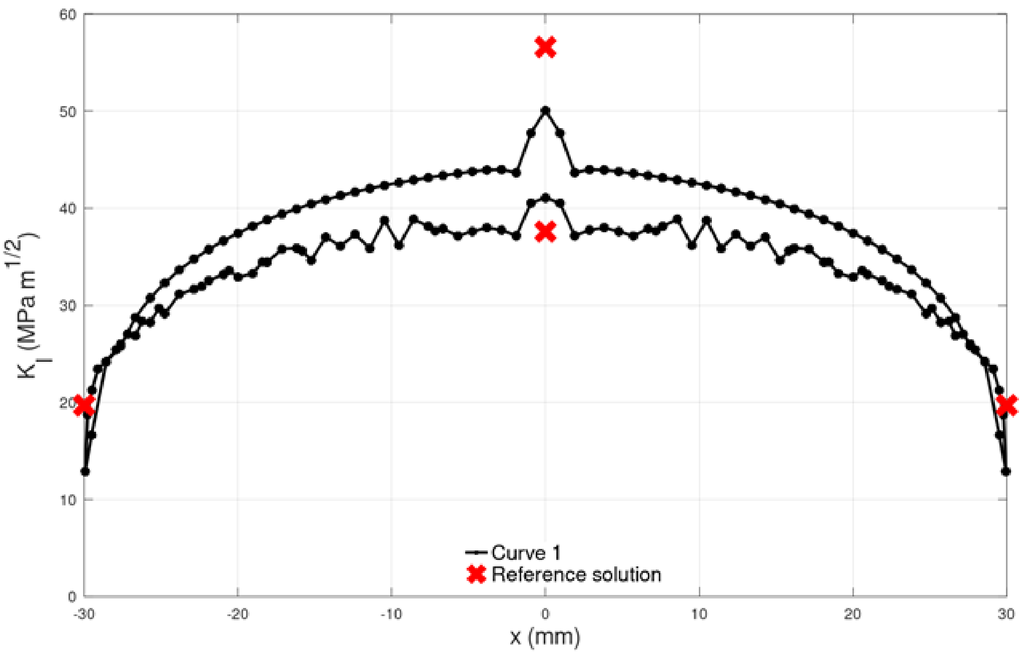

Figure F.13. Participant 16 – Benchmark C1

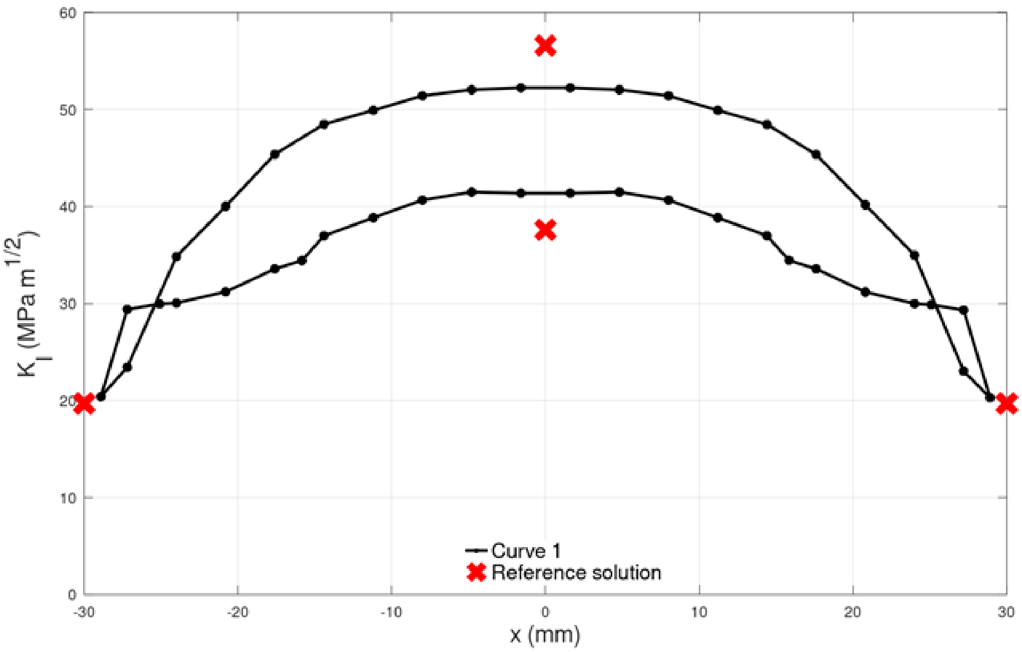

Figure F.14. K_I as function of time at point A

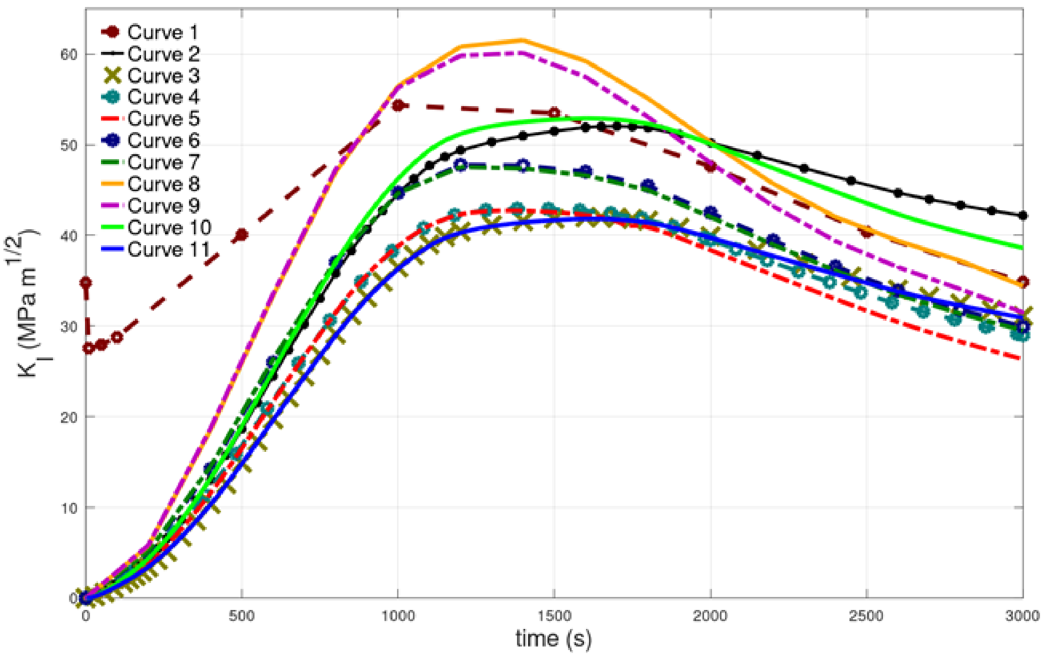

Annex G. Participants

A detailed list of the 18 participants to the X-FEM benchmark is given in Table G.1.

Table G.1. List of participants of the X-FEM benchmark

	Country	Organisation	Description of organisation	Contact person	Code used
1	Belgium	**Bel V** (Project co-leader) Walcourtstraat 148 B-1070 Brussels Belgium	TSO	VAN NUFFEL, Diederik diederik.vannuffel@belv.be Tel.: +32 (0)2 528 03 33	ABAQUS
2		**Tractebel Engineering (ENGIE)** Boulevard Simon Bolivar 34-36 B-1000 Brussels Belgium	Licensee support	DESMET, Michel michel.desmet@tractebel.engie.com Tel.: +32 (0)2 773 83 69	Morfeo Crack Software
3	Canada	**Candu Energy Inc.** 2285 Speakman Drive Mississauga, Ontario L5K 1B1 Canada	Research centre	DUAN, Xinjian xinjian.duan@snclavalin.com LEARY, Daniel daniel.leary@snclavalin.com SHI, Yihai yihai.shi@snclavalin.com	ABAQUS ANSYS
4	France	**Institut de Radioprotection et de Sûreté Nucléaire (IRSN)** (Project leader) B.P.17 92262 Fontenay-aux-Roses Cedex France	TSO	DELVALLÉE-NUNIO, Isabelle isabelle.delvallee@irsn.fr Tel.: +33 1 58 35 86 94	CODE_ASTER
5		**ESI Virtual Engineering solutions** Le Récamier - 70, rue Robert 69458 Lyon Cedex 06 France	Software developer	MOREAU, François francois.moreau@esi-group.com Tel.: +33 4 78 14 59 42	SYSTUS

6		**Electricité de France (EDF)** EDF R&D, Département ERMES EDF Lab Paris-Saclay – Bureau O2B24 7 Boulevard Gaspard Monge 91120 Palaiseau France	Utility	GENIAUT, Samuel samuel.geniaut@edf.fr Tel.: +33 1 78 19 37 83	CODE_ASTER
7	Germany	**MPA Universität Stuttgart** Dept Component Assessment and Reliability Pfaffenwaldring 32 D-70569 Stuttgart Germany	Research centre	STUMPFROCK, Ludwig ludwig.stumpfrock@mpa.uni-stuttgart.de Tel.: +49 711 685 63041	ABAQUS
8	India	**Bhabha Atomic Research Centre (BARC)** Mumbai-400085 India	Research centre	INGH, P.K. pksingh@barc.gov.in SHARMA, Kamal kamals@barc.gov.in	ABAQUS
9	Japan	**Japan Atomic Enegry Agency (JAEA)** Nuclear Science Research Institute 2-4 Shirakata, Tokai-mura, Naka-gun, Ibaraki 319-1195, Japan	Research centre	LI, Yinsheng li.yinsheng@jaea.go.jp	ABAQUS
10		**Central Research Institute of Electric Power Industry (CRIEPI)** Nuclear power plant Maintenance Research Team 2-6-1 Nagasaka, Yokosuka-shi, Kanagawa-ken 2400196 Japan	Research centre	MIURA, Naoki miura@criepi@denken.or.jp	NLXFEM3Dheat and NLXFEM3DStruc

11	Korea	**Korea Institute of Nuclear Safety (KINS)** Department of Mechanical and Materials Engineering 62 gwahak-ro, Yuseong-gu, Deajeon, 34142 Korea	TSO	YONG-BEUM, Kim ybkim@kins.re.kr Tel.: +82 42 868 0165	ABAQUS
12		**Korea Univ. (KoU)** Dept. of Mechanical Engineering 145, Anam-ro, Seongbuk-gu, Seoul Korea	Research centre	YUN-JAE, Kim kimy0308@korea.ac.kr Tel.:+82 10 2383 7459	ABAQUS
13		**Kyunghee Univ. (KyU)** Dept. of Nuclaer Engineering 1732, Deogyeong-daero, Giheung-gu, Yongin-si, Gyeonggi-do Korea	Research centre	YOON-SUK, Chang yschang@khu.ac.kr Tel.:+ 82 10 3020 6396	ABAQUS
14		**Korea Atomic Energy Research Institute (KAERI)** Nuclear Materials Research Division 1045, Daedeok-daero, Yuseong-gu, Daejeon Korea	Research centre	JONG-MIN, Kim jmkim@kaeri.re.kr Tel.:+82 10 2957 9780 HAN-BUM, Surh hbsurh@kaeri.re.kr Tel.: +82 42 866 6267	ABAQUS
15		**Seoul Tech Univ.(SeU)** Dept. of Mechanical System and Design Engineering 232, Gongneung-ro, Nowon-gu, Seoul Korea	Research centre	NAM-SU, Huh nam-su.huh@seoultech.ac.kr Tel.:+82 10 6276 2316	ABAQUS
16	Switzerland	**Paul Scherrer Institute (PSI)** 5232 Villigen PSI Switzerland	Research centre	NIFFENEGGER, Markus markus.niffenegger@psi.ch +41 (0)56 310 26 86 DIEGO, Mora diego.mora@psi.ch +41 (0)56310 43 64	ABAQUS

17	United States	**US Nuclear Regulatory Commission (USNRC)** Two White Flint North, M/S T-10 A36 11545 Rockville Pike Rockville, MD 20852-2738 United States	TSO and regulatory body	FACCO, Giovanni giovanni.facco@nrc.gov Tel.:301-415-0892 TREGONING, Robert robert.tregoning@nrc.gov Tel.: 301 415 2324 RAYNAUD, Patrick patrcik.raynaud@nrc.gov Tel.: 301-415-1987 IYENGAR, Raj raj.iyengar@nrc.gov Tel.: 301-415-0770	ABAQUS
18		**Structural Integrity Associates (SIA)** United States	Research centre /licensee support	SHIM, Do Jun dshim@structint.com DOMINGUEZ, Gary gdominguez@structint.com	ABAQUS